TECHNISCHE UNIVERSITÄT MÜNCHEN
Lehrstuhl für Proteomik und Bioanalytik

Time-resolved analysis of phosphoproteome dynamics in fibroblast mechanosensing

Laura Felicitas Mattner

Vollständiger Abdruck der von der TUM School of Life Sciences der Technischen Universität München zur Erlangung des akademischen Grades eines

Doktors der Naturwissenschaften

genehmigten Dissertation.

Vorsitzender: Prof. Dr. Dieter Langosch

Prüfer der Dissertation: 1. Prof. Dr. Bernhard Küster
2. apl. Prof. Dr. rer. nat. Silke Meiners

Die Dissertation wurde am 23.10.2020 bei der Technischen Universität München eingereicht und durch die TUM School of Life Sciences am 15.01.2021 angenommen.

Candidate's affiliations

"Everything is going to be fine in the end. If it's not fine, it's not the end."

Oscar Wilde

Abstract

Cells actively sense their environment by translating mechanical properties of the extracellular matrix, such as stiffness or shear stress, into biochemical signals. This cellular mechanosensing is crucial for development, tissue homeostasis and the outcome of many diseases. Mechanosensitive signaling pathways are important in the pathophysiology of fibrotic diseases, where the composition of the extracellular matrix (ECM) and its mechanical properties are altered in disease progression. The activity and survival of activated fibroblasts in fibrotic diseases may be largely controlled by mechanical signals. In this process, the structure and organization of the cytoskeleton is modified, which also induces long term gene expression changes. The precise molecular nature of many elements in these feedback connections is currently unknown. Posttranslational modifications (PTMs) are known to be essential mechanisms exploited by cells to diversify their protein functions and actively coordinate their signaling networks. Protein phosphorylation plays an important role in the transmission of cellular signals. Importantly, protein phosphorylation on serine, threonine and tyrosine residues (S,T,Y) was shown to regulate protein conformation, as well as protein interactions and subcellular localization. It is currently unclear which phosphorylation sites are directly regulated by substrate rigidity. Recent developments in phosphoproteomic workflows increase sensitivity of detection and sample throughput, which enabled me to follow the dynamic changes of the phosphorylation landscape of human lung fibroblasts to uncover phosphosites that are regulated during cell adhesion and by substrate rigidity. Up to date, only little is known about the contribution of the phosphoproteome in the context of cellular mechanosensing. In this work, a cell attachment time course (10, 20, 30, 60, 90, 120 min) was conducted as well as a mechanosensing experiment where fibroblasts were seeded for 2 h on a fibronectin-coated surface with varying rigidities (0.5, 2, 8, 16, and 32 kPa). The EasyPhos workflow for phosphopeptide enrichment in combination with a modern Orbitrap MS instrument enabled me to investigate the phosphoproteome at a depth of 10,000 to 12,000 unique phosphorylated peptides. The analysis revealed the identification of over 1000 significantly regulated phosphosites. Among those, differentially phosphorylated RNA-binding proteins, spliceosomal components, transcriptional regulators, chromatin modulators, and cytoskeletal proteins were detected. Through the combined analysis of the two phosphoproteomic data sets, it was possible to infer which stiffness sensitive phosphorylation sites are directly influenced by substrate rigidities and which phosphosites require the adaption of the cell to specific contractility and shape or are rather directly influenced by substrate stiffness. Furthermore, the comparison to primary human lung fibroblasts enabled me to

identify robust mechanosensitive signals that were reproducible in independent experiments. The data uncovers mechanosensitive protein phosphorylation sites, which were put in the context of established signaling pathways by my analysis. Overall, this study provides a deeper understanding of the signaling events on soft to stiff microenvironments and during cell spreading, which may have implications for fibroblast states in fibrotic diseases.

Zusammenfassung

Zellen nehmen ihre Umgebung aktiv wahr, indem sie mechanische Eigenschaften der extrazellulären Matrix, wie Steifigkeit oder Scherspannung, in biochemische Signale umsetzen. Diese zelluläre Mechanosensorik ist entscheidend für die Entwicklung, die Homöostase des Gewebes und den Ausgang vieler Krankheiten. Mechanosensitive Signalwege sind wichtig für die Pathophysiologie fibrotischer Erkrankungen, bei denen die Zusammensetzung der extrazellulären Matrix (ECM) und ihre mechanischen Eigenschaften im Krankheitsverlauf verändert werden. Die Aktivität und das Überleben von aktivierten Fibroblasten bei fibrotischen Erkrankungen können weitgehend durch mechanische Signale gesteuert werden. Dabei wird die Struktur und Organisation des Zytoskeletts verändert, was auch langfristige Veränderungen der Genexpression induziert. Die genaue molekulare Natur vieler Elemente in diesen Rückkopplungsverbindungen ist derzeit unbekannt. Posttranslationale Modifikationen (PTMs) sind bekanntlich wesentliche Mechanismen, die von Zellen genutzt werden, um ihre Proteinfunktionen zu diversifizieren und ihre Signalnetzwerke aktiv zu koordinieren. Die Proteinphosphorylierung spielt eine wichtige Rolle bei der Übertragung von zellulären Signalen. Es konnte gezeigt werden, dass die Proteinphosphorylierung an Serin-, Threonin- und Tyrosinresten (S,T,Y) die Proteinkonformation sowie die Proteininteraktionen und die subzelluläre Lokalisierung reguliert. Derzeit ist unklar, welche Phosphorylierungsstellen direkt durch die Substratrigidität reguliert werden. Neuere Entwicklungen in phosphoproteomischen Arbeitsabläufen erhöhen die Sensitivität der Detektion und des Probendurchsatzes, was es mir ermöglichte, die dynamischen Veränderungen der Phosphorylierungslandschaft menschlicher Lungenfibroblasten zu verfolgen, um Phosphorylierungsstellen aufzudecken, die während der Zelladhäsion und durch die Substratsteifigkeit reguliert werden. Bis heute ist nur wenig über den Beitrag des Phosphoproteoms im Zusammenhang mit der zellulären Mechanosensorik bekannt. In dieser Arbeit wurde ein Zeitverlauf während der Zelladhesion (10, 20, 30, 60, 90, 120 min) sowie ein mechanosensorisches Experiment durchgeführt, bei dem Fibroblasten für 2 h auf eine Fibronektin-beschichtete Oberfläche mit unterschiedlichen Steifigkeiten (0.5, 2, 8, 16 und 32 kPa) gesät wurden. Der EasyPhos-Workflow für die Phosphopeptid-Anreicherung in Kombination mit einem modernen Orbitrap MS-Gerät ermöglichte es mir, das Phosphoproteom in einer Tiefe von 10.000 bis 12.000 einzigartigen phosphorylierten Peptiden zu untersuchen. Die Analyse ergab die Identifizierung von über 1000 signifikant regulierten Phosphorylierungen. Unter diesen wurden differentiell phosphorylierte RNA-bindende Proteine, spliceosomale Komponenten, Transkriptionsregulatoren, Chromatinmodulatoren und Zytoskelettproteine nachgewiesen. Durch die kombinierte Analyse der beiden

phosphoproteomischen Datensätze konnte abgeleitet werden, welche steifigkeitssensitiven Phosphorylierungsstellen direkt von den Substratsteifigkeiten beeinflusst werden und welche Phosphorylierungen die Anpassung der Zelle an die spezifische Kontraktilität und Form erfordern oder vielmehr direkt von der Substratsteifigkeit beeinflusst werden. Darüber hinaus ermöglichte mir der Vergleich mit primären menschlichen Lungenfibroblasten die Identifizierung robuster mechanosensitiver Signale, die in unabhängigen Experimenten reproduzierbar waren. Die Daten decken mechanosensitive Proteinphosphorylierungsstellen auf, die durch meine Analyse in den Kontext der etablierten Signalwege gestellt wurden. Insgesamt bietet diese Studie ein tieferes Verständnis der Signalereignisse in weichen bis steifen Mikroumgebungen und während der Zelladhäsion, was Auswirkungen auf die Zustände von Fibroblasten bei fibrotischen Erkrankungen haben kann.

Table of contents

Introduction

Mechanobiology

Already the physical biologist D'Arcy Wenthworth Thompson was interested in the variety of shapes in the biological domain [1] - "Cell and tissue, shell and bone, leaf and flower, are so many portions of matter, and it is in obedience to the laws of physics that their particles have been moved, moulded and conformed. They are no exceptions to the rule that God always geometrizes. Their problems of form are in the first instance mathematical problems, their problems of growth are essentially physical problems, and the morphologist is, ipso facto, a student of physical science." D'Arcy Wentworth Thompson, *On Growth and Form* (1917), 7-8

Until today it is still unclear how a whole organism consisting of millions and trillions of cells is shaped and assembled in the right way, so that every single cell finds her spatial position in the system [1]. Throughout development of the complex morphology of different organs and tissues, cellular monolayers bend and distort. Hereby neighboring cells and the extracellular matrix (ECM) are key signals to establish a cells geometry form and maintain it. Cells can actively sense and respond to a variety of mechanical inputs from their environment [1, 2]. Tension and forces applied to cells are converted into chemical signals that enable cells to adopt their phenotype according to their surroundings [2]. Therefore, cell shape is often linked to biological functions [1].

Over the last two decades the field of mechanobiology, the interface and boundary of physics, biology and bioengineering [2], rapidly evolved and a variety of data shows that forces applied to cells as well as physico-chemical properties of the cell microenvironment affect almost all aspects of multicellular life [3, 4]. Cellular responses to mechanical forces are substantial in embryonic development and adult physiology and are involved in many diseases, such as atherosclerosis, hypertension, osteoporosis, muscular dystrophy, myopathies, cancer, metastasis formation and fibrosis [5, 6]. Therefore, a better understanding of the mechanosensory machinery is required to develop new molecular tools to treat and prevent those diseases associated with altered mechanosignaling.

Cells and forces acting on them

Forces experienced by cells and subcellular structures are either coming from the outside of a cell or evolve inside the cell via the cytoskeleton. Applied and endogenous forces are both of dynamic nature and oblige cells to constantly probe their environment and status to adapt their inner and outer morphology, accordingly. Through mechanosensory elements and mechanotransduction forces itself, biochemical signals are communicated from the cell periphery throughout entire cell including the nucleus [7-10].

Applied forces. Tension, shear stress, compression, membrane curvature and swelling are forces which are affecting cells. The elastic and prestressed contractile machinery reacts immediately to micrometric and nanometric changes in the geometry, topography or spatial distribution of its environment. The strength of cell-cell or cell-matrix connections is modulated by forces applied at the macro level. The forces are focused by specific pathways on protein complexes which include functional modules [11, 12]. Through those mechanotransduction events, cells can differentiate the stiffness and chemical composition of their subjacent surface and the specific type of ECM molecules [13].

Endogenous forces. During the assembly of the cytoskeleton, the filament subunits meet intermolecular binding forces that attract (pull or stretch) the adjacent subunits. These forces are balanced by an intramolecular resistance to compression [14]. The actomyosin machinery constitutes the contractile resistance to deformation under the effect of force/tension in non-muscle cells. Actomyosin is able to create a tension inside the cell by remodeling and applying traction forces to cell-cell and cell-matrix adhesions and the underlying substrate. The contractile machinery is strengthened upon experiencing an external force and therefore creates an opposite force within the ECM, leading to ECM remodeling. Homeostasis is thereby restored and adhesions are reinforced to be able to resist higher stress loads. This creates a feedback-loop within the mechanosensory machinery [7]. Fluctuation in the stress vs. strain homeostasis can influence which of the different mechanosensors interact to organize a concerted response and determine how the signal is integrated [15].

The process of mechanosensing

Mechanosensing describes a cells capability to perceive and process the mechanical cues of its microenvironment [16] by using myosin II mediated contractile forces [17, 18]. This process is essential for cells to react and adjust to their changing mechanical surrounding. Activation, differentiation, apoptosis and proliferation are examples for cell reactions and adjustments to the mechanical properties of the ECM [1]. Two types of mechanosensing are known, passive and active mechanosensing. Passive mechanosensing means 'outside-in' signaling, so forces from outside the cell are sensed and transduced across the cell membrane inside the cell [19]. An example for this process is the recognition of fluid shear stress by endothelial cells via mechanosensory cell membrane protein complexes [20]. Whereas active mechanosensing is called 'inside-out' signaling where internal forces are created in order to detect changes in the cell environment [19]. Durotaxis is a typical example for active mechanosensing, as cells move from softer substrates to stiffer substrates using traction forces [21].

Mechanical stimuli are perceived through many different mechanosensitive molecules such as integrins, growth factor receptors, G protein coupled receptors and stretch-activated ion channels [22]. Cell surface receptors are located at the frontline of mechanosensing and can transduce signals across the cell membrane upon mechanical stimulation. The following shows the process of mechanosensing broken down to a four-step model (**Figure 1**) [16].

Mechanopresentation. In the first step of the process, cells are exposed to a mechanical force. Mechanopresentation needs a ligand that is anchored on a surface in order to sense the mechanical input. The so called mechanopresenter supports the force upon its exertion. Soluble ligands however, are not capable of promoting force and cannot present mechanical stimuli.

Mechanoreception. After mechanopresentation the ligand-receptor constructs conformation in the binding site is changed or the bond properties are altered due to force acting on the cell. The receptor is termed mechanoreceptor since it is the molecule the force is approaching.

Mechanotransmission. In this step, the mechanical signal propagates from the ligand binding site inside the cell, by the mechanotransmitter. The transmitted mechanical signal is not limited to force only, also force-induced conformational changes on molecular level are part of mechanotransmission, as for example integrin-mediated mechanosensing.

Mechanotransduction. During the last step the mechanical signal gets converted into a biochemical signal. Conformational changes in the receptor or its linked subunits propagate

the force in waveform. Thereby, a biochemical event in the cytoplasm is enabled. All parts of the transduction process, the molecules undergoing conformational changes and the molecules needed for the chemical event are called mechanotransducers. The difference between mechanotransmission and mechanotransduction is, that the last-named process is translating mechanical signals into chemical signals, mechanotransmission not however.
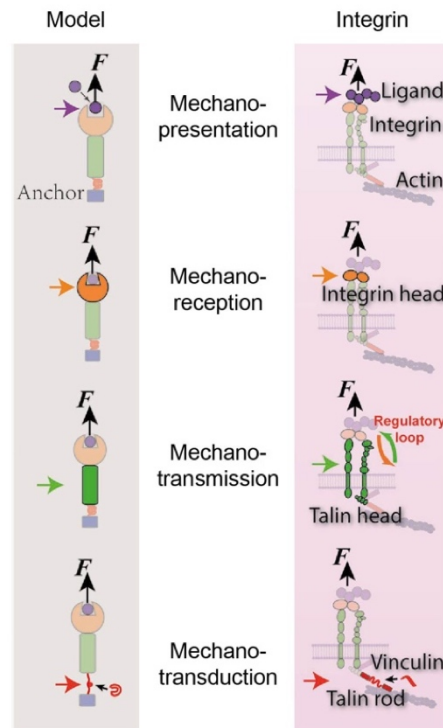
Figure 1 I Four step model of mechanosensing exemplarily represented by integrins. On the left the proposed model is shown in four steps: 1. Mechanopresentation, 2. Mechanorezeption, 3. Mechanotransmission and 4. Mechanotranduction. The colored arrows illustrate the where each is carried out by either a molecule or molecular assembly. The black arrows indicate external forces (F). In this figure only one possible mechanism of integrin mechanosensing is shown – the talin unfolding mechanism. Figure adapted form Chen et al., [16]

The main hub for cell-matrix interactions – focal adhesions

Almost 50 years ago adhesions sites between ECM and cultured cells were described for the first time by Abercrombie and Dunn using electron and interference reflection microscopy [23, 24]. They showed that those adhesions occurred along the cell membrane at various specialized small regions and are tightly connected with the underlying substrate. The observed sites are termed focal adhesions or contacts (FA) and play important roles in cell spreading, morphogenesis and migration through association and reorganization of actin filaments [25]. The most important adhesion complexes involved in mechanosensing are integrin-based, macromolecular, membrane-associated 3D FAs, consisting of various recruited proteins [26, 27]. Up to 180 proteins are known so far, to belong to the so called adhesome [28, 29]. The size and composition of the adhesome is influenced by mechanical cues and stimuli and is highly variable but the nanoscale architecture is conserved (**Figure 2**) [25, 26, 30]. The dynamic structures contain scaffolding proteins, kinases, phosphatases, adaptor proteins and cytoskeletal proteins. However, the major components of FAs are the 24 members of the integrin transmembrane receptor family [17, 31]. Integrins are heterodimers, consisting of an alpha and a beta subunit. Via the large extracellular domain they can bind to ECM proteins such as collagens, fibronectin and laminin. With the cytoplasmic tail of the ß subunit integrins are binding to proteins like talin and kindlin. Nevertheless, a direct binding of actin fibers and integrins is not possible but is indirectly mediated via adaptor proteins [26]. Integrins have, unlike growth factors, no intrinsic activity. Activation of integrins and as a consequence the starting of adhesion formation, is mediated either outside-in by binding of extracellular integrin domains to ECM molecules or inside-out by binding of proteins such as kindlin or talin at the intracellular part of the integrin molecules. This in turn recruits even more cytoplasmic proteins to the integrin tails to form the adhesion clutch [32]. A change of protein conformation and the opening of cryptic-binding sites in mechanosensitive adhesome proteins are enabled by force on cell-matrix adhesions (**Figure 2**). This leads to alterations in protein interactions and posttranslational modifications (PTMs), such as phosphorylation, affecting both the local adhesion site and signaling in the whole cell [33]. This means that the change of interaction between distinct proteins at the adhesion site can be transduced all the way to the nucleus. Furthermore, it leads to activation or inactivation of genes which in turn affects the fate of the entire cell.

A

B
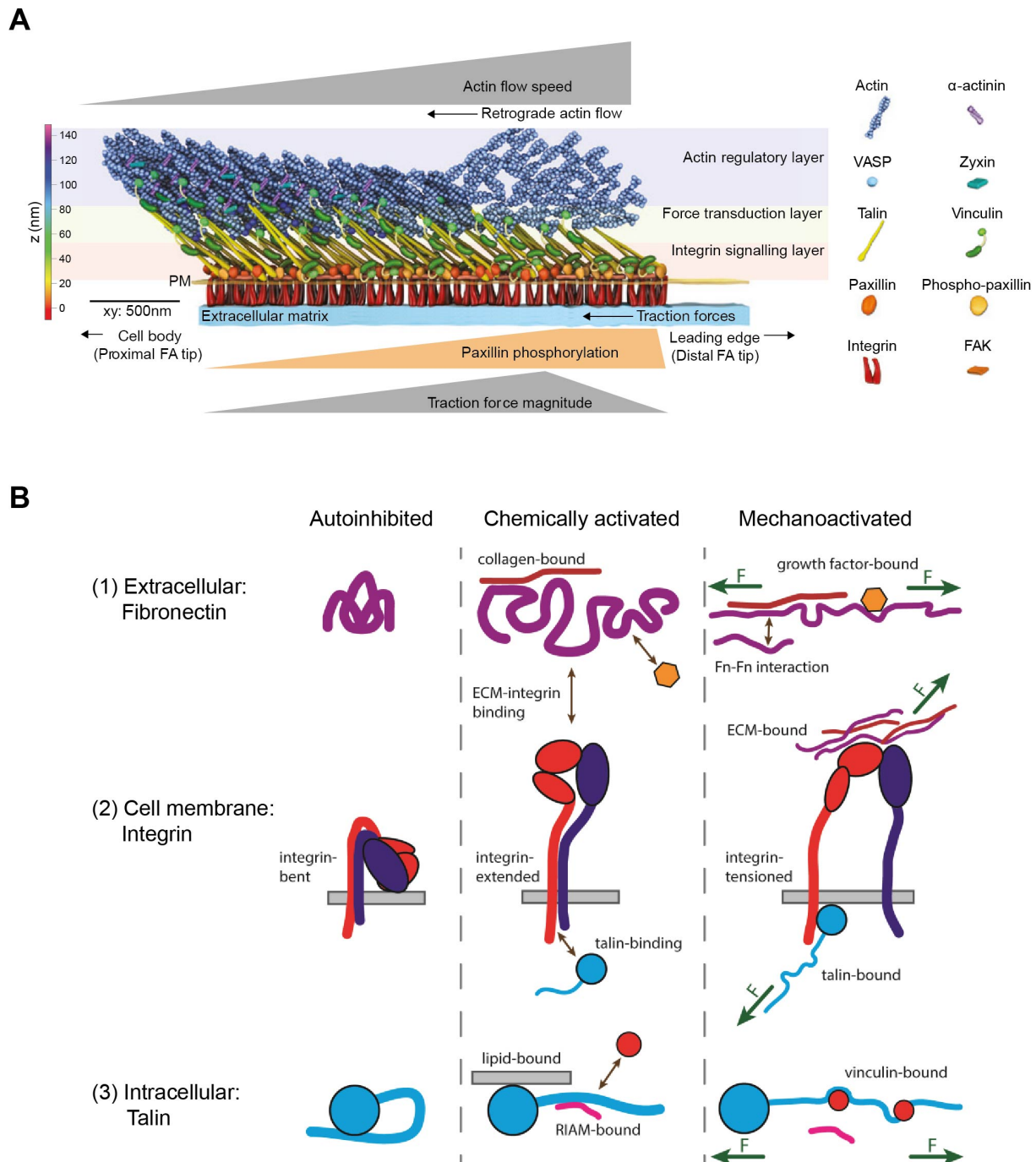
Figure 2 I A Focal adhesion architecture on nanoscale. Integrins connect the intracellular adhesome proteins to the ECM. FAs consist of different protein layers organized in 3D macrocomplexes. The integrin signaling layer is connected to the force transduction layer and these in turn to the actin regulatory layer. At the leading edge, the distal FA tip is interacting with lamellipodial dendritic actin and phosphorylated paxillin is enriched. Here high traction forces and a rapid retrograde flow are generated. At the proximal FA tip however, low traction forces and a slow retrograde flow are characteristically. At this location the FA interacts with actin stress fibers and a high number of actin binding proteins such as zyxin and VASP are accumulating. Adapted from Case and Waterman, 2015 [26] **B Regulation of the protein conformation and the cell-matrix contact by mechanical** tension (1) Fibronectin is present in an autoinhibited globular shape, if it is not bound to ECM proteins or integrins. Upon mechanical tension the fibronectin gets extended and polymerized into fibronectin fibers, which facilitates the binding of growth factors. (2) Before integrin is chemically activated through talin-binding or ECM-integrin binding, the protein is bent, inactive state. The high affinity conformation and strengthening of the connection to ECM proteins of integrin is induced via lateral force. (3) Only upon combination of two binding events e.g. lipid and RIAM binding, talin gets activated. This enables talin-integrin binding. Application of forces on talin opens binding sites for vinculin and weakens RIAM interaction. Adapted from Hytönen and Wehrle-Haller, 2016 [6].

Cell substrate stiffness matters

The spectrum of ECM stiffness in the body is immense and extends from soft and flexible brain tissue with a Young's modulus (specifies tensile elasticity of a material [34]) of 0.1 kilopascal (kPa) to hard and calcified bone with a modulus up to hundreds of megapascals (MPa), all other tissue types have rigidities in between those limits [35, 36]. Because there are many orders of magnitude between the softest and stiffest tissues in the body, these tissues contain cells that are adapted to the specific mechanical environments in which they are found [36]. This very specific physical microenvironment can be involved in the differentiation of stem cells. Engler et al. were the first to demonstrate the influence of substrate stiffness on stem cell fate *in vitro.* Human mesenchymal stem cells were seeded on polyacrylamide gels with varying rigidities according to the respective tissue stiffness of brain, muscle and osteoid but coated with equal amounts of collagen to ensure the interaction with the same ECM molecules. Over several days the transcriptomic and proteomic profile was tracked and the cells developed more towards neural, muscle and bone cells cultured on tissue-matched substrates [13]. Spreading and stiffness-dependent adhesion are processes with short time scales of one to two hours [37]. However, long-term cell fate decisions, associated with persistent changes in phenotype (lineage specification of stem cells), are based on activation or deactivation of distinct transcriptional programs. Mechanosensitive signaling pathways are needed to promote ECM rigidity signals to the nucleus. Those signaling pathways can regulate transcription factors that translocate into the cell nucleus adapting to microenvironmental cues [35].

The most famous stiffness dependent transcriptional cofactors YAP and TAZ were first described by Dupont et al., as mechanosensors in epithelial and mesenchymal stromal cells [38]. The activity of those proteins is dependent on F-actin and therefore enables the regulation and response to mechanical cues. The transcriptional cofactors are active and localized in the nucleus when cells are spreading on a stiff substrate. If the ECM or the underlying substrate is soft and cells are more rounded, YAP and TAZ are inactivated in the cytoplasm (**Figure 3**). This process is probably controlled by phosphorylation of YAP/TAZ [27].

Gupta et al. show that increasing substrate stiffness can cause the dynamic-mechanical properties of the actin cytoskeleton to switch from liquid-like to solid-like. With increasing substrate rigidity, the large-scale order of the actin filament arrangement also grows (**Figure 3**). Furthermore, the radial flow of actin and low-level friction promote round cell morphologies and less migratory behavior. On the other hand, the strongly ordered actin filaments on stiff substrates lead to alterations in cell shape and favour cell polarization. This could be one

explanation for a process termed durotaxis, where cells migrate along stiffness gradients to a more rigid environment [39].
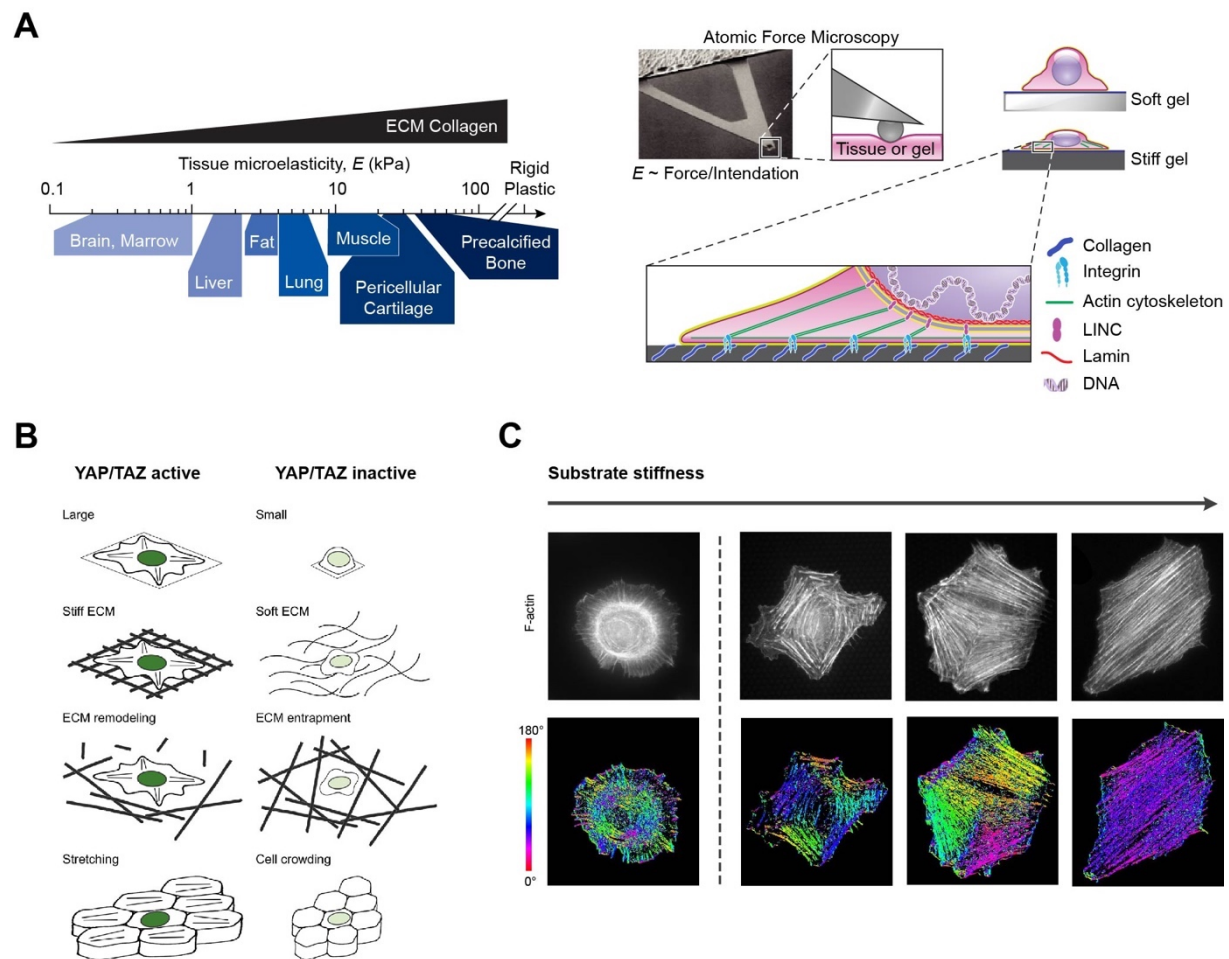
Figure 3 I A Scale of micro-stiffness of tissue/gel. Typically used plastic in cell culture is much more rigid than the whole tissue stiffness spectrum of the human body. Increase in tissue stiffness (measured in elasticity) is connected to the expression of collagen and is very variable from soft brain tissue to rigid bone. Using atomic force microscopy the stiffness of cells/gels can be measured. The most cell types seeded on stiff underlying substrate with appropriate coating of ECM molecules spread out and develop a strong cytoskeleton, with many stress fibres anchored by focal adhesions. On soft substrates however, cells are in a more circular shape. Adapted from Smith et al.[35]. B Experimental manipulation of ECM rigidity and cell shape modulate the nuclear activity of YAP/TAZ. The transcriptional cofactors are active if the underlying substrate is stiff, the cells are widely spread, ECM remodelling takes place and if the cells are stretched. In contrast, small cell shape, a soft ECM, confluent cells and an entrapment in ECM causes inactivation of YAP/TAZ. Adapted from Dupont et al., 2016 [27]. C Actin cytoskeleton depends on substrate stiffness. Rat embryogenic fibroblasts (REF-52) stained for F-actin on soft to stiff micropillar substrates. The different colours indicate different orientations of the actin fibres (see given colourmap). Uniformly coloured areas show microdomains of F-actin. Adapted from Gupta et al., 2015 [39].

ECM rigidity and mechanosensitive signaling pathways are also important in the pathophysiology of fibrotic diseases, where the composition of the ECM and its mechanical properties are altered with disease progression [40]. A physiological stiffness range (0.2 – 2 kPa) keeps human lung fibroblasts (CCL151) in a quiescent state, while substrates with higher stiffness (2-35 kPa), as observed in fibrotic lungs, induce a profibrogenic phenotype with high proliferation and matrix synthesis rates [41]. The activity and survival of activated fibroblasts

in fibrotic diseases may be largely controlled by mechanical signals. The precise molecular nature of many elements in these feedback connections is currently still unknown.

Cell spreading

It is well-known that matrix rigidity affects cell size and morphology [42-44]. But also cell spreading is influenced by the stiffness of the substrate. Cell spreading describes the transition from rounded cells in suspension to polarized cells on appropriate substrates [45]. Especially the spreading area has long been considered a key structural property in determining the internal structure and fate of cells [44]. The adhesion of cells is one of the first interactions occurring between ECM and cell surface. Receptor-ligand complexes are formed to anchor the cell to the underlying ECM. The complexes comprise interactions between adhesion receptors of the cell for example integrins and ligands such as fibronectin [46].
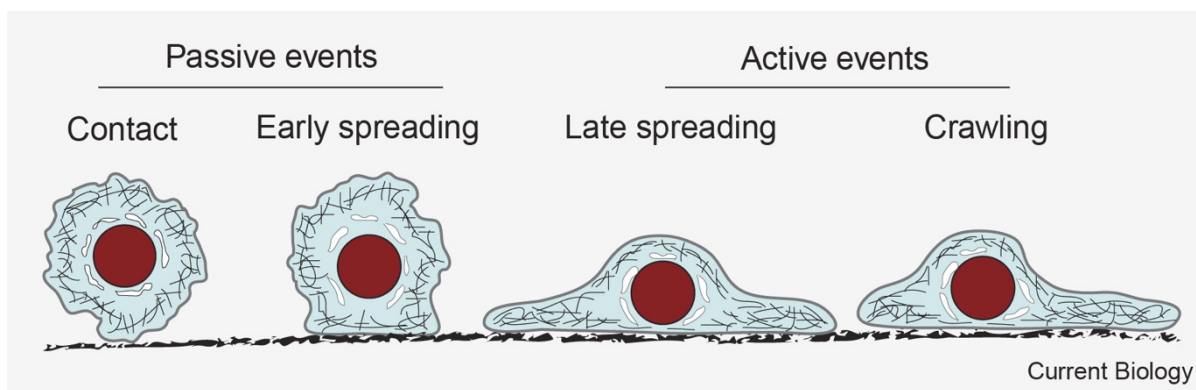
Figure 4 I Attachment and cell spreading. In the process of early cell spreading does not involve metabolic energy expenditure. In late spreading events however, myosin contraction and the actively actin polymerization are engaged. Those processes are essential for polarized cells to crawl. Figure adapted form [47].

The spreading process of eukaryotic cells can be classified in distinct stages, whereas the first contact is defined by passive adhesion and cell deformation [47]. This first contact can be described similarly to the way a liquid initially adheres to a surface, which is a passive event [48]. The active events, namely late cell spreading and cell crawling require metabolic energy to rearrange the cytoskeleton and contract myosin. Cell substrate adhesions are formed and the plasma membrane gets deformed [48] (**Figure 4**). Cuvelier et al. proposed a model which captures the underlying physics by a universal mechanism for the passive events of early cell spreading [49]. The model compensates the energy gained by cell adhesion to a surface with the energy released by deformations in the actin cortex of the cell. Hence, despite the obvious molecular differences in these experiments such as different cell lines and different ligands, the results point to a common physics. Although, certain experimental details, for instance the specific amounts of ligand and receptor on the substrate and the cell itself influence the strength of the adhesion and the time to full propagation, they do not alter the physical

processes at work [47]. The capacity of adherent cells to spread has significant implications. Very early studies of cell culture showed, that the substrate contact area can dictate whether or not cells die [50], become quiescent [51] or proliferate [52]. Whilst it is most likely that active mechanisms provide the feedback that drives these spreading responses, the results of Cuvelier et al. are crucial in explaining how a cell gets "foot" on a surface in any case [47, 49].

Mechanosensing and Fibrosis

Normal tissue architecture and function are maintained by mechanical homeostasis, which gets disrupted upon tissue injuries caused by varying origins such as chemical, microbiological or mechanical threads [53, 54]. Failure to repair the injury and restore homeostasis leads to progressive fibrosis (**Figure 5**) [53]. Fibrosis is defined by the overgrowth, rigidification and/or scarring of tissue accompanied by persistent changes in the mechanical surrounding as a result of pathological deposition of ECM components including collagen [53, 55]. The microenvironment of fibrotic scar tissue continues to progress steadily towards a mechanically altered state that is marked by increasing tissue stiffness [56]. Compared to normal lung tissue, fibrotic lungs are significantly more rigid [57]. The stiff matrix promotes fibroblast activation, thereby creating feedback loops which in turn promote fibrotic remodeling and ECM deposition [41].
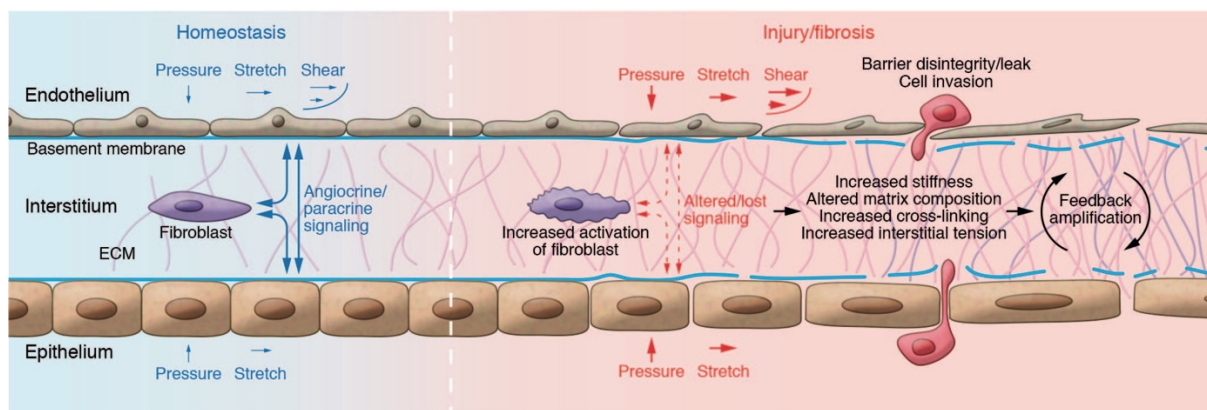
Figure 5 I Comparison of homeostasis/tissue integrity to injury/fibrosis states. Schematic depiction of the ECM containing interstitium framed by endothelial and epithelial barriers. During Homeostasis, tissue integrity and function is maintained. Upon injury the mechanical homeostasis is impaired through cell-generated forces, endothelial and epithelial disintegration, increased strain, pressure and shear forces, ECM deposition and cell invasion. While temporary disturbances of mechanical homeostasis promote fibroblast functions essential for normal wound healing, malfunctioned healing or failed injury repair can lead to persistent changes in the mechanical environment. Increased matrix stiffening causes a feedback amplification and promotes even more matrix deposition and stiffening. Figure taken from Tschumperlin et al., 2018 [53]

It is remarkable that by culturing cells on decellularized matrices of fibrotic lung tissue the fibrotic phenotypes are restored. Vice versa culturing of activated fibroblasts from patients with lung fibrosis on physiologically compatible matrices enables the deactivation of fibrotic reprogramming [58]. This suggests, that the biochemical and physical tissue environment are tremendously important in defining the behavior of adherent growing cells [59, 60]. Thus, ongoing cell activation through changed mechanical environment drives disease progression [61]. That the mechanical environment plays a major role in fibrosis is commonly accepted but questions about the evolution of distinct matrix properties, especially during the shift from regular injury repair to a fibrotic state, and reversibility of those changes in the mechanical

milieu of the matrix remain [62]. Also epithelial and endothelial cells are capable of sensing forces such as pressure, stretch and shear and can amplify the mechanoresponses by transmitting the signal to the nearby cells or the surrounding microenvironment [53]. For example, epithelial cells communicate mechanical stimuli to the adjacent mesenchyme by paracrine signaling [63]. In the liver, those kind of signals keep nearby hepatic stellate cells quiescent and suppress the transdifferentiation to activated myofibroblasts [64]. A similar homeostasis signaling to prevent activation of fibroblasts to myofibroblasts is observed in the lung [53]. Tschumperlin et al. hypothesizes that fibrosis constitutes an ultimate failure in restoring mechanical homeostasis. Tissue destruction and ECM deposition are caused by activation of cell-matrix–mediated transcriptional changes and epigenetic remodeling induced by aberrant mechanosensitive signaling. The advances in research on fibrosis, tissue regeneration and mechanoregulation mechanisms shed light on the formation of mechanical environments and the mechanical homeostasis in healthy and in fibrotic states. Gaining new insights may enable the development of novel approaches to treat fibrotic remodeling [53].

Idiopathic pulmonary fibrosis

The interstitium of the lung is a lacy network of tissue that extends across the entire lung and supports the pulmonary alveoli. Gas exchange between air and blood is enabled through fine blood vessels. Idiopathic pulmonary fibrosis (IPF) belongs to the interstitial lung diseases (ILD). ILDs can be acute or chronic, progressive and irreversible. In all cases the interstitium of the lung is affected in many ways such as edema, elevated inflammation and/or fibrosis. This causes a thickening of the interstitium and impaired gas exchange, leading to exertional breathlessness and/or cough. Furthermore, IPF is characterized by progressive lung scarring and the diagnosis of usual interstitial pneumonia (UIP) by radiography and/or histopathology and the exclusion of other ILDs for this pattern. UIP is defined by 'honey-combing' meaning enlarged cystic airspaces with fibrotic walls and bronchodilatation. The disease originates from the periphery of the lungs and spreads steadily throughout the whole organ [65]. IPF is the most studied and most widespread ILD and is generally associated with the elderly, with most patients being between 50 and 70 years of age at the time of diagnosis and often affecting more men than women. The majority of patients have a history of smoking, which is discussed as one of the risk factors for IPF. [66, 67]. IPF is self-sustaining and causes a progressive deterioration of lung function, respiratory symptoms and thus quality of life, so that it is currently an incurable disease whose molecular pathophysiology is understood only to a limited extent and for which lung transplantation is the only definitive therapy. Hence, IPF is associated with the poor prognosis of a median survival of 3 to 5 years after diagnosis [68]. At present, the only approved drugs to slow the progression of disease are *Nintedanib* and

Pirfenidone, both are antifibrotic therapies. With Pirfenidone treatment over one year the decline in FVC of IPF patients is slowing down. Furthermore, the disease progression, the death risk and hospitalization can be reduced [69-73]. Although *Pirfenidone* has been shown to have antifibrotic, anti-inflammatory, antioxidant effects, the exact molecular mechanism of action is not well known. The other available approved drug for IPF, *Nintedanib,* is a receptor tyrosine kinase inhibitor. The targeted receptors are the fibroblast growth factor (FGF), the platelet-derived growth factor (PDGF) and the vascular endothelial growth factor (VEGF). With this medication a significant slowdown on lung function decline and a prolongation of the time until the first exacerbation was observed [74, 75]. As the term "idiopathic" indicates, the etiology and pathogenesis of IPF is not yet fully understood. Further research and a better understanding is necessary to allow early diagnosis as well as the development of new therapeutics [76].

Pathobiology of idiopathic pulmonary fibrosis

The capacity of the lungs to recover and repair upon injury is noteworthy. Therefore, a cascade of subtle synchronized biological processes is needed. Nevertheless, repetitive injury of the alveolar epithelium over several weeks to years may result in profibrotic reprogramming, epithelial cell senescence, profuse production of pro-fibrotic factors and continuous activation of mesenchymal cells. All those processes result in failure to repair injury and restore homeostasis and could potentially lead to development of IPF and the destruction of original tissue architecture (**Figure 6**) [65].
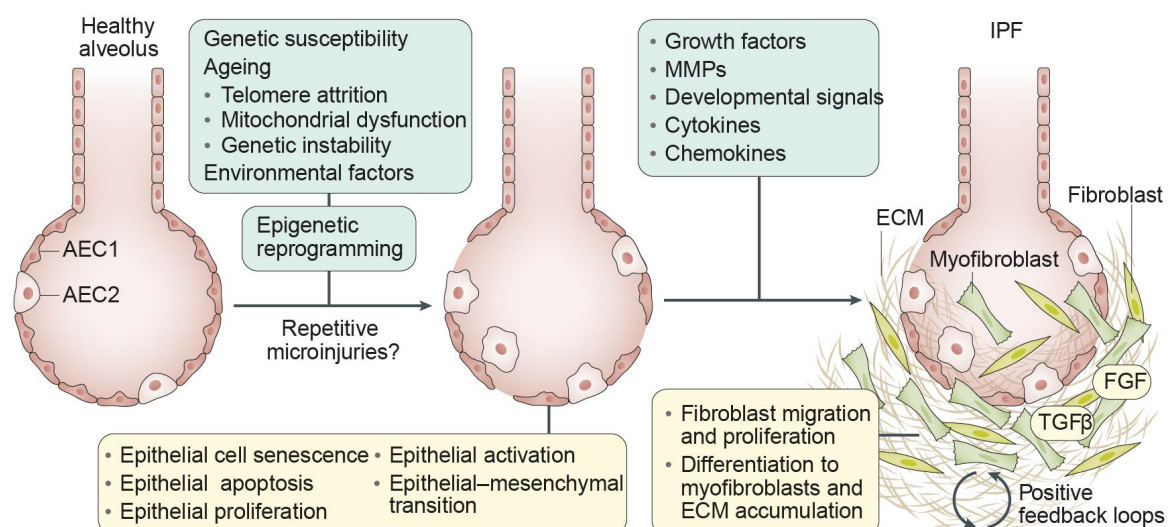
Figure 6 I Model of pathogenesis in Idiopathic pulmonary fibrosis. The interaction of the three factors, genetic susceptibility in particular health changes in epithelial cells, environmental factors such as smoking and age-related cell changes lead to epigenetic reprogramming, which promotes dysregulated epithelial activation and may ultimately lead to IPF. Repeated micro-injuries could induce or even accelerate this process. Disturbed wound healing then triggers fibrotic Tissue modelling of the lung. Figure taken from Martinez et al., 2017 [65]

The pathobiological paradigm of IPF being a disease related to age and the accompanying alveolar epithelial cell disfunction has arisen since the prevalence and incidence increases drastically with age [77]. Multiple risk factors are known to play a role in the pathogenesis of IPF, these include smoking and other environmental exposures, chronic viral infections and certain comorbidities (**Figure 6**). But genetic variants are thought to account for up to one third of the inherited individual risk of disease [65]. Sustained inflammation is usually involved in fibrotic diseases in several different organs [78, 79]. The role of inflammation in IPF is albeit arguable, since fibrotic remodeling occurs without substantial inflammatory response. This goes in line with observations of clinicians that anti-inflammatory therapies in IPF patients show only poor efficiency [78, 80]. Considering age as the strongest demographic risk factor for IPF, ageing of the lung might be the main driver for IPF development. It was observed that alveolar epithelial type 2 cells display a lot of hallmarks of cell ageing in IPF lungs. This includes genomic instability, altered intercellular communication and cellular senescence [81, 82]. IPF is still a complex disease resulting from the interaction of several of risk factors and where the relative contribution of each factor depends on the individual patient [82].The complexity of IPF is also influenced by countless multidirectional interactions between mesenchymal cells, epithelial cells and the ECM. But the precise mechanisms by which these factors interact to cause IPF remain elusive [65].

Role of fibroblasts in lung fibrosis

Fibroblasts are considered as main workhorses of connective tissue, which is so important in holding the human body together. All other tissues are interconnected and supported by connective tissue. In the interstitium of organs fibroblasts are widely distributed in an extensive ECM of fibrous proteins and gelatinous basic substances. Fibroblast identity can show considerable plasticity, therefore fibroblasts can be activated by various chemical signals to promote migration and proliferation as well as differentiation to myofibroblasts [83]. One hallmark of fibrosis is the massive expansion of the fibroblast population and its activation to myofibroblasts [65]. Fibroblasts are spindle-shaped, mesenchymal cells derived from the embryonic mesoderm. In the lung, they are located in highly complex, multicellular environments that are normally adjacent to the epithelium or endothelium. They are the primary producers of extracellular matrix proteins, adhesive proteins as well as glycosaminoglycans and proteoglycans, the ground substance of the ECM [83, 84]. In lung fibrosis these activated fibroblasts or myofibroblasts migrate to the site of injury and expand in

numbers. This results in accumulation of fibrogenic patches where massive amounts of ECM proteins, such as fibronectin, elastin and collagens, are secreted [78]. Myofibroblasts share high contractile features with smooth muscle cells and can be identified by large stress fibers in fibrotic foci [85, 86]. Controlled and temporarily myofibroblast expansion plays an important role for restoration of integrity upon injury by forming a collagenous scar [86]. Scar formation is a protection mechanism in organs to prevent further disruption upon mechanical challenge [87]. Nevertheless, myofibroblast expansion can escalate if the cells resist programmed cell death or dedifferentiate to their initial ground state. This turns the beneficial process of wound healing into progressive scarring leading to fibrotic remodeling and ultimately to fibrosis [88]. Myofibroblasts are barely seen in healthy tissue but form *de novo* upon injury [87]. However, the exact origin and source for myofibroblasts remains elusive even though different hypotheses have been made. Hoyles et al. suggest that myofibroblasts arise from resident fibroblasts expressing high affinity type-2-TGF-ß receptor [89]. Another hypothesis proposes an origination from bone-marrow derived circulating fibrocytes which differentiate into myofibroblasts after migration to the injured tissue [90]. Others postulate that they might stem from pericytes in respect of comparable gene expression signatures between these cell types [91]. Also transitions from epithelial, mesothelial or endothelial to mesenchymal cells seem to be reasonable explanations [65]. Even though many different precursor cell types have been reported to be involved in myofibroblast generation, resident fibroblast stromal cells seem to be the major contributor to activation of fibroblasts to myofibroblasts and the progression of fibrotic diseases such as IPF. Fibroblasts and/or myofibroblasts are also believed to play a role in processes such as blood clotting and angiogenesis. Furthermore, reactive oxygen species, chemokines, and paracrine signals produced by fibroblasts further promote fibrotic remodeling. Fibroblasts are therefore a suitable therapeutic target. Given the many factors involved in fibrosis, it is likely that a combinatorial therapy targeting fibroblasts will be more effective in treating organ fibrosis than single-target approaches [83]. However, the exact mechanisms and pathways are still unknown and need further investigation.

Protein phosphorylation: The function of kinases and phosphatases

Phosphorylation is one of the five most common covalent additions to proteins [92] and an important posttranslational modification (PTM) for cellular signaling, involved in nearly all biological functions. Besides the biological relevance, the stability of phosphorylation, the availability of suitable enrichment strategies and the analytical detection methods are the major reasons that phosphorylation is one of the most widespread and extensively researched PTM in eukaryotes [93, 94]. As the name suggests, PTMs are modifications that arise after the DNA has been transcribed into RNA and translated into proteins [92]. The covalent addition of a γ-phosphate (PO_4) to amino acid residues of proteins from a donor adenosine 5'-triphosphate (ATP) is catalyzed by kinases. Whereas phosphatases catalyze the removal of phosphate from protein side chains [95]. Phosphorylation and dephosphorylation follows the "reader-writer-eraser" paradigm, whereas kinases are the "writers", phosphatases are the "erasers" and the phosphate moieties are recognized by reader modules to transmit effects downstream [96, 97]. (**Figure 7**).
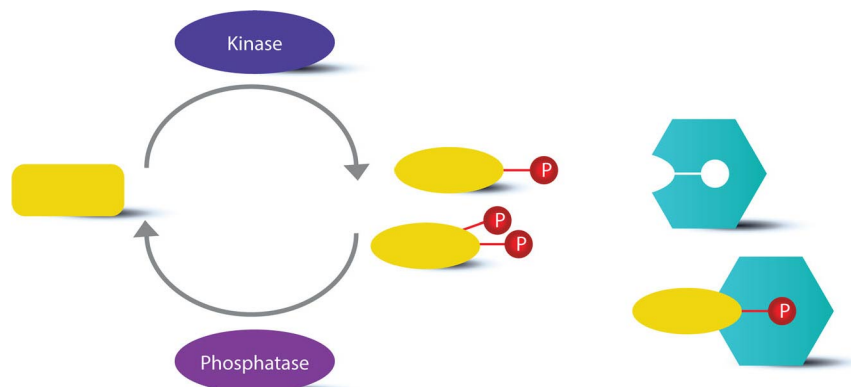
Figure 7 I Protein phosphorylation - covalent addition of a phosphate group to protein side chains. Phosphorylation of proteins is based on a simple and modular "reader-writer-eraser" system, which represents the compositional principle of higher order signal cascades. (Figure taken from Low et al. [98])

Consequently, phosphorylation causes changes in the chemical properties of a protein, shifting from hydrophobic apolar to hydrophobic polar, thereby enabling a protein conformation change to interact with other proteins or molecules [99]. The main element of a phosphate group is phosphorus which has five outer electrons and can therefore form up to five covalent bonds. This, the high water solubility and its ability to from mono, di, trialkyl or aryl esters and acid anhydrides with hydroxyl groups, explains its interactive capacity [100]. In mammalians the amino acid side chains of serine, threonine and tyrosine can get phosphorylated (*Figure 8*), whereas bacterial and fungal phosphoproteomes also have phosphorylated histidine and asparagine residues. However, there is increasing evidence that they might also be relevant

in eukaryotes [101] and additionally also phosphorylation of lysine, aspartate, gluatmate and cysteine has been reported [98, 102-104].
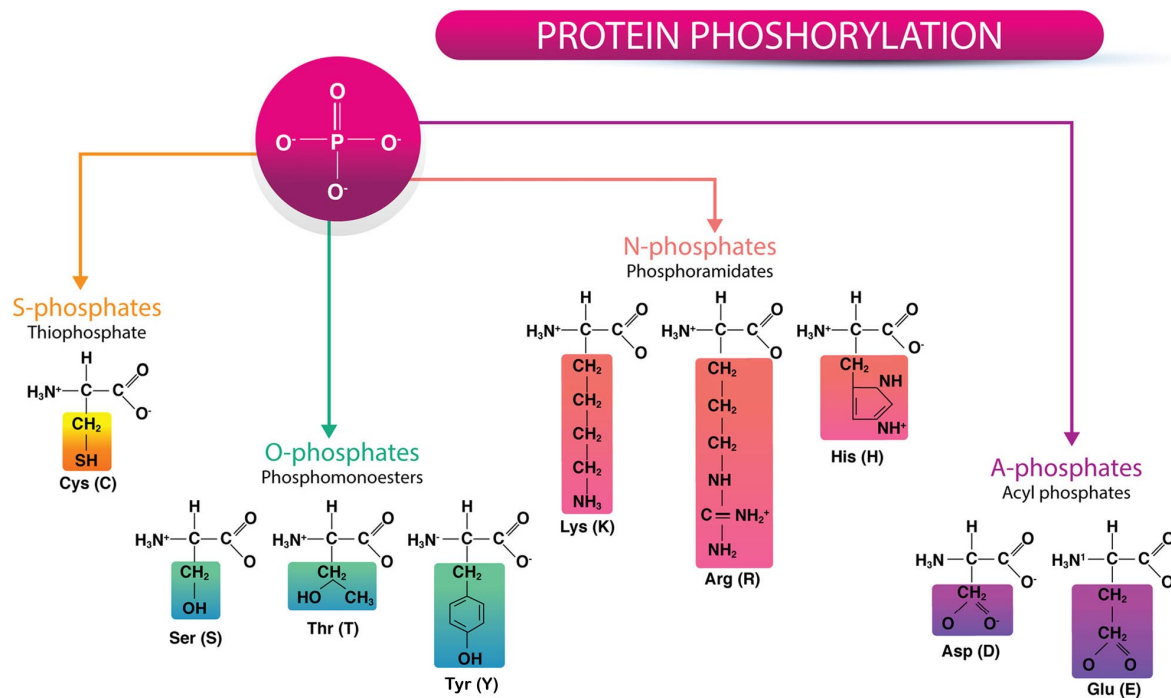
Figure 8 l Protein phosphorylation. There are nine different amino acids which can be phosphorylated on their side chains, with four different types of phosphate bonds. S-phosphates are formed by transfers of a phosphate to cysteine forming a thiophosphate. O-phosphates are formed by the most common phosphorylated amino acids serine, threonine and tyrosine. The transfer of phosphate on lysine, arginine and histidine side chains forms phosphoramidates and are called N-phosphates. Acyl phosphates constitute the last type of phosphates linkages with aspartate and glutamate. (Figure taken from Low et al. [98])

In contrast to serine, threonine and tyrosine phosphorylation, phosphorylation of those amino acid residues is rare and also acid- and thermolabile. This makes conventional enrichment methods impracticable, which is why this thesis will not go into this any further [98, 101]. Serine phosphorylation is the most common one and accounts for about 90 % of the phosphoproteome, the remaining 10 % are covered by threonine and tyrosine phosphorylation [92]. The PhosphoSitePlus data base ("http://www.phosphosite.org") lists 172,399 serine, 71,354 threonine and 44,556 tyrosines non-redundant phosphorylation sites. It has turned out that more than two-thirds of human proteins can be phosphorylated. However, it is more likely that this accounts for actually about 90 % of the proteome [105].

Protein kinases

In the later 1950s, Krebs and Fischer discovered the phosphorylation of proteins as a regulatory mechanism through their research on glycogen phosphorylase [106]. Protein kinases are in fact key regulators of cell function, representing one of the biggest and functionally broadest gene families. By the addition of phosphate groups to substrates, they control the activity, localization and overall function of many proteins and serve to regulate the activity of nearly all cellular processes such as growth, division, differentiation, motility, organelle trafficking, membrane transport, muscle con- traction, immunity, learning and memory [107, 108]. The gene family of protein kinases constitute ~ 2% of the human genome. Those gene
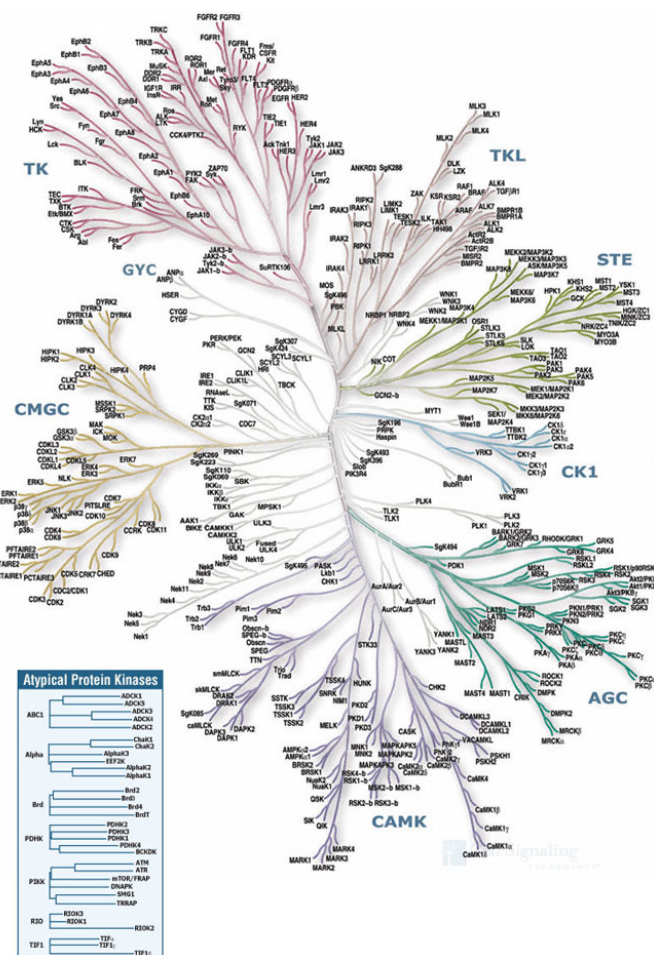
Figure 9 I Kinome tree. The genetic homology of the catalytic domain defines seven major protein kinase families arranged in a kinome tree. Illustration reproduced courtesy of Cell Signaling Technology, Inc. (www.cellsignal.com).

sequences are transcribed and translated to 518 kinases which can be divided into 478 typical and 40 atypical kinases [108]. The typical protein kinases belong to one super family with sequence similarities in the catalytic domain and can be clustered based on general sequence similarity, sequence comparisons of the catalytic domain and overlapping biological function into seven major families :AGC-, CAMK-, CK1- ,CMGC-, STE-, TK-, and TKL-kinases (**Figure 9**) [108].

Protein phosphatases

A single signaling event triggers a cascade of phosphorylations by kinases; but protein phosphatases play an equally important regulatory role in all signaling networks by reversing the effect of kinases via phosphate removal from proteins [109]. About 189 phosphatases are currently known. Reflecting the large proportion of phosphorylation of serine/threonine residues in human cells, protein-serine/threonine phosphatases (PSP) regulate a lot cellular processes, including transcription, metabolism, mitosis, protein synthesis and numerous other biochemical pathways. Obviously there is a huge demand for dephosphorylation in cellular signaling networks. Nevertheless, only 43 serine/threonine phosphatases are encoded by the human genome which represents only 10 % of the number of serine/threonine kinases. The enormous progress made in the development of kinase inhibitors for clinical application has stimulated discussions about the possibility of protein phosphatases as drug targets [110]. Although protein phosphatases seem to be promising drug targets since they regulate so many important cellular processes, the design for inhibitors is challenging. Unlike kinases phosphatases are more diverse in catalytic mechanisms and structure and are often found in with non-catalytic subunits [111]. Instead of simply matching each serine/threonine kinase with a phosphatase to reverse the modification, phosphatases have developed diversified strategies to coordinate their function with that of the kinases and act on a greater variety of substrates. The substrate specificity of phosphatases is generated by a combinatorically strategy, where a distinct number of catalytic subunits is combined with a huge number of regulatory subunits to obtain the required high selectivity for precise signaling [110].

Phosphorylation in cell signaling

Over the last 100 years, cell signaling has become a common mechanism for most physiological processes. The exponential growth of the field was provoked by the interdisciplinary support from chemistry, physics, mathematics and bioinformatics, even though most of the principles originally resulted from hormone studies [112]. A signal is defined as perturbation of the cellular homeostasis and can be of chemical, electrical or mechanical nature. Signaling activities can be divided in endocrine, paracrine, juxtracrine as well as neuronal-neurotransmitter mediated [112]. Ligand binding to the extracellular domain of a receptor entails many intracellular, biochemical reactions which have great impact on a cells phenotype by altering metabolism, the cytoskeleton and even gene expression. Mostly normal and essential processes are regulated, but incorrect signaling leads to various diseases [113]. Although, many biomolecules, such as lipids, second messengers, amino acids and hormones are involved in cell signaling, one of the most studied signaling regulation is protein phosphorylation. The reason for that is, that protein kinases are often mutated or overexpressed in disease context, most importantly in cancer [113]. Signaling can be regulated by phosphorylation in many ways (**Figure 10**). The phosphorylation of proteins can lead to their activation. One example is the phosphorylation of amino acid residues in kinase activation loops which accomplishes an active kinase conformation. But this also accounts for the reversed effect, the deactivation of proteins. The SH2 domain is a prominent example for the establishment of binding sites through phosphorylation. In this case distinct proteins can only bind another protein if it is phosphorylated, thereby regulating protein complex formation. Furthermore, this phosphorylation-dependent complex formation can also regulate the protein localization and protein trafficking [113].

Not only the regulatory role of phosphorylation is manifold, additionally a lot of different factors are affecting phosphorylation-dependent signaling. Cells are capable of integrating information from several signaling pathways in order to make decisions. The underlying principle is shown in **Figure 10 B**. Signal transduction in cell populations is often not universal but shows a biologically relevant cell-to-cell variability [113]. For example in tumor tissue, the temporal and spatial heterogeneity of signaling dependent on protein phosphorylation influences several phenotypes [114]. But also the microenvironment plays a pivotal role in cell signaling. Especially stiff extracellular matrices can promote aberrant signaling by upregulating of distinct transcription factors and signaling pathways. This is seen for instance, in ductal adenocarcinoma of the pancreas. SMAD4 mutant tumors use STAT3-dependent signals that are in part controlled by integrins, resulting in tumor stiffening and fibrosis and thereby enhancing tumor progression [115].
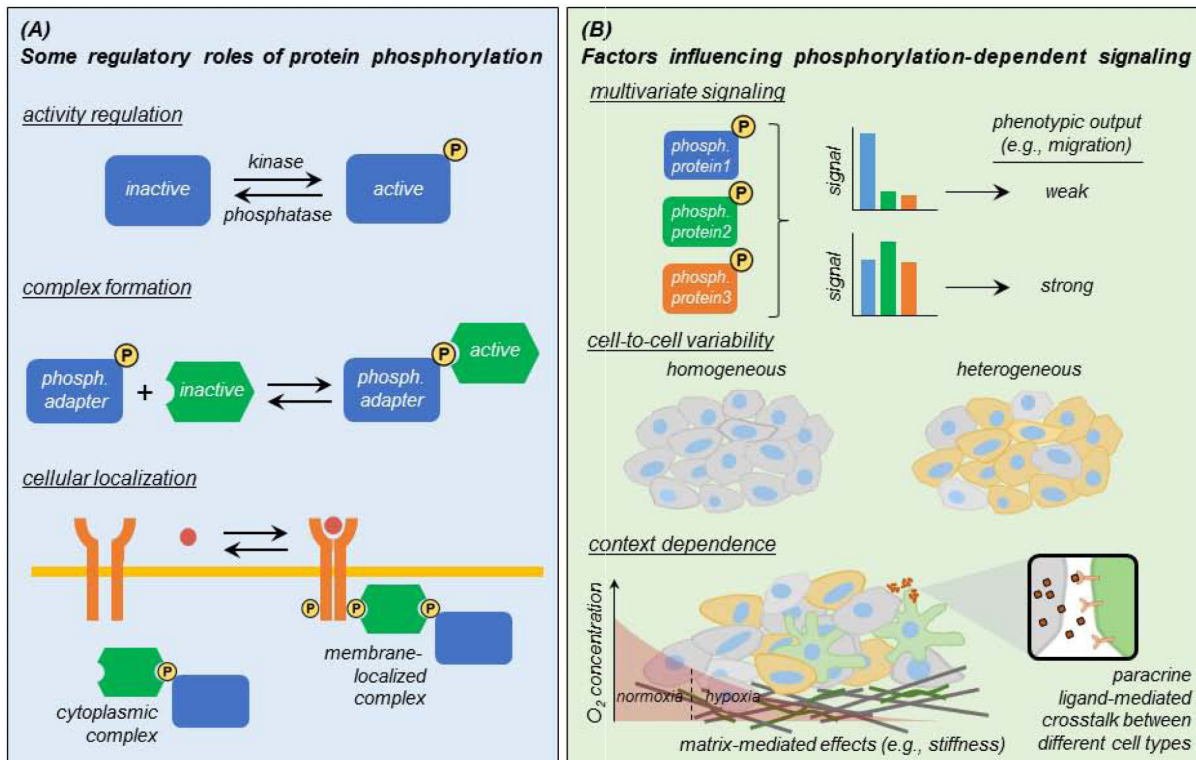
Figure 10 I A Some regulatory roles of protein phosphorylation. Through phosphorylation of proteins their activity, cellular localization and binding properties can be regulated. **B Factors influencing phosphorylation-dependent signaling.** For a complete understanding and analysis of phosphorylation-dependent signaling mechanisms also following factors have to be considered: the coordination between multiple signaling pathways to form complex phenotypes, heterogeneous cell signaling processes between cell populations and the microenvironment. Figure taken from Day et al., 2016 [113].

A variety of micro-environment systems have been developed to reveal the physical basis for such findings. Cells can be grown on two- or three-dimensional gels of varying stiffness. The stiffness of polyacrylamide gels can be adjusted and their surfaces can be coated with collagen or other ECM proteins, facilitating to reconstruct *in vivo* contexts [116]. But of course also other factors such as oxygen concentration or cross talk between different cell types can influence cell signaling [113].

Whilst kinase signal transduction has been studied with various experimental methods for over 100 years, the latest generation of mass spectrometry-based phosphoproteomic profiling enables the study of phosphorylation on global scale [117]. However, large-scale studies on phosphoproteomics are still a challenge and generally require substantial resources and time [118]. To achieve a system-level view of signaling, it is critical to be able to acquire high-dimensional measurements of the phosphoproteome [119].

Kinases and phosphatases, together with their respective substrates and proteins, form a complex, dynamic signaling network mediated by protein phosphorylation to transmit

information throughout the cell in response to cellular stimuli. Over the last decade, the emergence of new analytical methods at the systems biology level has begun to reveal the true complexity of these signaling networks [120]. It has often turned out that what was once considered a rectilinear signaling pathway has now turned out to be a dynamically regulated network with several layers of positive and negative feedback loops. New analytical methods make it possible to uncover new potential substrates in addition to the few already known substrates of distinct kinases. Thus, helping to better understand the distribution of signals across many network nodes, that probably regulate many different aspects of cell biology. The specific sites of phosphorylation within a given cellular signaling network must be mapped and their temporal response to several different levels of cellular stimulation must be accurately quantified, in order to shed light on the underlying signaling. But the large background of phosphorylation sites in a cell makes it difficult for researchers to identify and quantify the sites affected by a particular stimulus. There are numerous different analytical strategies for quantifying activated signaling networks. These strategies can be divided into different categories: global strategies, to quantify as many phosphosites as possible in order to detect enough sites to map the altered sites in the network; semi targeted approaches, with a focus of a subset of the phosphoproteome; and targeted concepts, using a previous knowledge of the signalling network to outline the analytical approach. Of course, each of these approaches has specific advantages, limitations and different requirements for instruments, expertise and samples.

Mass spectrometry based proteomics and phosphoproteomics

Proteomics is the large-scale study of all proteins, the so called proteome [121]. The focus lies on expression of proteins, their function, structure, possible modifications, interactions and the influence of the environment [122]. Marc Wilkins first introduced the term proteomics in 1995 and defined it as "the protein complement expressed by a genome" [123]. By the use of two-dimensional (2D) gel electrophoresis in 1970 first attempts were made to analyse proteins in its whole [124]. Anyhow, identifications from 2D-gels were often unsuccessful or required prior knowledge of the protein. A first step towards a connection of protein level and genome was made by Henzel et al. by searching molecular masses of peptide fragments in protein sequence databases [125]. Only the invention of new ionization methods and the development of computational analysis made it possible to use mass spectrometry for protein and peptide research. The ever better bioinformatic processing, the improvement in ionization methods and new mass analysers led to a drastic increase in a better understanding of the proteomic network [122]. Mass spectrometers reach accuracy and precision in the ppm-area. Nevertheless, not every single protein of a cell can be measured in one analysis, but it is nowadays possible to measure up to 10.000 proteins in one experiment [126] and answer numerous biological questions ranging from analyzing of signaling pathways, to protein expression profiling, or the detection of biomarkers [122]. Different aspects of the proteome can be investigated by selecting the right combination of sample preparation, MS instrumentation and data processing. The highly dynamic proteome of a cell is dependent on spatiotemporal conditions, such as subcellular location, environment and stage of development. It is assumed that humans have about 20.000 to 22.000 genes [127]. This relatively small number of genes raised questions, particularly in view of the fact that apparently less complex and less developed organisms have the same or even more coding genes. It was therefore concluded that the complexity of an organism cannot be explained by the number of coding genes. It is the number of proteins and protein isoforms expressed by a single gene, as well as the protein modifications, that define the complexity and developmental stage of an organism (**Figure 11**) [128, 129]. The genome of a cell is mostly stable with the exception of chromatin remodeling and epigenetic modifications. In contrast, the proteome is dynamically regulated and therefore better depicts cellular conditions, adapting to external and internal stimuli [130].
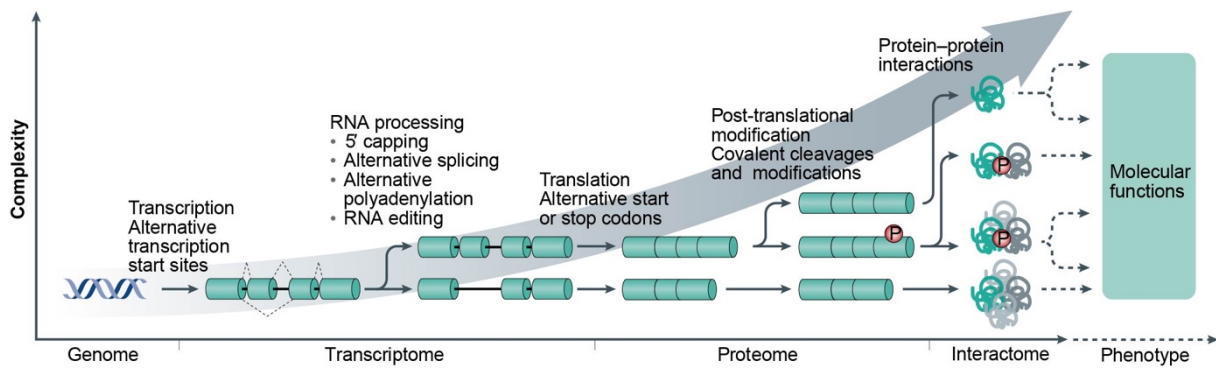
Figure 11 I The emergence of functional diversity at multiple molecular dimensions. Contrary to the paradigm "one gene, one protein, one function", cellular complexity emerges from many mechanisms that expand molecular diversity over and beyond the genome encoded by the protein. (Adapted from Bludau and Aebersold, 2020 [130]).

Splicing of mRNA and tissue-specific alternative splicing constitute one way to promote proteome expansion and complexity. The second mechanism to expand the coding capacity in eukaryotic genes are PTMs, this includes covalent modifications, such as phosphorylation of proteins, as well as covalent cleavages [130]. During those processes of diversification, the molecular complexity and the number of potential molecules derived from a protein-coding gene increases enormously (**Figure 11**).

Besides proteins, the overall extent of phosphorylation can also be determined by mass spectrometry [131], which enables large scale sensitive, site-specific and quantitative measurement of protein phosphorylation. Innovations in MS technology have created the field of phosphoproteomics – the identification and quantification of phosphorylated proteins at the exact amino acid residue where the protein contains the phosphate group [94]- which emerged from groundbreaking studies at the turn of the century. Large scale studies on phosphoproteomics conducted under different biological contexts have further deepened our understanding of the limits of the phosphoproteome and revealed exceptional magnitudes and complexity [94]. It appears that the phosphoproteome forms highly interconnected networks, far from view of simple linear pathways in a textbook context. Interferences of kinases and phosphatases therefore often affect large parts of the phosphoproteome and not only their direct substrates [132]. Phosphoproteomics is a powerful tool to screen these complex intertwined networks in order to find signaling nodes important in disease states.

Bottom up proteomics workflow

In recent years, several different bottom-up proteomics experimental protocols have been published for protein digestion, peptide separation, ionization, MS data acquisition and computer-aided data analysis. The most common protocol involves protein digestion by trypsin protease, followed by reversed phase high performance liquid chromatography (HPLC), electron spray ionization (ESI) and subsequent MS data acquisition and analysis [130]. Those steps are depicted in **Figure 12**. Bottom-up ("shotgun") proteomics is the most widely used approach to identify and quantify proteins obtained from complex biological samples. In contrast to top-down proteomics the bottom-up approach is based on the measurement of peptides instead of full-length proteins [133, 134]. The workflow starts with the extraction of proteins from their cellular context, either by denaturing or native lysis. Using a proteolytic enzyme which cleaves the peptide bond at distinct amino acid motifs the extracted proteins are digested to peptides [135-137]. Trypsin is most commonly used for proteolytic digestion, the enzyme cleaves C-terminal of lysines and arginines [133]. The tryptic peptides are separated before mass spectrometric measurement by an on-line liquid chromatography setup. Each peptide is retained to a different extent due to its size and hydrophobic properties and therefore elutes at a certain point of the LC gradient. Subsequent to elution, the peptides are ionized and then subjected to the mass spectrometer, which measures the mass-to-charge ratio and intensity of the peptides. [122, 138, 139].
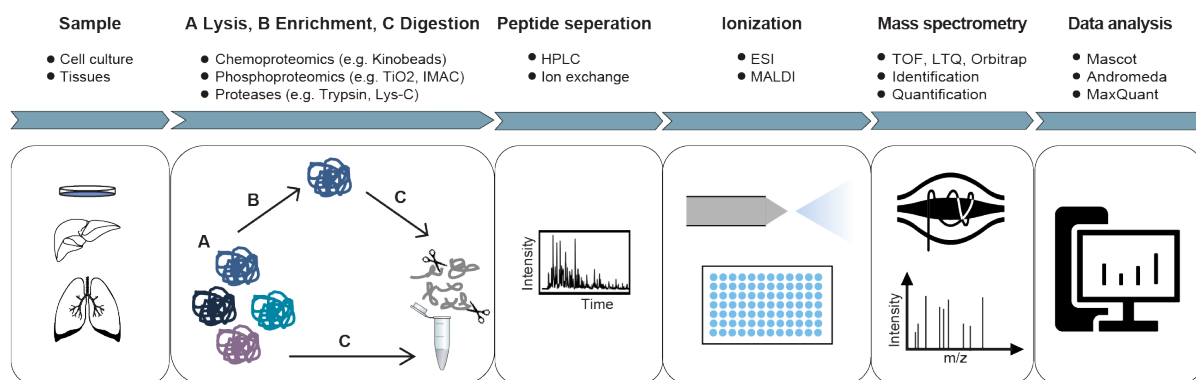
Figure 12 I Schematic overview of a typical bottom-up proteomics workflow. (Adapted from Steen et al. [133])

The standard proteomics workflow can be expanded by different enrichment or fractionation steps if need for the respective sample type and experimental setup. Enrichment strategies can be performed on protein level after protein extraction by antibodies, chemical probes or affinity matrices or on peptide level to enrich for post-translationally modified peptides such as phosphorylated peptides for example via immobilized metal affinity chromatography [140].

Mass spectrometry

Mass spectrometers function as a „scale" for individual molecules by converting them into ions and measuring their response to electric or magnetic fields. The main components of a mass spectrometer include: the ion source, the mass analyzer and the detector. A mass spectrometer measures not the actual mass of the molecule but the ratio of mass to charge ratio (*m/z*) of ions in the gas phase. Therefore, proteins and peptides must be ionized in the ion source before entering the mass analyzer, where the actual m/z ratio is determined. Finally, the ions reach a detector which creates the output spectra [121, 141]. In this study, a quadrupole Orbitrap mass spectrometer, in particular a Q Exactive HF [142] (**Figure 13**) was used and the subsequent section provides an overview of the underlying technology.
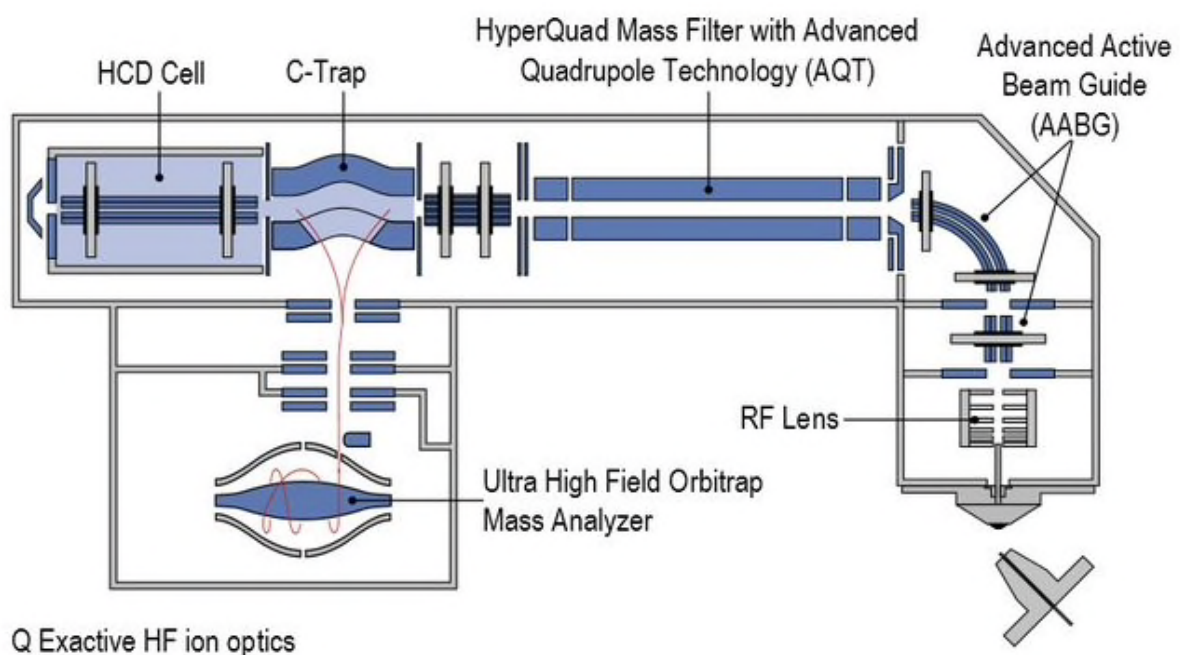
Figure 13 Schematic overview over the Q Exactive HF (Thermo Fisher Scientific).

Ionization. Several types of ionization methods are used in MS approaches. The classic methods include the Matrix-Assisted Laser Desorption/Ionization (MALDI) and the Electrospray Ionization (ESI). MALDI is a soft ionization technique that uses a laser energy absorbing matrix to create ions from the condense phase. In other words, proteins are embedded in matrices, such as α - cyano-4-hydroxycinnamic acid, that can absorb laser beams. The energy of the laser ionizes the matrix molecules and subsequently transfer their charge to the proteins. This causes the release of various ions by desorption from the condensed phase to the gas phase. MALDI primarily produces singly charged ions [121, 143].

In the Q Exactive HF peptide ionization is accomplished by ESI. The method uses electrical energy to facilitate the transfer of ions in solution into the gas phase via spraying. This process involves three steps: (1) dispersal of liquid in very small droplets in an electrostatic field, (2) solvent evaporation in the vacuum and (3) ion ejection from the highly charged droplets (**Figure 14**). Finally, the charge ends up on the now gas phased molecules, which then entry the first chamber of the mass analyzer. ESI ions are predominantly multiply charged. One advantage of ESI compared to MALDI, is the possibility of coupling it with prior liquid chromatography (LC). Two main hypotheses explain the mechanism of the charge transfer from the droplets to the molecules. The ion evaporation model (IEM) describes that the droplets get smaller by evaporation. When the field strength at their surface is large enough, the solvated ions can be expelled from the droplet. This model is only feasible for small ions. For large ions such as, proteins or peptides the charged residue model (CRM) is more plausible. For the CRM, in the end every small droplet contains a single analyte and evaporates to dryness. The charge finally gets transferred to the molecule when the last solvent shell disappears. This hypothesis also elucidates the feasibility of multiple charged ions [121, 141, 144].
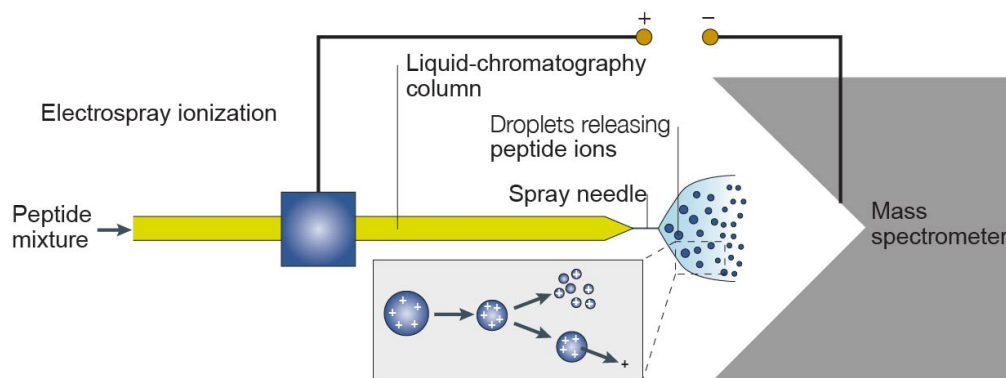
Figure 14 I Scheme of electrospray ionization. By applying a high electrical potential to a capillary, a Taylor cone at the end of the capillary is formed. The peptide mixture is eluting from the chromatography to multiple charged drops though solvent dispersion by coulomb repulsion. When reaching the vacuum of the mass spectrometer the drops get smaller and smaller and the charge gets transferred to the molecule. (Figure adapted from Steen and Mann [133])

Sample separation. Prior to MS analysis, the sample complexity has to be reduced by separation via ion-pair reversed-phase LC [121]. The technique allows the separation of neutral molecules in solution driven by hydrophobicity. The separation is based on the molecules partition coefficient between the hydrophobic stationary phase and the polar mobile phase [139]. Non-polar side chains bind to the hydrophobic surface and charged side chain residues interact with adsorbed amphiphiles of the mobile phase in an electrostatic manner. Elution is conducted by increasing the concentration of the organic solvent in the mobile

phase, therefore peptides are eluted with increasing unpolarity [145]. A powerful analytical tool is the combination of high-resolution MS and LC. Even tough reversed-phase LC is the most often used possible combination, also ultra-high pressure LC or multi-dimensional LC can be coupled on-line (direct) to the MS [146].

Mass analyzers. Ions are separated according to their *m/z* ratio. Many types of mass analyzers have been developed: time-of flight devices (TOF), quadrupoles, ion traps, Fourier Transform ion cyclotron resonance (FT-ICR) and orbitraps. They differ with their resolution, sensitivity and accuracy. The orbitrap is the most prominent technique for MS [147]. The advantages of the orbitrap are exceedingly high resolution, a low-ppm (parts per million) mass accuracy and the possibility for online coupling with an LC separation. Since its commercial introduction in 2005 it has become the instrument of choice for many proteomics approaches and shall be described in more detail [148]. The orbitrap is an ion trap, where ions are caught in an electrostatic field. After injection of the ions vertical to the z-axis, the electrostatic field forces them to cycle around the inner electrode on elliptical trajectories. Different *m/z* states have characteristic oscillations, whereas the axial component of these oscillations is independent of initial energy, angels and positions and can be detected as an image current on the two halves of an encapsulating electrode (**Figure 15 A**). After a Fourier Transformation the *m/z* of different ions in the orbitrap can be determined from respective frequencies of oscillation [147, 148]. A very high resolution is possible, since the resolution is dependent on the number of oscillations.

Tandem MS/MS. Molecular spectrometric analyzers are arranged one after the other to determine the peptide sequence. It is also called tandem MS because in the first lap the ion is generated (precursor ion), which further is fragmented via collision induced dissociation (CID), electron transfer dissociation (ETD) or high collusion induced dissociation (HCD). The fragments are separated as before according to their *m/z* ratio. Ideally, each peak will vary only by one amino acid. The difference in size between the peaks determines the amino acid sequence [121]. Thus, protein identification in complex mixtures is feasible. The peptide fragments containing an N-terminus are called a_n-, b_n-, c_n-ions and fragments containing an C-terminus are called x_n-, y_n- or z_n-ions (**Figure 15 B**). The most common used fragmentation methods are CID and HCD, where peptides collide multiple times with an inert gas, such as N_2, He or Ar. The breakage of of the peptide bond is induced through kinetic energy transfer [149]. CID and HCD differ in the energy which is applied to initiate the bond breakage. The lower energy CID is performed in ion traps and the breakage is a result of multiple collisions with gas molecules. On the other hand HCD fragmentation applies a beam type fragmentation

using high energy to the precursor ions, which leads to almost immediate bond breakage [150, 151].
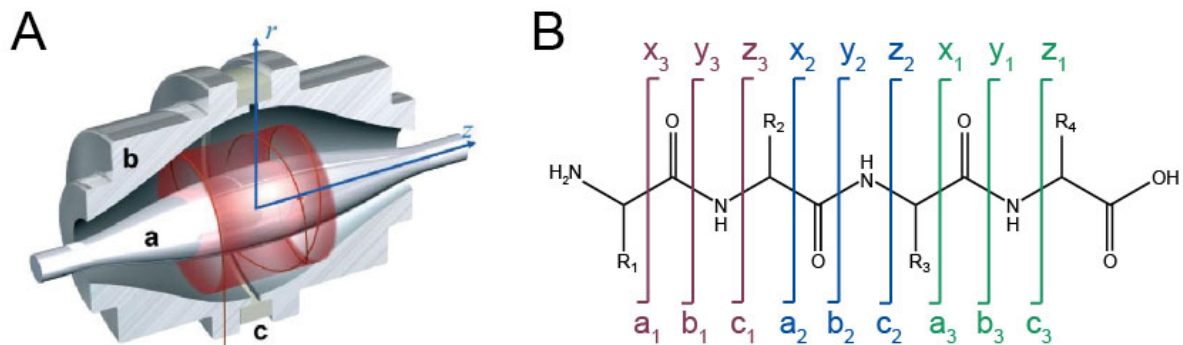
Figure 15 l A Model of the orbitrap mass analyzer. **A** Ions move spirally around a central electrode. An insulating ceramic ring splits the outer electrode **B** in half. After a FT the m/z of different ions in the orbitrap can be determined from respective frequencies of oscillation. (Adapted from Scigelova et al. [148]) B Peptide fragmentation in MS/MS according to Roepstorff and Fohlman (1984). Peptides produce a, b and c ions when the N-terminal residue is retained on the fragment, and x, y and z ions when the C-terminal residue is retained on the fragment. The mass-difference between two of the same ions equals the residual mass of the amino acid [152].

Protein/peptide identification and quantification. A first and central step in proteomics data processing is the correct allocation of the acquired spectra to peptide sequences [153]. The MS2 fragment spectra is used to derive the amino acid sequence of the peptides. Since the sequence is often not resolved completely, the approach of choice to identify peptides/proteins from tandem spectra is database searching. However, it has to be noted that only proteins whose sequence is listed in the database can be identified, a *de novo* identification is not possible [133, 153]. Theoretical spectra are generated by *in silico* tryptic digest of all proteins contained in the data base and are then correlated to the measured MS/MS spectra. A search algorithm can take into account protease specificity, missed cleavage sites, fixed or variable modifications of PTMs to match as many peaks as possible. Also other factors are considered such as the length of sequential ion series, the overlap of ion series, the number of matched precursor and peptide fragments and their mass deviations. To obtain high confidence identifications, a false discovery rate is determined (FDR) for filtering by searching the experimental spectra against a decoy database [153]. This database contains the reverse versions of the *in silico* generated tryptic peptides. A number of search engines, such as Mascot [154] or Andromeda (MaxQuant) [155], have been implemented to allow the identification of peptides and to subsequently match them with proteins. Often it is not possible to assign peptides to one particular protein, if the identified peptide is not unique but present in other related proteins or protein isoforms. This is the reason why proteomics experiments often report protein groups when no unique peptide was found to unmistakably assign the peptide to a distinct protein. Therefore, proteomic experiments using database searching can

mostly not accomplish to distinguish between protein isoforms from splicing events or post-translational protein processing.

Besides the identification of peptides and proteins also the abundance of them plays an important role in proteomics experiments [156, 157]. However, mass spectrometry is not quantitative in itself, due to different physiochemical properties of peptides such as charge, size and hydrophobicity which lead to huge changes in mass spectrometric response. To ensure an accurate quantification only the behavior of the same peptide can be compared between different MS runs which allows relative quantification of peptide abundance [156]. In this study the MS1-based label-free quantification was applied [158-160]. The label-free quantification MaxLFQ in MaxQuant utilizes the precursor intensities and elution times of MS1 spectra to derive an elution peak of each peptide precursor. The LFQ intensities result from the integration of the peak area in the MS1 space but the identification of the peptide species is still done from the MS2 spectra [155, 161, 162]. But data-dependent acquisition may result, in particular for low abundant peptides, in missing quantification and missing identification. Using the match-between-runs option in MaxQuant [163], this can be overcome to a certain extent by aligning the retention time of multiple runs, thereby enabling sequence information derived from one sample to be used for the same precursor mass found in another sample. This quantification strategy eases the relative quantification of the same protein across multiple samples but does not allow comparison of different proteins within the same sample.

MS based phosphoproteomics workflow

Typically a phosphoproteomics workflow starts with cell or tissue lysis to extract proteins and the elimination of impeding factors [98]. In most cases phosphatase and protease inhibitors are added to prevent dephosphorylation and protein degradation once the compartmentalization of enzymes is disrupted by cell lysis [164]. However, heat treatment directly after cells lysis is the preferable approach because chemical inhibitors could differentially inhibit the action of different enzymes and therefore affect certain phosphopeptide populations differentially [165]. The samples are digested to peptides mostly using trypsin as protease [98]. This step is followed by an enrichment step for phosphorylated peptides [166]. Enrichment is necessary because of the low frequency and sub-stoichiometric levels of most post-translational modification events. Many different enrichment methods for phosphopeptides have been developed but usually the chemical interaction of phosphoamino acids with distinct binding partners is the one being taken advantage of. The enriched phosphorylated peptides are subjected to LC-MS/MS and by matching the tandem spectra to protein databases the respective phosphorylation sites are determined [98].

In this work the so called EasyPhos method, where the phosphopeptide enrichment is based on TiO_2-beads, was used to generate phosphoproteomics MS data sets [118]. The hybrid Ti^{4+}-Immobilized metal ions chromatography (IMAC) technology exploits the interaction of positively charged metal ions with negatively charged phosphate groups via electronic attraction and metal chelation (**Figure 16**).
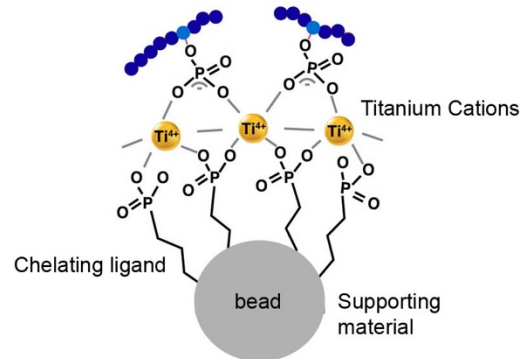
Figure 16 I Ti^{4+}IMAC material.
(Adopted from Low et al., [98])

Three components are needed to construct a IMAC column, support matrices, metal cations and chelating ligands [98]. For the EasyPhos workflow self-made IMAC columns are used. They are prepared out of pipette tips where a small portion of C8 material is put inside, the so called StageTips [167]. This single layer stops the TiO_2-beads thereby forming the IMAC column. Only phosphorylated peptides bind to the TiO_2-beads and all non-phosphorylated peptides are eliminated by washing steps before the phosphorylated peptides are eluted with low pH elution buffer.

Outline and Objectives

Mechanosensitive signaling pathways are highly relevant in the pathophysiology of fibrotic diseases, where the composition of the extracellular matrix and its mechanical properties are altered in disease progression [40]. A physiological stiffness range (0.2 – 2 kPa) keeps human lung fibroblasts (CCL151) in a quiescent state, while substrates with higher stiffness (2-35 kPa), as observed in fibrotic lungs, induce a profibrogenic phenotype with high proliferation and matrix synthesis rates [41]. The activity and survival of activated fibroblasts in fibrotic diseases may be largely controlled by mechanical signals. When cells encounter their extracellular substrate, they respond to the stiffness of this substrate. This mechano reciprocity is produced by a feedback connection between cell-matrix adhesions and the cytoskeleton, which adjusts the strength of the contractile forces to a balance of applied force and tensile strength of the ECM substrate [17]. The precise molecular nature of many elements in these feedback connections is currently unknown. In most cases, the conversion of extracellular and mechanical stimuli into intracellular cues is encoded by post-translational modifications (PTMs). One of the five most common PTMs is protein phosphorylation [92], which is a key modification for cellular signaling and is involved in nearly all biological functions [94]. Importantly, protein phosphorylation on serine, threonine and tyrosine residues (S,T,Y) was shown to regulate protein conformation, as well as protein interactions and subcellular localization [28]. It is reasonable to assume that the regulation of cellular mechanosensory properties is likely to occur in proteins with functions in cell-matrix adhesions and the cytoskeleton. Both integrin- and cadherin-mediated adhesions attach to the filamentous (F-) actin cytoskeleton using a diversity of adaptor and signaling proteins. These proteins join together to form a dense, highly dynamic network that is visible as a protein plaque on the plasma membrane, which we call an adhesome. Remarkably, the recruitment of multiple plaque proteins into the adhesome requires myosin II-mediated mechanical tension [18, 168]. As there are many thousands of phosphorylation sites that are regulated in an integrin and therefore, mechanosensing dependent manner it is obvious that the function of most of these molecular switches remained uncharacterized so far.

So it is currently unclear which phosphorylation sites are directly regulated by substrate rigidity. Also the spreading area of cells plays a major role in cell fate decision and tissue morphogenesis [44]. The acquisition of cytoskeleton structure and polarity is organized by elastic stresses which develop in the cell during spreading [169]. Migration and cell spreading are controlled both by biochemical activity within the cell and by the rigidity of the underlying substrate. Such activities are generally intensified on more rigid substrates [170]. Through an increase in tension in the cytoskeleton, adhesion receptors are activated and the nucleus gets deformed which triggers biochemical signals thereby mediating differentiation and growth

control [44]. A comprehensive map of signaling cascades that occur during cell spreading and while rigidity sensing is currently lacking. Recent developments in phosphoproteomic workflows substantially increased sensitivity of detection and sample throughput thereby promising to greatly improve our understanding of complex biological networks [134]. A better understanding of the mechanosensory machinery is required to develop new molecular tools to treat and prevent fibrotic diseases, especially lung fibrosis, associated with altered mechanosignaling.

Here the aim was, to explore molecular changes in protein phosphorylation during mechanosensing and cell spreading in human lung fibroblasts in a systemic and unbiased manner using mass spectrometry driven phosphoproteomics. I used a label-free approach, allowing me to include several time points, substrate rigidities and replicates in our experimental workflow. The EasyPhos workflow for phosphopeptide enrichment [118] in combination with a modern Orbitrap MS instrument enabled me to investigate the phosphoproteome at a depth of 10,000 to 12,000 unique phosphorylated peptides. The analysis of differential phosphorylation on varying substrates stiffnesses allowed me to identify rigidity- dependent regulated phosphosites. Furthermore, the analysis of a phosphorylation time course during cell spreading reveals different dynamic patterns of regulated phosphosites. The data illustrates the phosphorylation dynamics and status of well-known focal adhesion molecules, as well as that of novel mechanosensitive proteins. Overall, this study provides a deeper understanding of the signaling events on soft to stiff microenvironments and during cell spreading and may advance the enlightenment of mechanical cues and signaling.

Material and Methods

Material

Antibodies
Table 1 I Primary antibodies.

Antigen	Product number	Host	Type	Appli-cation	Dilution	Provider
Actin/αSMA	A5228	Mouse	Monoclonal	IF	1:750	Sigma Aldrich, St. Louis, USA
GAPDH (HRP-linked)	14C10	Rabbit	Monoclonal	WB	1:80,000	Cell Signaling, Danvers, USA
Phospho-CK2 Substrate Motif [(pS/pT)DXE]	8738	Rabbit	Monoclonal	WB	1:1000	Cell Signaling, Danvers, USA
Phospho-HP1γ/CBX3 (S93)	2600	Rabbit	Polyclonal	WB, IHC	1:1000, 1:200	Cell Signaling, Danvers, USA
Phospho-Myosin Light Chain 2 (T19/S20)	3674	Rabbit	Polyclonal	IF	1:200	Cell Signaling, Danvers, USA
Phospho-PXN (S126)	441022G	Rabbit	Polyclonal	WB, IHC	1:1000, 1:20	Life Technologies, Carlsbad, USA
YAP1	Ab205270	Rabbit	Monoclonal	IF	1:200	Abcam, Cambridge,USA

Table 2 I Secondary antibodies.

Antigen	Product number	Host	Application	Dilution	Provider
Anti-mouse 488	A21202	Donkey	IF	1:250	Thermo Fisher Scientific, Waltham, USA
Anti-mouse IgG HRP-linked	7076S	Horse	WB	1:20 000	Cell Signaling, Danvers, USA
Anti-mouse IgG HRP-linked	7074S	Goat	WB	1:20 000	Cell Signaling, Danvers, USA
Anti-rabbit 568	A10042	Donkey	IF	1:250	Thermo Fisher Scientific, Waltham, USA

Cell culture

Table 3 I Cell lines.

Cell line	Origin	Specification
CCL151	Human lung fibroblasts	ATCC-Nr. CCL-151
phLF	Primary human lung fibroblast	Donor lung

Table 4 I Cell culture media.

Cell type	Cell culture medium	Product number	Provider
CCL151	DMEM-F12 10 % FBS Superior 100 U/mL Penicillin/Streptomycin	31330 S 0615 15140-122	Thermo Fisher Scientific, Waltham, USA Biochrom, Berlin, Germany Thermo Fisher Scientific, Waltham, USA
phLF	DMEM-F12 20 % FBS Superior 100 U/mL Penicillin/Streptomycin	31330 S 0615 15140-122	Thermo Fisher Scientific, Waltham, USA Biochrom, Berlin, Germany Thermo Fisher Scientific, Waltham, USA

Consumables

Table 5 I Consumables.

Product	Provider
Cell culture dishes (6 cm, 10 cm 15 cm)	Nunc, Wiesbaden, Germany
Falcon tubes (15 mL, 50 mL)	BD Bioscience, Heidelberg, Germany
Glass pasteur pipettes	VWR International, Darmstadt, Germany
Microplate 96-well, PS, flat bottom (for BCA assay)	Greiner Bio-One, Frickenhausen, Germany
Pipet tips	Biozym Scientific, Hessisch Oldendorf, Germany
PVDF membrane	Bio-Rad, Hercules, USA
Sterican cannulas	BD Bioscience, Heidelberg, Germany
Syringes (10 mL)	Neolab, Heidelberg, Germany
Whatman blotting paper 3 mm	GE Healthcare, Freiburg, Germany
6/24/96 well plates	TPP, Trasadingen, Switzerland
Ibidi µ-Dish, 35 mm, high ESS uncoated (0.5 and 28 kPa)	Ibidi, Martinsried, Germany
Petrisoft, Easy Coat hydrogels 100 mm dish (0.5 and 25 kPa)	Matrigen, San Diego, USA
Petrisoft, Easy Coat hydrogels 35 mm dish (0.5 and 25 kPa)	Matrigen, San Diego, USA
Protein LoBind tube (1.5 mL and 0.5 mL)	Eppendorf, Hamburg, Germany
CytoSoft 6-well plate Elastic Modulus (0.5, 2, 8, 16 and 32 kPa)	Advanced BioMatrix, Carlsbad, USA
SafeSeal reaction tubes (0.5 mL, 1.5 mL, 2.0 mL)	Sarstedt, Nümbrecht, Germany
Cryovials 1.5 ml	Greiner Bio-One, Frickenhausen, Germany
Serological pipettes Cellstar 5, 10, and 25 mL	Greiner Bio-One, Frickenhausen, Germany

Buffer formulations

All buffers were prepared with Milli-Q® water.

Table 6 l Composition of buffers.

Buffer	Reagent	Concentration
10x WB transfer buffer	Tris	250 mM
	Glycine	1.92 M
1x WB transfer buffer	10x WB transfer buffer	1x
	Methanol	20 %
6 M GdmCl lysis buffer	GdmCl	6 M
	TCEP	10 mM
	CAA	40 mM
	Tris HCl pH 8.5	100 mM
6x Laemmli buffer	Tris	300 mM
	Glycerol	50 % (v/v)
	SDS	6% (w/v)
	Bromophenol blue	0.01 % (w/v)
	DTT	600 mM
	NaF	50 mM
	ß-glycerophosphate	100 mM
Citrate buffer pH 6.0	Citric acid monohydrate	1.8 mM
	Sodium citrate tribasic	8.2 mM
Digestion buffer	TFE	10 %
	Ammonium bicarbonate	100 mM
Elution buffer	ACN	40 %
	NH_4OH (25 % HPLC grade)	15 %
EP elution buffer	NH_4OH (25 % HPLC grade) to 800 µl 40 % ACN	
EP transfer buffer	TFA	0.1 %
	Isopropanol	60 %
EP wash buffer	TFA	5 %
	Isopropanol	60 %
Loading buffer/EP loading buffer	ACN	80 %
	TFA	6 %
MS loading buffer	ACN	2 %
	TFA	0.3 %
PBS pH 7.4	NaCl	137 mM
	KCl	2.7 mM
	Na_2HPO_4	10 mM
	K_2HPO_4	2 mM
PBS-T washing buffer	NaCl	
	KCl	
	Na_2HPO_4	1 % (v/v)
	KH_2PO_4	
	Tween-20	
Reduction/alkylation buffer (brought to pH 7-8 with KOH)	TCEP	100 mM
	CAA	400 mM
RIPA lysis buffer pH 7.5	Tris/HCl pH 7.5	50 mM
	NaCl	150 mM
	IGEPAL CA 630	1 % (v/v)
	Sodium deoxycholate	0.5 % (w/v)
	SDS	0.1 % (w/v)
	cOmplete® protease inhibitor	1x
SDBRPS elution buffer	ACN	80 %
	NH_4OH (25 % HPLC grade)	5 %
SDBRPS StageTip loading buffer	TFA	1 %
	Isopropanol	99 %
SDBRPS StageTip wash buffer I	TFA	1 %
	Isopropanol	99 %
SDBRPS StageTip wash buffer II	ACN	5 %
	TFA	0.2 %
SDBRPS wash buffer	TFA	0.2 %
SDC lysis buffer	SDC	4 %

	Tris HCl pH 8.5	100 mM
SDS PAGE running buffer	Tris	25 mM
	Glycine	192 mM
	SDS	0.1 % (w/v)
TBS pH 7.6	Tris pH 7.6	20 mM
	NaCl	135 mM
TBS-T pH 7.6	Tris pH 7.6	20 mM
	NaCl	135 mM
	Tween-20	0.1 % (v/v)
Transfer buffer	ACN	80 %
	Acetic acid	0.5 %
Wash buffer	ACN	60 %
	Acetic acid	0.5 %

Reagents and Kits

Table 7 I Reagents and Kits.

Product	Solvent	Stock concentration	Provider
30 % acryl amide mix			Carl Roth, Karlsruhe, Germany
4',6-Diamidin-2-phenylindol (DAPI)	PBS	1:2000	Sigma-Aldrich, St. Louis, USA
Alexa Fluor 647 phalloidin	MeOH		Thermo Fisher Scientific, Waltham, USA
Bovine serum albumin (BSA)	PBS	1 %, 5 %	AppliChem, Darmstadt, Germany
cOmplete™ protease inhibitor cocktail	H_2O	50x	Roche, Basel, Switzerland
Dako Antibody diluent			Agilent Technologies, Santa Clara, USA
Dithiotreitol (DTT)	H_2O	1 M	Life Technologies, Carlsbad, USA
FBS Superior standardized (S 0615)			Merck Millipore, Darmstadt, Germany
Fibronectin from bovine plasma		2 mg/mL	Sigma-Aldrich, St. Louis, USA
Fluorescent Mounting Medium	-	-	Dako, Hamburg, Germany
Luminata™ Classico Western HRP Substrate	-	-	Merck Millipore, Darmstadt, Germany
Luminata™ Forte Western HRP Substrate	-	-	Merck Millipore, Darmstadt, Germany
Nuclease-Free Water	-	-	Ambion, Thermo Fisher Scientific, Waltham, USA
Penicillin/Streptomycin	-	-	Thermo Fisher Scientific, Waltham, USA
Phosphatase Inhibitor Cocktail Tablets PhosSTOP	H_2O	25x	Roche Diagnostics GmbH, Mannheim, Germany
Pierce™ BCA Protein Assay Kit			Thermo Fisher Scientific, Waltham, USA
Protein Marker IV (10-245 kDa)			AppliChem, Darmstadt, Germany
Roti-Block	H_2O	10x	Carl Roth, Karlsruhe, Germany
SeeBlue®Plus2 Prestained (C592)			Invitrogen Life Technologies Inc, Carlsbad, USA
Trypan Blue Stain (0.4 %)			Thermo Fisher Scientific, Waltham, USA
Trypsin (0.25 % EDTA)	-	-	Thermo Fisher Scientific, Waltham, USA
Vector True View Autofluorescence Quenching Kit			Vector Laboratories, Burlingame, USA

Chemicals

Table 8 I List of chemicals.

Product	CAS number	Provider
2-Chloracetamid	79-07-2	Sigma-Aldrich, St. Louis, USA
2,2,2-Trifluorethanol	75-89-8	Sigma-Aldrich, St. Louis, USA
Acetic acid	64-19-7	Sigma-Aldrich, St. Louis, USA
Acetone	67-64-1	Merck Millipore, Darmstadt, Germany
Acetonitrile	75-05-8	Sigma-Aldrich, St. Louis, USA
Ammonium bicarbonate	1066-33-7	Sigma-Aldrich, St. Louis, USA
Ammonium hydroxide	1336-21-6	Carl Roth, Karlsruhe, Germany
Ammonium persulfate	7727-54-0	BioRad Laboratories, Hercules, USA
APS	231-786-5	Sigma-Aldrich, St. Louis, USA
Bromophenol blue	62625-28-9	AppliChem, Darmstadt, Germany
Citric acid monohydrate	5949-29-1	Thermo Fisher Scientific, Waltham, USA
Dithiotreitol (DTT)	3483-12-3	Life Technologies, Carlsbad, USA
DMSO	67-68-5	Carl Roth, Karlsruhe, Germany
EDTA	6381-92-6	Sigma-Aldrich, St. Louis, USA
Ethanol	64-17-5	AppliChem, Darmstadt, Germany
Glycerol	56-81-5	AppliChem, Darmstadt, Germany
Glycine	56-40-6	Sigma-Aldrich, St. Louis, USA
IGEPAL CA 630	9002-93-1	Sigma-Aldrich, St. Louis, USA
Isopropanol	67-63-0	AppliChem, Darmstadt, Germany
Methanol	67-56-1	AppliChem, Darmstadt, Germany
Paraformaldehyde	30525-89-4	AppliChem, Darmstadt, Germany
Potassium chloride	7447-40-7	AppliChem, Darmstadt, Germany
Potassium dihydrogen phosphate	7778-77-0	AppliChem, Darmstadt, Germany
Sodium chloride	7440-23-5	AppliChem, Darmstadt, Germany
Sodium citrate tribasic	68-04-2	Sigma-Aldrich, St. Louis, USA
Sodium deoxycholate	302-95-4	AppliChem, Darmstadt, Germany
Sodium dodecyl sulfate	151-21-3	AppliChem, Darmstadt, Germany
Sodium fluoride	7681-49-4	Sigma-Aldrich, St. Louis, USA
ß-glycerophosphate	13408-09-8	Merck Millipore, Darmstadt, Germany
TCEP	51805-45-9	Sigma-Aldrich, St. Louis, USA
TEMED	110-18-9	Merck Millipore, Darmstadt, Germany
Trifluoroacetic acid	76-05-1	Sigma-Aldrich, St. Louis, USA
Tris	77-86-1 1185-53-1	AppliChem, Darmstadt, Germany
Triton X-100	9002-93-1	Life Technologies, Carlsbad, USA
Tween-20	9005-64-5	AppliChem, Darmstadt, Germany
Xylene	1330-20-7	AppliChem, Darmstadt, Germany

Software

Table 9 I Software.

Software	Provider
Adobe Illustrator 2020	Adobe Systems, San Jose, USA
Adobe Photoshop 2020	Adobe Systems, San Jose, USA
GraphPad Prism 8	GraphPad Software, La Jolla, USA
Image Lab 5.0	Bio-Rad, Hercules, USA
Ingenuity Pathway Analysis	Quiagen, Hilden, Germany
Magellan Software	Tecan, Crailsheim, Germany
MaxQuant 1.5.3.34	Cox Lab, MPI, Munich
Microsoft Office Professional Plus 2010	Microsoft, Redmond, USA
Persus 1.6.5.0	Cox Lab, MPI, Munich
Python	Python Software Foundation
ZEN 2.3 (blue edition)	Zeiss, Jena, Germany
ZEN 2.3 SP1 (black)	Zeiss, Jena, Germany

Technical devices and further equipment

Table 10 I List of technical devices and other equipment.

Technical device	Provider
-20 °C freezer MediLine LGex 410	Liebherr, Biberach, Germany
-80 °C freezer	Eppendorf, Hamburg, Germany
-80 °C freezer U570 HEF	New Brunswick, Hamburg, Germany
Analytical scale XS20S Dual Range	Mettler-Toledo, Gießen, Germany
Autoclave DX-45	Systec, Wettenberg, Germany
Autoclave VX-120	Systec, Wettenberg, Germany
Bioruptor Plus	Diagenode s.a. BELGIUM EUROPE, Seraing, Belgium
Concentrator Plus	Eppendorf, Hamburg, Germany
Cell culture work bench Herasafe KS180	Thermo Fisher Scientific, Waltham, USA
Centrifuge MiniSpin plus	Eppendorf, Hamburg, Germany
Centrifuge Rotina 420R	Hettich, Tuttlingen, Germany
Centrifuge with cooling, Micro220R	Hettich, Tuttlingen, Germany
CO_2 cell incubator BBD6620	Thermo Fisher Scientific, Waltham, USA
Dry ice container Forma 8600 Series, 8701	Thermo Fisher Scientific, Waltham, USA
Electrophoretic Transfer Cell, Mini Protean Tetra Cell	Bio-Rad, Hercules, USA
Gel imaging system ChemiDoc XRS+	Bio-Rad, Hercules, USA
Hemocytometer	Brand, Wertheim, Germany
Intell-Mixer RM-2	Schubert & Weiss Omnilab, Munich, Germany
Liquid nitrogen cell tank BioSafe 420SC	Cryotherm, Kirchen/Sieg, Germany
Liquid nitrogen tank Apollo 200	Cryotherm, Kirchen/Sieg, Germany
Magnetic stirrer KMO 2 basic	IKA, Staufen, Germany
Microm STP 420D Tissue Processor	Thermo Fisher Scientific, Waltham, USA
Milli-Q® Advantage A10 Ultrapure Water Purification System	Merck Millipore, Darmstadt, Germany
Milli-Q® Integral Water Purification System for Ultrapure Water	Merck Millipore, Darmstadt, Germany
Mini Centrifuge MCF-2360	Schubert & Weiss Omnilab, Munich, Germany
Multipette stream	Eppendorf, Hamburg, Germany
Nalgene Freezing Container (Mister Frosty)	Omnilab, Munich, Germany
NanoDrop 1000	PeqLab, Erlangen, Germany
pH meter InoLab pH 720	WTW, Weilheim, Germany
Plate centrifuge 5430	Eppendorf, Hamburg, Germany
Plate reader Sunrise	Tecan, Crailsheim, Germany
Plate reader TriStar LB941	Berthold Technologies, Bad Wildbach, Germany
Refrigerator Profi Line	Liebherr, Biberach, Germany
Ice machine ZBE 110-35	Ziegra, Hannover, Germany
Research plus pipettes	Eppendorf, Hamburg, Germany
Roll mixer	VWR International, Darmstadt, Germany
Scale XS400 2S	Mettler-Toledo, Giessen, Germany
Shaker Duomax 1030	Heidolph, Schwabach, Germany
Thermomixer compact	Eppendorf, Hamburg, Germany
Thermomixer C	Eppendorf, Hamburg, Germany
Vacuum pump NO22AN.18 with switch 2410	KNF, Freiburg, Germany
Vortex mixer	IKA, Staufen, Germany
Zeiss 710	Carl Zeiss AG, Oberkochen, Germany
Axio Imager.M2	Carl Zeiss AG, Oberkochen, Germany
Water bath Aqua Line AL 12	Lauda, Lauda-Königshofen, Germany

Methods

Cell culture

Cultivation of mammalian cell lines. CCL151 and CCL206 cell lines were obtained from American Type Culture Collection and tested negative for mycoplasma. Cells were maintained in Dulbecco's modified Eagle's medium (DMEM)/F-12K medium supplemented with 10 % fetal calf serum (FCS), 1 % penicillin/streptomycin (PS). Human primary lung fibroblasts from healthy donor tissue were cultured in DMEM/F12 medium with 20 % FCS and 1% penicillin/streptomycin. All cells were cultivated at 37 °C and 5 % CO_2 in a humidified atmosphere.

Passaging, Defrosting and Freezing of adherent cells. All cells were cultivated at 37 °C and 5 % CO_2 in a humidified atmosphere. CCL206 and CCL151 cells were cultured in DMEM with 10 % FCS and 1 % PS**.** Cells were passaged at a confluence of 80-90 %. Used culture medium was sucked off and remaining medium and death cells were washed away with PBS (w/o Mg^{2+}/Ca^{2+}). Cells were detached with an adequate amount of trypsin and incubation for 5 – 10 min at 37 °C. The trypsin was stopped by adding the same volume of growth medium. Afterwards cells were spun down 5 min, room temperature (RT), 300 g, resuspended in medium and counted. The requested cell number was spread to new cell culture dishes containing fresh medium.

For freezing, cells were washed with PBS (w/o Ca^{2+}/Mg^{2+}) and were detached with trypsin. Medium was added to stop the trypsin, the cells were centrifuged for 5 min, RT, 300 g and the supernatant was discarded. Afterwards, the cells were resuspended in cold freezing medium (culture medium with 50 % FBS and 10 % DMSO). Then the cells were transferred into cryo vials. The cryo vials were cooled down over-night (o/n) in the -80 °C freezer and were afterwards stored in liquid nitrogen (-196 °C).

For defrosting, cells were thawed in the 37 °C water bath and then quickly resuspended in pre-warmed growth medium. Cells were spun down 5 min, RT, 300 g to remove DMSO and resuspended in fresh medium.

Determination of cell number. Cell number was determined using a hemocytometer. A coverslip was wet slightly with distilled water and then put on top of the Neubauer counting chamber. Cell suspension was mixed with a suitable volume of trypan blue and was pipetted to both sides in the counting chamber. Counting was conducted with a phase contrast microscope. Four 16 blocks were counted twice and the average was calculated. Cell number was calculated using the following formula:

Cell number per mL = average value x chamber factor (10^4) x dilution factor   (1)

Protein biochemistry

Coating with Fibronectin (FN). Cytosoft or Softwell cell culture dishes and ibidi imaging dishes as well as glass cover slips were coated with 10 µg/mL FN in PBS at 4°C overnight or for 1 h at RT. After coating the FN solution was aspirated and the dishes were washed with PBS. The coated dishes could either be used immediately for cell seeding or could be stored covered with PBS for some days at 4°C.

Protein extraction from cells. Unless indicated otherwise, cells were lysed in RIPA lysis buffer with proteinase and proteases inhibitors, at a volume suitable for the petri dish size. If cells were scraped from dishes with soft substrate, the cell culture dish was quickly dipped in liquid nitrogen to freeze the soft substrate slightly in order to improve cell scrapping. After 30 min incubation on ice, the lysate was centrifuged for 20 min, 4 °C, 14000 g. To remove insoluble debris, the clear supernatant was transferred to pre-chilled tubes and protein concentration was measured using the BCA protein assay, according to the manufacturer´s instructions.

Finally, 6x Laemmli buffer was added to denature proteins via SDS and the sample was boiled for 5 min at 95 °C.

Bicinchoninic acid (BCA) assay. Protein concentration was determined by BCA Assay. The BCA assay uses the reduction of Cu^{2+} to Cu^{1+} by proteins in an alkaline medium which results in a purple-colored reaction. The equation to calculate protein concentration was derived from linear regression of a bovine serum albumin (BSA) dilution series of 2000-0µg/mL in ddH_2O (see Table 11). The sample was diluted 1:10 and 1:20 in the respective buffer and each sample/standard was measured in three replicates. The BCA working reagent was prepared by mixing 50:1 of BCA reagent A with BCA reagent B. For the measurement sample/standard were thoroughly mixed with BCA working reagent in the ration 1:8 on a plate shaker for 30 sec. After 30 min of incubation at 37 °C, the plate was cooled to RT and the measurement of absorbance at λ= 562nm was carried out in SUNRISE[TM] microplate reader.

Table 11 I Pipetting scheme BCA Assay standard.

vial	volume dilution solution [µL]	volume and origin of BSA [µL]	final concentration BSA [µgmL^{-1}]
A	0	300 (stock solution)	2000
B	125	375 (stock solution)	1500
C	325	325 (stock solution)	1000
D	175	175 (dilution B)	750
E	325	325 (dilution C)	500
F	325	325 (dilution E)	250
G	325	325 (dilution F)	125
H	400	100 (dilution G)	25
I	400	0	0 = reference

SDS-PAGE and Western blot analysis. Gels were prepared freshly before use (Table 12, Table 13). Protein samples were boiled with 1/6 volume Laemmli buffer and incubated for 5 min 95 °C. Samples and a molecular weight marker were loaded onto SDS polyacrylamide gels and subjected to gel electrophoresis in running buffer at 80–120 V. After gel electrophoresis, proteins were transferred to a membrane for immunoblot analysis.

Separating gel
Table 12 I Pipetting scheme for different separating gels.

A volume of 15 mL is sufficient for two gels.

Gel	8 %	10 %	12 %	15 %
Protein size	75-150 kDa	50 -100 kDa	40-75 kDa	25-60 kDa
30 % acryl amide mix	2.7 mL	3.3 mL	4 mL	5 mL
1.5 M Tris pH 8.8	2.5 mL	2.5 mL	2.5 mL	2.5 mL
10 % SDS	0.1 mL	0.1 mL	0.1 mL	0.1 mL
dH$_2$O	4.59 mL	3.99 mL	3.29 mL	2.29 mL

Directly before use, TEMED and 10 % APS were added to the separating gel in a ratio of 1:1000 and 1:100.

Stacking gel
Table 13 I Pipetting scheme for stock solution of stacking gel.

A volume of 3 mL is sufficient for two gels.

Reagent	volume
30 % acryl amide mix	8 mL
1.5 M TRIS, pH 8.8	6.25 mL
10 % SDS	0.5 mL
dH$_2$O	35 mL
total	50 mL

Directly before use, TEMED and 10 % APS were added to the stacking gel stock solution in a ratio of 1:1000 and 1:100.

Immunoblotting. Western blot was performed using the Mini PROTEAN Tetra Cell (BioRad Laboratories, Inc.) according to the manufactures instructions. The PVDF membrane (Immun-Blot® BioRad Laboratories, Inc.) was activated for 3 min in 100 % methanol, rinsed with dH$_2$O water and stored in 1x transfer buffer. The blot was run for 2 h at 100 V, on ice in 1x transfer buffer. The membrane was blocked using 1x RotiBlock in dH$_2$O and incubated for 1 h, RT. After blocking, the membrane was quickly washed with PBS-T or in case of phospho antibodies with TBS-T. Primary antibody mix (1:1000) was prepared with 1x RotiBlock. Incubation with the primary antibody was carried out overnight (4 °C, gently shaking). The membrane was washed 3 x 5 min with PBS-T /TBS-T and was then incubated with the secondary antibody mix (1:20,000) in 5 mL 1x RotiBlock solution for 1 h, RT. Afterwards, the membrane was washed 3 x 10 min with PBS-T/TBS-T.

Finally, visualization was conducted with Immobilon™ Western solution using the ChemiDoc™ System.

Immunofluorescence microscopy. Glass coverslips or ibidi microscopic dishes (0.5 kPa and 28 kPa) were coated with FN. Cells were seeded for 120 min. Then the cells were washed three times with PBS and fixed with 4 % PFA for 20 min, RT. Afterwards, cells were washed three times for 5 min with PBS/TBS and permeabilized with 0.1 % TritonX-100 in PBS/TBS for 10 min. After three times of washing for 5 min cells were blocked with 5 % BSA in PBS for 30 min, RT and incubated with primary antibodies diluted in 1 % BSA in PBS/TBS o.n., 4 °C. After that, cells were washed three times for 5 min with PBS/TBS followed by 2 h incubation with the secondary antibodies diluted in 1 % BSA in PBS. After washing three times for 5 min with PBS/TBS, cells were incubated with DAPI for 10 min, RT, followed by washing with PBS/TBS times for 5 min. Cells on glass cover slips were mounted with Fluorescent Mounting Medium, whereas cells on ibidi microscopic dishes were covered with PBS/TBS. Samples were examined using Zeiss LSM 710 or AXIO Imager.

For staining of formalin-fixed, paraffin-embedded (FFPE) lung tissue sections were cut at 3.5 µm. The slides were dried at 60 °C for 30 min to 60 min. Deparaffinization and rehydration was performed according to the following scheme:

1. Xylene I (5 min)
2. Xylene II (5 min)
3. 100 % Ethanol I (3 min)
4. 100 % Ethanol II (3 min)
5. 90 % Ethanol (3 min)
6. 80 % Ethanol (3 min)
7. 70 % Ethanol (3 min)
8. Milli-Q water (5 min)

Antigen retrieval was performed by pressure cooking in citrate buffer (30 s at 125 °C and 10 s at 90 °C). After a cool down step for 20-25 min at RT, slides were washed twice with PBS for 5 min. Unspecific binding was blocked with 5 % BSA in PBS for 1 h, RT, in a wet chamber. The slides were tilted and 100 µL primary antibody solution in antibody diluent solution were added. Incubation was carried out overnight at 4 °C in a wet chamber. After removal of the primary antibody solution, the slides were washed twice in PBS, 5 min each. The secondary antibodies diluted in 1 % BSA solution were added and incubated for 2 h, RT in a dark wet chamber. The slides were washed twice for 5 min in PBS in the dark. Then, the tissue sections were counterstained with DAPI (1:2000 in Milli-Q water) for 10 min. The DAPI solution was washed away with Milli-Q water, twice for 5 min in the dark. Autofluorescence blocking was performed with Vector TrueVIEW Autofluorescence Quenching Kit according to the manufacturer's instructions. After that the tissue sections were mounted with DAKO fluorescence mounting medium.

Human lung material form the CPC-M bioArchive

Human lung tissue and human lung explant material were received from the CPC-M bioArchive at the Comprehensive Pneumology Center (CPC), Munich, based on the bioArchive proposal BA-067/2019. I gratefully acknowledge the provision of human biomaterial and clinical data form the CPC-M bioArchive and its partners at the Asklepios Biobank Gauting, the Klinikum der Universität München and the Ludwig-Maximilians-Universität München.

Phosphopeptide enrichment – EasyPhos Workflow

The phosphopeptide enrichment was conducted as described by Humphrey et al. 2015 *[118]*.

Substrate rigidity testing. In this experiment cells were exposed to different degrees of substrate stiffness for 120 /180 min, this was done with Cytosoft plates**.** CytoSoft® Elastic Modulus Plates are used for the cultivation of cells on substrates with different defined stiffnesses which cover a wide physiological range. At the bottom of each well there is a thin layer of specially formulated biocompatible silicone whose Young's modulus (stiffness) is carefully measured. The surfaces of the gels in CytoSoft® products are functionalized to form covalent bonds with amines on proteins. CytoSoft 6-well dishes with elastic modules 0.5, 2, 8, 16 and 32 kPa were coated with 10 µg/mL FN for 1h, RT. 500,000 cells were seeded per well for 120 min.

Cell spreading. In this experiment, cells were allowed to spread on very stiff substrates (normal plastic cell culture dishes) for 10 min, 20 min, 30 min, 60 min, 90 min and 120 min before cells were lysed. The 6-well plastic dishes were also coated with FN before seeding 500,000 cells per well.

Lysis and protein precipitation. Cells were lysed in a suitable volume of 6M Gdm lysis buffer. Lysate was heated for 5 min, 95 °C, then cooled on ice for 15 min. Afterwards, the lysate was sonicated (Bioruptor; max. energy; 10x 30 sec cycle) and then heated again for 5 min, 95 °C. To increase the precipitation efficiency, the 6M GdmCl lysate was diluted 1:2 with water before 100 % acetone (-20 °C) was added until a volume of 50 mL was reached and incubated o/n at – 80°C.The precipitated protein was collected by centrifugation for 10 min, 4 °C, 4000 g. The supernatant was discarded and the pellet was resuspended with 80 % acetone (-20 °C). The resuspended pellet was incubated for 30 min, -20 °C and centrifuged 10 min, 4 °C, 4000 g. The pellet was resuspended in 80 % acetone (-20 °C), sonicated in Bioruptor for 4 cycles and spun down (10 min, 4 °C, 4000 g). The pellet was air dried for around 10 min at RT or until no residual acetone odor remained. Thereafter, the pellet was resuspended in maximum 500 µL of TFE digestion buffer and sonicated (Bioruptor, 5 min, 4 °C). Then, samples were snap frozen and stored at -80 °C.

Protein digestion. The following steps were performed in 96-well deep well plates (DWP). Digestion was initiated by addition of 1:100 Lys-C for 30 min and 1:100 trypsin (resuspended in 0.05 % acetic acid, 2 mM $CaCl_2$) for 18 h, 37 °C, 2000 rpm.

Phosphopeptide enrichment. To the digested peptides in 500 µL TFE digestion buffer KCl, KH$_2$PO$_4$, 100 % ACN and 100 % TFA were added in this order to a final volume of 1.6 mL and final concentrations of 300 mM KCl, 5 mM KH$_2$PO$_4$, 50 % CAN and 6 % TFA. The peptide solution was mixed for 1h, RT, 2000 rpm. Samples were centrifuged for 30 min, RT, 3500 g and the supernatant was transferred to a clean 2 mL Eppendorf DWP.

For preparing the TiO$_2$ beads, the TiO$_2$ beads (GL Sciences, Titansphere Phos-TiO$_2$) were weighed out for all samples at a ratio of 10:1 to protein. The beads were resuspended in loading buffer (see Table *6*) per sample. The bead suspension was incubated for 1 min, 4 °C in the bioruptor to disaggregate the beads. Thereafter, the bead suspension was transferred to each DWP well, and incubated for 5 min, 40 °C, 2000 rpm in a ThermoMixer. To pellet the beads, the suspension was centrifuged for 1 min, RT, 3500 g. The supernatant containing the non-phosphopeptides was discarded by aspiration and the non-specifically bound peptides were washed from the TiO$_2$ beads. Therefore, the beads were resuspended in wash buffer (see Table *6*) and transferred to a clean DWP. Any remaining beads were collected with wash buffer (see Table *6*). The beads were incubated for 30 sec, RT, 2000 rpm in a ThermoMixer, centrifuged for 1 min, RT, 3500 g and the supernatant was discarded by aspiration. Cell pellets were washed four additional times with wash buffer (see Table *6*), incubated 30 sec, RT, 2000 rpm for every wash step. After the final washing step, transfer buffer (see Table *6*) were added to each well and incubated for 30 sec, RT, 800 rpm in a ThermoMixer.

Hereafter, the beads were transferred in transfer buffer on top of a C8 (single layer) StageTip and centrifuged for 5 min, RT, 500 g. For elution of the phosphopeptides 2 x 30 µL elution buffer (see Table *6*) was added to each StageTip containing TiO$_2$ beads. The eluates were collected into a PCR tube after centrifugation for 3 min, 4 °C, 500 g. The samples were concentrated in a SpeedVac for 20 min, RT or until approximately 20 µL of volume remained. Immediately 10 µL 10 % TFA were added to each sample.

The StageTips had to be pre-equilibrated in three steps. Pre-equilibration was conducted with ACN (washing), 30 % MeOH (activation), 0.2 % TFA and 0.1 % TFA. After adding the respective solution to the StageTips, the StageTips were centrifuged for 5 min, RT, 500 g. Then each sample was loaded onto the StageTips with 3x layers of pre-equilibrated SDBRPS material and 100 µL SDBRPS wash buffer were added and centrifuged for 5 min, RT, 500 g. Subsequent SDBRPS wash buffer (see Table *6*) was added and centrifuged for 5 min, RT, 500 g or until less than 5 µL liquid remained. For elution of phosphopeptides 60 µL SDBRPS elution buffer (see Table *6*) was added to each SDBRPS StageTip. The phosphopeptides were collected into clean PCR tubes by centrifugation for 5 min, RT, 500 g or until the SDBRPS material was dry. Immediately the samples were placed into the SpeedVac for 30 min, RT or until around 2 µL remained. To the phosphopeptides 7 µL MS loading buffer (see Table *6*) were added and resuspended by sonication in an ultrasonic water bath for 1 min.

Mass spectrometric phospho data analysis

MS analysis. The Peptides were loaded onto a 40-cm column with a 75 µM inner diameter, (packed in-house, 1.9 µM C18 ReproSil particles, Dr. Maisch GmbH). Column temperature was maintained at 50 °C. The mass spectrometer was connected to an EASY-nLC 1000 system (Thermo Fisher Scientific) with a nanospray ion source. Peptides were separated at a flow rate of 300 nL/min with a binary buffer system of 0.1% formic acid (buffer A) and 60% ACN plus 0.1% formic (buffer B). Peptides were eluted with a gradient of 5–25% buffer B over 85 or 180 min followed by 25–50% buffer B over 35 or 60 min, resulting in ~2 h or 4 h gradients respectively. Peptide analysis was performed with a Q Exactive benchtop Orbitrap mass spectrometer (Thermo Fisher Scientific), with one full scan (300–1,600 m/z, R = 60,000 at 200 m/z) at a target of $3e^6$ ions and up to five data-dependent MS/MS scans with higher-energy collisional dissociation (HCD) (target 1e5 ions, max ion fill time 120 ms, isolation window 1.6 m/z, normalized collision energy (NCE) 25%, underfill ratio 40%), detected in the Orbitrap (R = 15,000 at 200 m/z). Dynamic exclusion (40 s or 60 s) and apex trigger (4 to 7 s) were activated.

MaxQuant. Raw MS data files were processed using MaxQuant Version 1.5.3.34 [163]. The spectra were searched with the Andromeda search engine using a false discovery rate (FDR) of < 0.01 on protein level as well as on peptide and modification level. In general the default settings of MaxQuant were used but with following changes. Methionine (M), acetylation (protein N-terminus) and phosphorylation (STY) were selected as variable modification. Carbamidomethyl (C) was selected as fixed modification. Furthermore, only peptides with a minimal length of seven amino acids were taken into account. The 'match between runs' option was turned on using a matching time window of 0.7 minutes. Peptide and protein identification was done by using the UniProt data base from human (April, 2018) which contained 20,138 entries. Each raw file was handled as one experiment. For the rigidity phosphoproteomic data set replicate 1 of 0.5 kP was removed for the final analysis because of low identification number and outlier clustering within the replicates. Exactly the same was done with the phosphoproteomic spreading data set. Here the following replicates were not considered for the final analysis: replicate 2 of 20 min and replicate 4 of 30 min.

Bioinformatic and statistical data analysis

Perseus. The processed data files were uploaded in the Perseus software [171] in order to perform bioinformatic data analysis. First, the label-free phosphorylation data was filtered to retain only these sites that have a localization probability > 0.75. In the next step, the data was

rearranged, so that the different number of phosphorylations per peptide are not formatted as separate columns but just as one column per sample and three rows per phosphosite alternatively. The phosphorylation intensities were log2 transformed and filtered from reverse (decoy) database hits. Following protein annotations were added: GOBP name, GOMF name, GOCC name, GOPB slim name, GOMF slim name, GOCC slim name, KEGG name, Pfam, GSEA, Keywords and Corum. The different annotations were obtained from http://annotations.perseus-framework.org. Then, phosphosite-specific data such as sequence features, linear motifs, known sites, kinase substrate relations and regulatory sites were added to the data set obtained from the PhopshoSitePlus database. The respective replicates were grouped according to stiffness or spreading time.

Both data sets were filtered for valid values. In the rigidity data set three values in at least one group had to be valid in order to pass the filter. For the spreading data set four values in at least one group had to be valid to not filter out the phosphorylation sites, since here five replicates per group were measured and not just four replicates as for the rigidity data set. The data was normalized by subtracting the median of each column.

Missing values were imputed using a width of 0.3 and a down shift of 1.8 for the total matrix. ANOVA testing for identification of regulated phosphosites was performed with and without prior imputation of the data. The phosphorylation sites found to be significantly regulated by ANOVA testing without imputation of the data were combined with the results of the performed ANOVA test with imputed values. In the next step, a matrix which only contained the significantly regulated phosphorylation sites was created. A principal component analysis was performed to further explore the data. Before proceeding with hierarchical clustering, the data was z-scored. This means, that the mean of each row is subtracted from each value and the result is divided by the standard deviation of the row. Based on the hierarchical clustering the data was split into distinct cluster.

Relative enrichment of annotations for the IPA predicted CK2A1 regulated sites was achieved using Fisher's exact test enrichment analysis (FDR 5 %).

Ingenuity Pathway analysis. IPA is a web-based software application that facilitates the analysis, integration and understanding of data from gene expression, miRNA and SNP microarrays as well as metabolomics, proteomics and RNAseq experiments. IPA enables the search for specific information about genes, proteins, chemicals and drugs and the construction of interactive models of experimental systems. Data analysis and search functions help to understand the meaning of data, specific targets or candidate biomarkers in the context of larger biological or chemical systems. The software is supported by the Ingenuity Knowledge Base, which contains highly structured, detailed biological and chemical knowledge (IPA, Qiagen, Redwood City, www.qiagen.com/ingenuity).

The z-scored averages of the distinct significantly regulated phosphosites of each condition (stiffness or spreading time) were uploaded into the program. Observations were inferred and the identifier was assigned. After the data upload a core phosphorylation analysis was performed using the z-scored intensity of the phosphosites as base for analysis. Once all core analyses were calculated, a comparison analysis was run to obtain regulated Canonical Pathways, Upstream Regulators and Diseases and Functions. Canonical Pathways show the molecules of interest in known and well-established signaling pathways. Furthermore, if possible the likelihood is determined whether the pathway is activated or inhibited. Upstream analysis predicts which upstream regulators (any molecule that can affect the phosphorylation of another molecule) could be activated or inhibited to explain the phosphorylation changes in the data set. Diseases & Functions relates the molecules in the data set to known disease conditions and biological functions. Where applicable, IPA derives from the activity of the protein whether the associated disease or function is likely to be increased or decreased.

Metascape analysis. The members of the clusters defined by hierarchical clustering of the phospho data in Perseus were submitted to the web-based analysis tool Metascape [172]. This portal combines functional enrichment, gene annotation, membership search and interactome analysis of over 40 independent knowledgebases to comprehensively analyze OMICs-based data. After inserting the gene list, the express analysis was performed for each cluster. In the settings species h. sapiens was selected as input and also used for analysis. All pathway and process enrichment analysis for each cluster were combined in one heatmap.

Scanpy packages. Scanpy is a Python-based, scalable toolkit which was originally designed for the analysis of single-cell gene expression data (https://github.com/theislab/Scanpy) [173]. Even though the analysis tool was intended for the analysis of single-cell gene expression data, it was used in this work for the analysis of phosphorylation intensity data. Scanpy can be used for clustering and visualization of data and can easily be run on Jupyter notebooks, which represents an interactive web-based environment (www.jupyter.org).

Tables generated in Perseus containing the significantly regulated phosphosites were exported and imported into Scanpy and a scanpy object was created. This was done for the CCL151 stiffness dataset, the CCL151 spreading dataset, the merged dataset spreading and stiffness and the combined phosphorylation data from CCL151 and phLFs on different substrate rigidities. The merge of data sets was performed in Excel by making use of the unique identifiers for each phosphorylation site which were generated by processing all phospho data together in MaxQuant.

After calculation of the PCA for each imported data set, the phospho data was visualized by the Uniform Manifold Approximation and Projection (UMAP) method [174]. The scaled phosphorylation intensities were overlaid on the generated UMAPs. Furthermore, dot plots showing the scaled phosphorylation intensities and the cluster memberships of each site were created in Scanpy.

"Nothing in life is to be feared, it is only to be understood. Now is the time to understand more, so that we may fear less."

Marie Curie

Results

The work presented here has been drafted into a manuscript that will be submitted to a scientific journal. By the time of submission of this thesis, the paper has not yet been peer-reviewed. The PhD student, as first author of this manuscript, was involved in all parts of this study, performed most of the practical work, analyzed the data, drafted all the figure panels and was part in conceiving the manuscript. Credit goes to Meshal Ansari for providing the code to analyze the phosphoproteomics data with Scanpy, Christoph Mayr for assisting in MS measurements of the phosphoproteomes and Dr. Anita Wasik for conducting an immunofluorescence staining.

Mapping phosphorylation sites in human lung fibroblasts seeded on varying substrates stiffnesses from soft to stiff

In a first step the mechanosensing properties of the human lung fibroblast cell line CCL151 was visualized by seeding the cells for 120 min on soft (0.5 kPa) and stiff substrates (28 kPa) followed by immunofluorescence staining of YAP1 and the actin cytoskeleton (**Figure 17 A**). Spread cells and cells grown on rigid ECM exhibit increased YAP/TAZ activity correlating with their nuclear localization [38]. In CCL151 cells grown on 28 kPa PDMS gels YAP1 is mainly found in the nucleus and not in the cytoplasm, while on soft substrate YAP1 is localized throughout the whole cell (**Figure 17 A**).
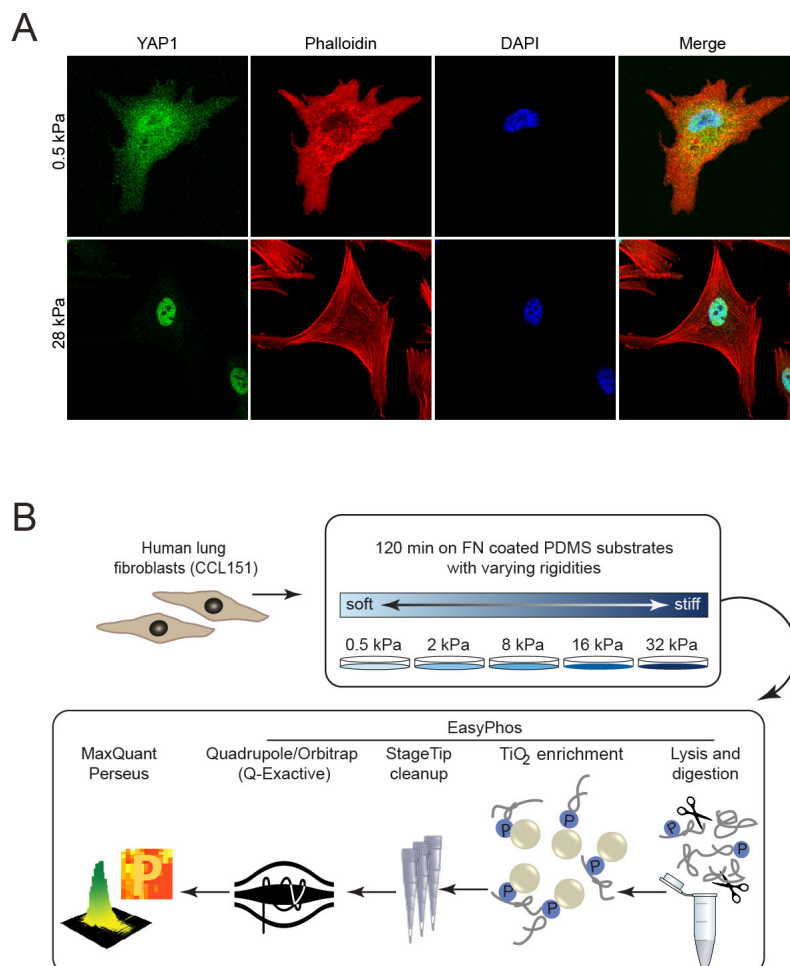

Figure 17 I Cell line validation and phosphoproteomic workflow. A Immunofluorescence staining of YAP (green) in CCL151 cells seeded for 2 h on 0.5 kPa and 28 kPa. **B** Experimental workflow to analyze the phosphoproteome of human lung fibroblasts seeded on varying substrate stiffnesses.

To generate a comprehensive data set of phosphorylation events taking place in human lung fibroblast while they are sensing substrate rigidity, CCL151 cells were seeded for 120 min on fibronectin coated PDMS gels with varying rigidities from soft to stiff (0.5, 2, 8, 16 and 32 kPa). After cell lysis, sample preparation and data acquisition was performed as described in the 'EasyPhos' protocol. This approach is capable of maximizing the coverage and reproducibility of phosphorylation sites quantification in single MS runs and gets along without fractionation [118] (**Figure 17 B**).
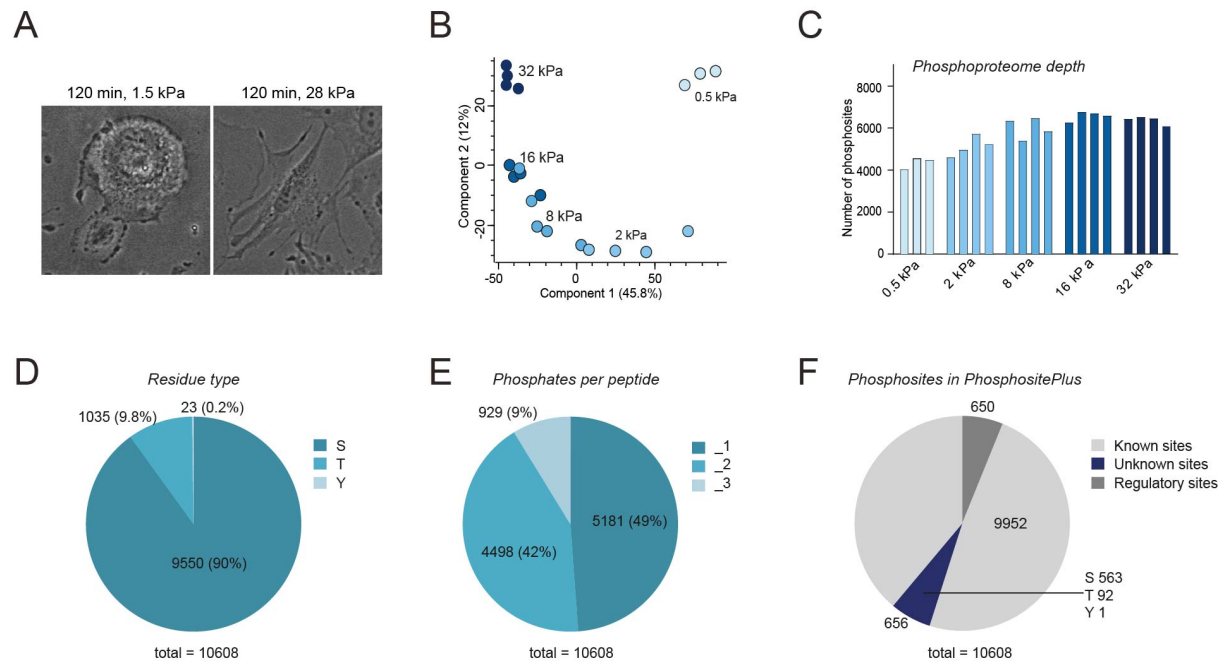
Figure 18 I Description of the phosphoproteomic data set measured in dependence of substrate stiffness. **A** CCL151 cells seeded on FN-coated 0.5 kPa and 28 kPa substrates after 120 min of spreading time. **B** Phosphoproteome depth of the phosphoproteomic data set of varying substrate rigidities. **C** Principal component analysis (PCA) of the stiffness regulated phosphoproteome. Two major components separate the data according to stiffness **D** Pie chart presenting the percentage of identified phosphorylated serines (S), threonines (T) and tyrosines (Y) residues in the rigidity data set. **E** Pie chart presenting the percentage of identified singly, doubly and triply (or more) phosphorylated peptides in the rigidity data set. **F** Pie chart showing the number of already known sites, previously unreported sites and known sites with an assigned regulatory function in the PhosphoSitePlus database (www.phosphosite.org) of the rigidity data set.

Substrate stiffnesses have differential influence on cells (**Figure 18 A**).The lung fibroblasts on both substrate rigidities were seeded for 120 min, but show huge differences in cell shape and spreading status. Using the unbiased MS approach, I identified 10,608 class I phosphosites with a localization probability > 0.75. In each replicate, included in the analysis, at least 4000 phosphosites were measured. With increasing stiffness more phosphorylation sites were recorded in a range between 5400 and 6700 sites (**Figure 18 C**). The performed principle component analysis showed a good separation of the distinct substrate rigidities and high reproducibility between the single replicates (**Figure 18 B**). The 10,608 class I phosphosites correspond to mainly serine residues (S) with 9550 sites, followed by 1035 phosphothreonines

(T) and only 23 phosphorylated tyrosine residues (Y) (**Figure 18 D**). Almost half of all identified phosphosites (5181) are localized on phosphopeptides which have only one phosphate group as modification. But 4498 phosphosites are found on doubly phosphorylated peptides and 929 sites are located on phosphopeptides with at least three phosphorylations (**Figure 18 E**). Interestingly, 656 phosphosites were identified which were previously unknown without entry in the PhosphoSitePlus data base. Those sites split up in phosphorylations on 563 serine, 92 threonines and one tyrosine residues. On the other hand, 650 phosphorylation sites identified are already better characterized and known to be functionally relevant (**Figure 18F**). After filtering for sites that were at least measured three times in one of the stiffness conditions 8349 phosphorylation sites remained and were used for further analysis.

To validate the experimental setup, the data was searched for already known phosphorylation sites in context of mechanosensing such as phosphorylation of threonine 18 and serine 19 of myosin light chain (MYL9) and various phosphorylation sites of the adaptor protein paxillin (PXN). Phosphorylation of T19 and S20 of MYL9 showed the expected increase with increasing substrate stiffness. It is known that the activity of MYL9 is increased via phosphorylation of those residues in dependence on substrate rigidity [175]. The increase in phosphorylation measured by mass spectrometry was also seen in immunofluorescence stainings in cells seeded for 120 min on soft (0.5 kPa) und stiff (28 kPa) substrates (**Figure 19 A**) As a second positive control for the accuracy of the experimental workflow serves the increase in phosphorylation of serine 126 on the focal adhesion protein paxillin with increasing substrate stiffness, which is related to a raised turnover of paxillin in focal adhesions [176]. The elevated phosphorylation of serine 126 on paxillin was also validated by western blotting (**Figure 19 B**). Also other phosphorylation sites of paxillin are increasing with rising stiffness, S341, S106, S250, S258, S261, S130, S137, and S109.
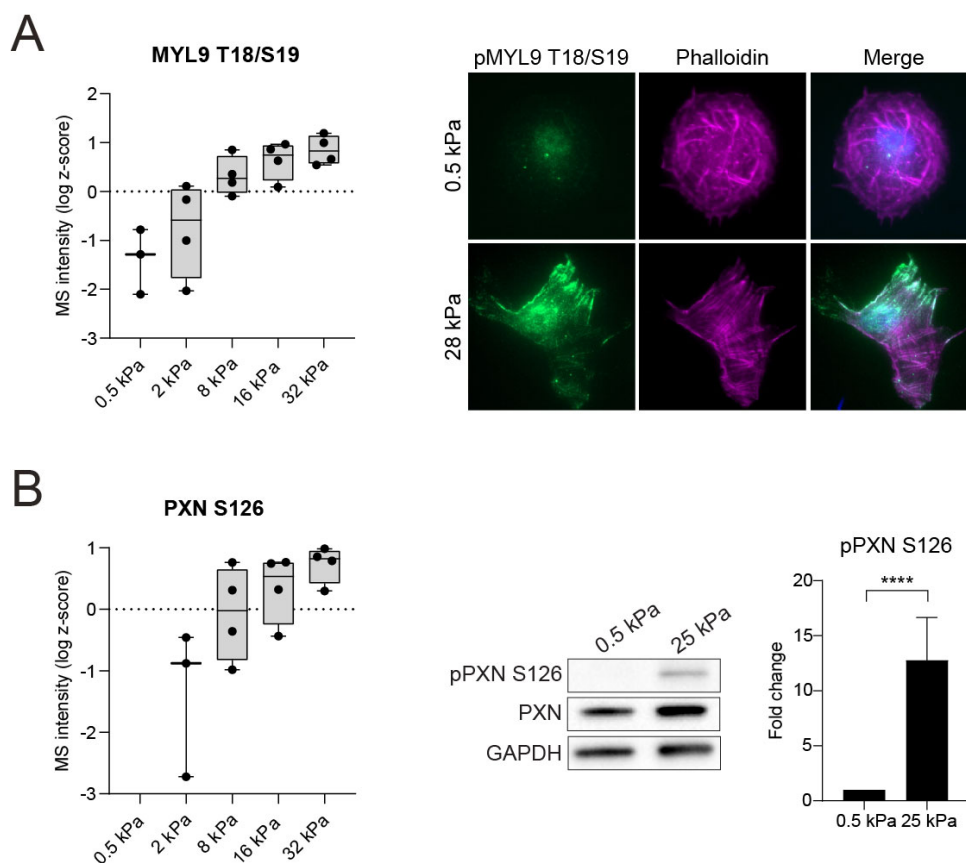
Figure 19 I Validation of experimental setup and accuracy of the method. **A** Phosphorylation status of MYL9 on residues 18 and 19 with increasing stiffness serves as positive control. MS intensity values are log z-scored and shown without imputation.. Immunofluorescence staining of cells seeded for 120 min on 0.5 and 28 kPa substrates coated with FN, probed with phosphospecific MYL9 T18/S19 antibody and phalloidin to stain the actin cytoskeleton. Nuclei (DAPI) are colored in blue, MYL9 T18/S19 appears in green, and actin in magenta. **B** Increasing phosphorylation of PXN with increasing stiffness serves as positive control. MS intensity values are log z-scored and shown without imputation. Immunoblot analysis of equal amounts of proteins from total cell lysates seeded for 120 min on 0.5 and 25 kPa substrates coated with FN, probed with phosphospecific PXN S126 antibody and PXN antibody. GAPDH served as a loading control.

Identification of stiffness-dependent regulated phosphorylation sites

I sought to identify phosphosites, whose phosphorylation was regulated in a rigidity-dependent manner. After label-free relative quantification across all stiffness conditions, an ANOVA-based statistical approach was used to find significantly regulated sites. The ANOVA test was performed both with and without prior imputation of the data. Then, the results of these two test strategies were combined. With this approach, 1631 phosphosites were found to be significantly regulated across the different substrate rigidities (1 % FDR) (**Figure 20 A**). These regulated sites account for around 20 % of the phosphorylation sites in the total data set and belong to 721 different proteins. Mainly phosphosites with phosphorylation on serine residues were regulated, namely 1463 sites, and only 164 threonines and four tyrosines were found to

be dependent on stiffness. A heatmap depicting the difference of phosphorylation between the stiffness conditions was generated by hierarchical clustering (Pearson correlation) of the z-scored MS intensities (**Figure 20 A**). More than half of the regulated sites enhance in phosphorylation with increasing substrate stiffness. Within the heatmap I identified ten different clusters containing between 52 to 648 phosphorylation sites. The course of phosphorylation for each of the different clusters are presented in **Figure 20 B**. Cluster 8 is the largest of the ten clusters and already shows a rise in phosphorylation at 2 kPa, whereas the phosphorylation in cluster 9 is only increased from a rigidity of 8 kPa. In contrast, the phosphosite contained in cluster 10 start to be enhanced upon a substrate stiffness of 16 kPa. The 78 phosphorylation sites present in cluster 4 show also increasing phosphorylation with increasing stiffness, but solely at the most rigid condition with 32 kPa. Only cluster 2 displays decreasing phosphorylation of the contained phosphosite with increasing stiffness. Cluster 1, 3, 5, 6 and 7 show no gradually change in phosphorylation, but rather vary in between the rigidity conditions. The phosphosites in cluster 6 get more phosphorylated starting from 2 kPa, but decrease again on 32 kPa. In cluster 7, on the other hand, the phosphorylation status peaks on 8 kPa but decreases on 16 kPa and increases again on 32 kPa. The course of cluster 3 is similar to cluster 7 but without the sharp increase form 0.5 kPa to 8 kPa. The phosphorylation of sites contained in cluster 5 are high on soft, decrease from 2 to 8 kPa and are increased in the stiff conditions 16 and 32 kPa.

Analysis of annotations enriched within the set of phosphorylation sites in a given cluster was performed with the web-based tool Metascape [172]. This portal combines functional enrichment, gene annotation, membership search and interactome analysis of over 40 independent knowledgebases to comprehensively analyze OMICs-based data. The analysis revealed, that especially the clusters 2, 8, 9 and 10 are enriched with sites corresponding to 'supramolecular fiber organization', 'actin filament based process' and 'actin cytoskeleton organization'. Interestingly only cluster 2 contained phosphosites enriched for the term 'focal adhesion' and 'fibroblast migration'. Furthermore, the analysis revealed that proteins associated with the terms 'hippo signaling', 'mesenchymal cell differentiation' and 'Rho A signaling' enhanced in cluster 10 were impacted by mechanical stimulation. It is striking, that especially proteins in cluster 8 are enriched for annotations like 'mRNA processing', 'regulation of mRNA stability' and 'RNA splicing', indicating that substrate stiffness is a trigger for changes in gene expression.
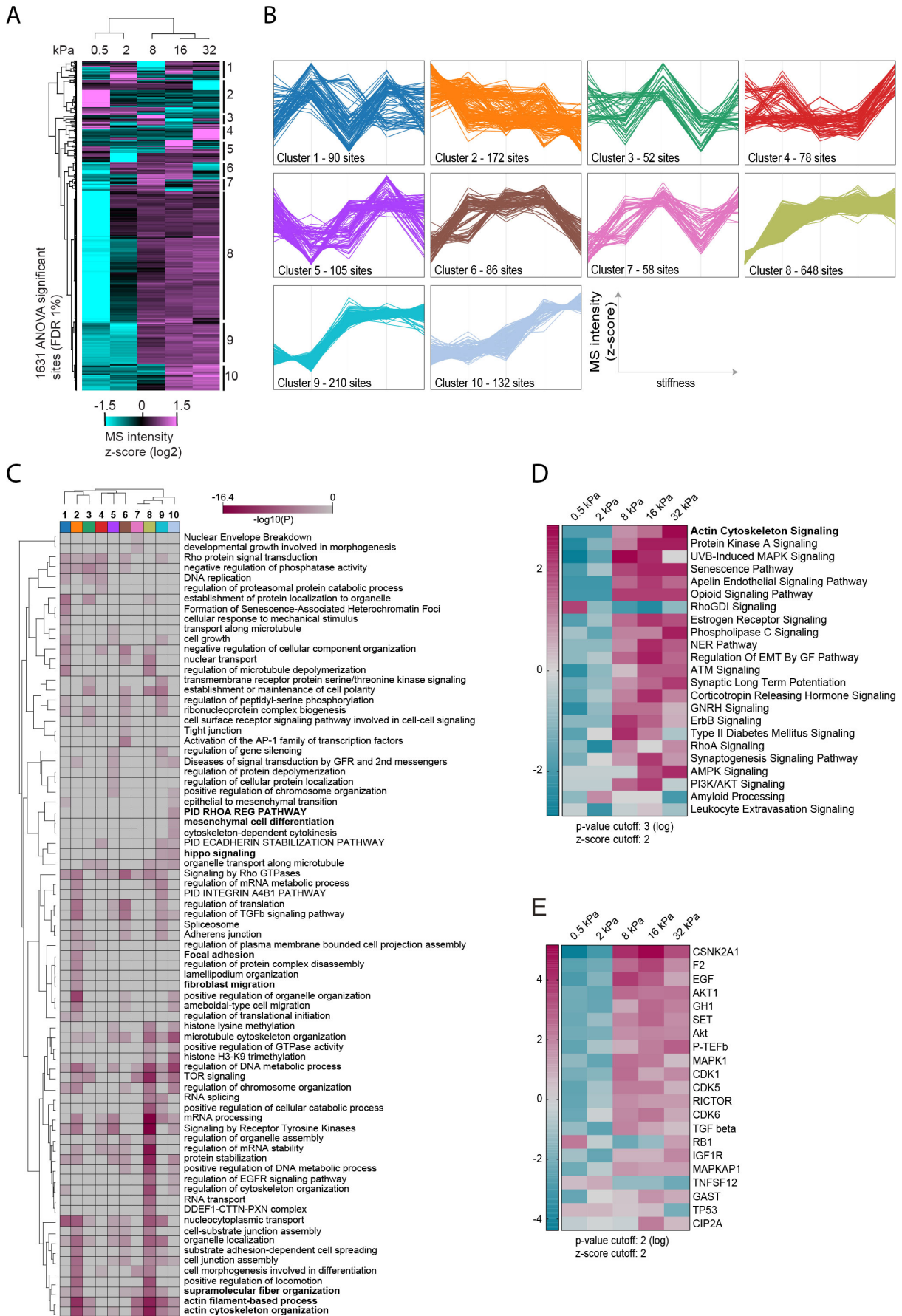
A

kPa 0.5 2 8 16 32

1631 ANOVA significant sites (FDR 1%)

1
2
3
4
5
6
7
8
9
10

-1.5 0 1.5
MS intensity
z-score (log2)

B

Cluster 1 - 90 sites
Cluster 2 - 172 sites
Cluster 3 - 52 sites
Cluster 4 - 78 sites
Cluster 5 - 105 sites
Cluster 6 - 86 sites
Cluster 7 - 58 sites
Cluster 8 - 648 sites
Cluster 9 - 210 sites
Cluster 10 - 132 sites

MS intensity (z-score)

stiffness

C

-16.4   0
-log10(P)

1 2 3 4 5 6 7 8 9 10

Nuclear Envelope Breakdown
developmental growth involved in morphogenesis
Rho protein signal transduction
negative regulation of phosphatase activity
DNA replication
regulation of proteasomal protein catabolic process
establishment of protein localization to organelle
Formation of Senescence-Associated Heterochromatin Foci
cellular response to mechanical stimulus
transport along microtubule
cell growth
negative regulation of cellular component organization
nuclear transport
regulation of microtubule depolymerization
transmembrane receptor protein serine/threonine kinase signaling
establishment or maintenance of cell polarity
regulation of peptidyl-serine phosphorylation
ribonucleoprotein complex biogenesis
cell surface receptor signaling pathway involved in cell-cell signaling
Tight junction
Activation of the AP-1 family of transcription factors
regulation of gene silencing
Diseases of signal transduction by GFR and 2nd messengers
regulation of protein depolymerization
regulation of cellular protein localization
positive regulation of chromosome organization
epithelial to mesenchymal transition
PID RHOA REG PATHWAY
mesenchymal cell differentiation
cytoskeleton-dependent cytokinesis
PID ECADHERIN STABILIZATION PATHWAY
hippo signaling
organelle transport along microtubule
Signaling by Rho GTPases
regulation of mRNA metabolic process
PID INTEGRIN A4B1 PATHWAY
regulation of translation
regulation of TGFb signaling pathway
Spliceosome
Adherens junction
regulation of plasma membrane bounded cell projection assembly
Focal adhesion
regulation of protein complex disassembly
lamellipodium organization
fibroblast migration
positive regulation of organelle organization
ameboidal-type cell migration
regulation of translational initiation
histone lysine methylation
microtubule cytoskeleton organization
positive regulation of GTPase activity
histone H3-K9 trimethylation
regulation of DNA metabolic process
TOR signaling
regulation of chromosome organization
RNA splicing
positive regulation of cellular catabolic process
mRNA processing
Signaling by Receptor Tyrosine Kinases
regulation of organelle assembly
regulation of mRNA stability
protein stabilization
positive regulation of DNA metabolic process
regulation of EGFR signaling pathway
regulation of cytoskeleton organization
RNA transport
DDEF1-CTTN-PXN complex
nucleocytoplasmic transport
cell-substrate junction assembly
organelle localization
substrate adhesion-dependent cell spreading
cell junction assembly
cell morphogenesis involved in differentiation
positive regulation of locomotion
supramolecular fiber organization
actin filament-based process
actin cytoskeleton organization

D

0.5 kPa 2 kPa 8 kPa 16 kPa 32 kPa

Actin Cytoskeleton Signaling
Protein Kinase A Signaling
UVB-Induced MAPK Signaling
Senescence Pathway
Apelin Endothelial Signaling Pathway
Opioid Signaling Pathway
RhoGDI Signaling
Estrogen Receptor Signaling
Phospholipase C Signaling
NER Pathway
Regulation Of EMT By GF Pathway
ATM Signaling
Synaptic Long Term Potentiation
Corticotropin Releasing Hormone Signaling
GNRH Signaling
ErbB Signaling
Type II Diabetes Mellitus Signaling
RhoA Signaling
Synaptogenesis Signaling Pathway
AMPK Signaling
PI3K/AKT Signaling
Amyloid Processing
Leukocyte Extravasation Signaling

p-value cutoff: 3 (log)
z-score cutoff: 2

E

0.5 kPa 2 kPa 8 kPa 16 kPa 32 kPa

CSNK2A1
F2
EGF
AKT1
GH1
SET
Akt
P-TEFb
MAPK1
CDK1
CDK5
RICTOR
CDK6
TGF beta
RB1
IGF1R
MAPKAP1
TNFSF12
GAST
TP53
CIP2A

p-value cutoff: 2 (log)
z-score cutoff: 2

60

Figure 20 I Identification and dynamics of substrate stiffness regulated phosphosites. A Hierarchical clustered heat map with the intensities (log2 z-scored normalized) of stiffness sensitive phosphosites (1631 ANOVA significant phosphosites) **B** Clustering analysis of rigidity-regulated sites. The 10 clusters were defined by hierarchical clustering (Pearson correlation). **C** Heat map showing enriched terms across gene lists of clusters 1 - 10, colored by p-values. Enrichment analysis was performed with Metascape (www.metascape.org). **D, E** Phosphoproteomic data was analyzed in IPA. Significance of term enrichment is indicated through shading as log p-value. Regulated pathways belonging to "Canonical pathways" (**D**) and predicted "Upstream regulator" **(E)** with significant enrichment are shown and color-coded according to their activation z-score.

In order to infer pathway activities and potential upstream regulators each rigidity condition was analyzed separately using Ingenuity Pathway Analysis platform (IPA, Qiagen, Redwood City, www.qiagen.com/ingenuity). Separate analyses for each rigidity were combined to form an overall comparison, which is shown in **Figure 20 D** for canonical pathways and in **Figure 20 E** for upstream regulators. The data indicates that the stiffness of 8 kPa is a critical threshold in this cell line. Exceeding this stiffness threshold triggers a change in the activity of several kinases and associated pathways. That the actin cytoskeleton signaling is regulated with increasing substrate stiffness shows that it is feasible to capture events dependent on substrate stiffness with this phosphoproteomic workflow. Also other important pathways such as RhoA signaling, PI3K/AKT signaling and phospholipase C signaling are activated by substrate stiffness. Many well-known kinases were identified as potential upstream regulators of phosphorylation changes in this data set, such as AKT, CKD1, CDK1, MAPK1. The kinase CK2A1 was identified as top upstream regulator for the phosphoproteomic data. But also other proteins not only kinases have a predicted regulatory effect on the measured phosphorylation and are probably involved in mechanosensing such as TGFbeta, EGF or RB1.

To map out regulated phosphosites on a functional representation of interconnected signaling pathways**,**

Figure *21* shows a schematic representation of phosphorylation sites found to be significantly regulated upon rigidity sensing in this study. Sections of the pathways HIPPO signaling, actin cytoskeleton signaling, integrin signaling, phospholipase C signaling, RHO A signaling, PI3K/AKT signaling, p70S6K signaling, ERK5 signaling, p38 MAPK signaling and mTOR signaling are illustrated. A lot of the phosphosites in this map do not have a known function yet, but are significantly regulated by substrate stiffness. Further investigations will be needed to assign functional relevance to them.
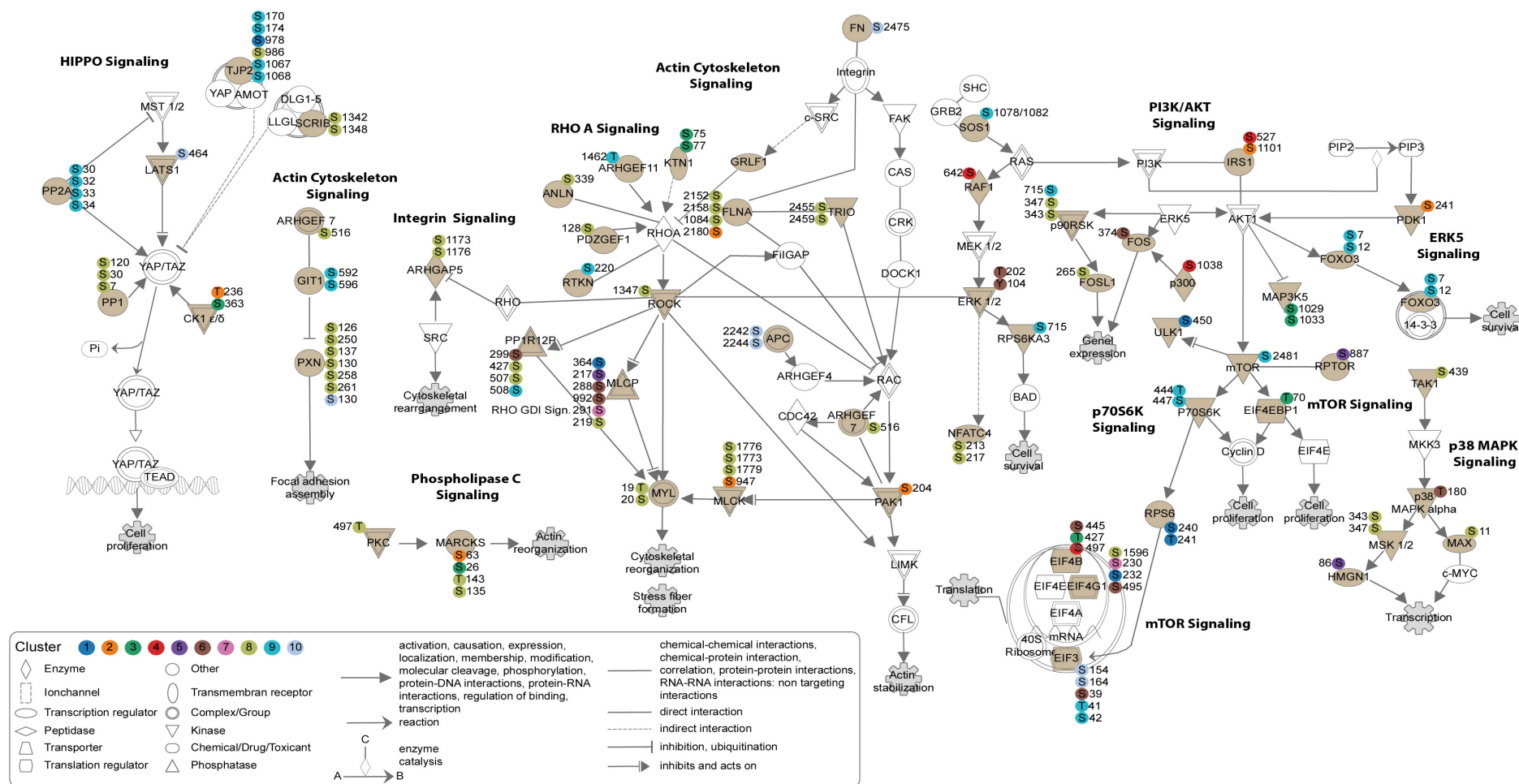
Figure 21 I Mapping of a subset of rigidity regulated phosphosites on canonical signaling pathways/networks. Phosphosites are color-coded according to their dynamic on different substrate stiffnesses as presented in **Figure 20 B**. Proteins color coded in light brown are contained in the stiffness regulated data. The white colored proteins where either not found to be phosphorylated in the data set or measured but were excluded by the settings of the performed ANOVA test.

Using the database PhosphoSitePlus (www.phosphosite.org), which provides information and tools to study PTMs including phosphorylation, 112 known regulatory phosphosites were identified among the ANOVA significantly regulated sites. The phosphorylation sites were sorted by their regulatory site process known from literature such as cell adhesion, cytoskeletal reorganization, cell motility and transcription. The dynamics of those sites on soft to stiff substrates according to their phosphorylation status and assigned cluster were summarized in **Figure 22**.
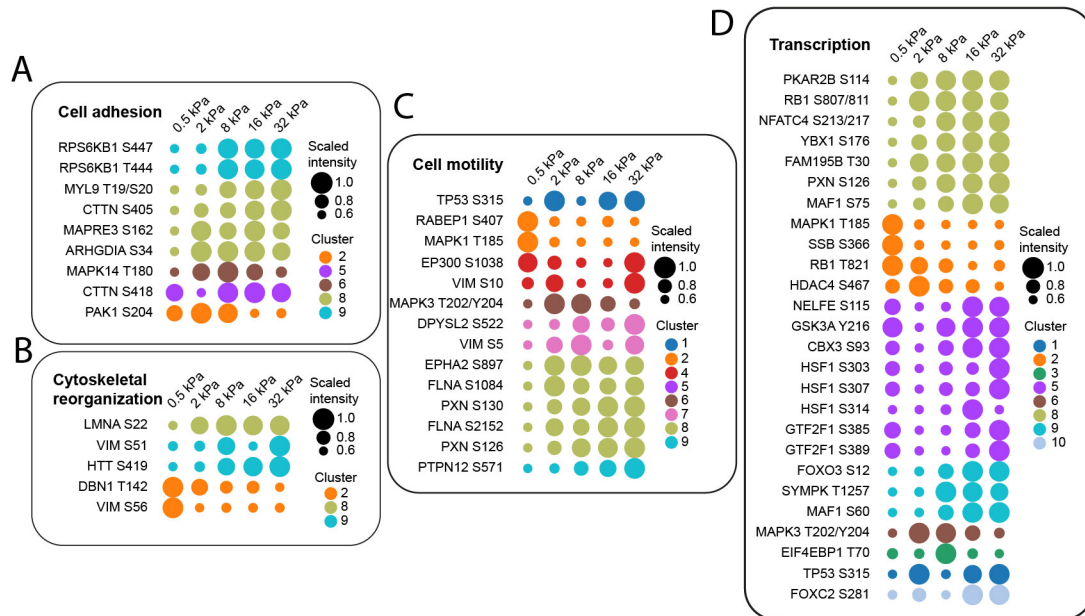
Figure 22 I Response of known regulatory phosphosites to stiffness. Dot plots showing the dynamics of scaled phosphorylation intensities on soft to stiff substrate of selected phosphosites associated with the regulatory sites process **A** 'Cell adhesion', **B** 'Cytoskeletal reorganization', **C** 'Cell motility' and **D** 'Transcription' (dots are color-codes per cluster as presented in **Figure 20 B**).

The data suggests that several kinases involved in cell adhesion and cell motility are differentially phosphorylated in a rigidity dependent manner such as PAK1, where serine 204 gets dephosphorylated with increasing stiffness. The phosphosite regulates the protein conformation and enzymatic activity of PAK1 and plays an important role in the formation of nascent adhesions and cell protrusions [177], indicating that this process gets turned off with increasing substrate stiffness. Phosphorylation of T444 and S447 of p70S6 kinase leads to boosted enzymatic activity [178-180], suggesting that the activity of this serine/threonine kinase is enhanced on stiff substrates and therefore is involved in the processing and transduction of mechanical signals. Furthermore, the MAP kinases MAPK1, MAPK3 and MAPK14 are differentially phosphorylated with changing mechanical stimuli. MAPK1 and MAPK3 are also known as ERK2 and ERK1. On soft substrate the phosphorylation of ERK2 on threonine 185 is high and then decreased on stiffer substrates, meaning that ERK2 activity

is likely higher on soft substrates, since T185 enhances ERK2 activity [181]. Also the activity of ERK1 is regulated via phosphorylation, here T202 and Y204 are the key phosphosites [181] and increased in phosphorylation on 2 and 8 kPa. Threonine residue 180 of MAPK14 is highest phosphorylated on 8 kPa and also this phosphosites accounts for induced activity of the kinase [182]. Also a phosphosite, namely serine 571, belonging to a PTPN12 phosphatase is increasing with stiffness and is relevant in the context of cell motility, since phosphorylation allows the interaction between PTPN12 and FAK and leads to dephosphorylation of Y397 of FAK, thereby promotion of migration [183]. Not only differentially phosphorylated kinases and phosphatases were detected but also various cytoskeletal associated proteins were phosphorylated in dependence on substrate stiffness.

Serine residues 405 und 418 of the actin-binding protein cortactin are get more phosphorylated with increasing stiffness. If phosphorylated on those sites cortactin is localized to sites of dynamic actin assembly in tumor cells and is essential in motility based cell processes [184]. The implications of increasing phosphorylation of T18/S19 on myosin light chain was already discussed. LMNA is a component of the nuclear lamina and the phosphosite serine 22 is found in cluster 8, which increase in intensity with increasing stiffness of the substrate. This phosphosite is required in the process of lamin A/C disassembly and is relevant during cytoskeletal rearrangement [185]. Various phosphosites of vimentin are regulated in a rigidity dependent manner, which is plausible since vimentin is part of the cytoskeleton as intermediate filament [186]. Drebrin1 is an actin-filament binding protein and contains a cryptic F-actin-bundling activity which is regulated by phosphorylation of threonine 142 [187]. The function of paxillin phosphorylation at serine 126 was already explained but also accounts for S130, which is also increasing in intensity with increasing substrate stiffness. Phosphorylation of paxillin S130 by ERK primes the molecule for following phosphorylation of S126 by GSK3B [176].

Substrate stiffness may induce long-term gene expression changes via phosphorylation of transcription factors. Here the changes in phosphorylation status of transcriptional regulators are shown (**Figure 22 D**). The phosphorylation of serine 126 of PXN is not only relevant for its turnover in focal adhesion, but also translocates the protein into the nucleus upon phosphorylation by ERK and acts as a coactivator to induce cyclin D1 transcription, thereby increasing cell proliferation [188]. Phosphorylation sites of RB1, PKAR2B, YBX1, NFATC4, FAM95B, MAF1, SYMPK and FOXO3a are also increasing in intensity, the more stiff the substrate gets. Phosphorylation of RB1 on serine 807 and 811 functionally inhibits tumor suppressor activity of the protein [189]. Another phosphosite of RB1, T821, is also regulated by stiffness, but the intensity is decreasing with increasing stiffness. This phosphosite stimulates tropoelastin transcription by facilitating the binding of RB1 to the transcription factor SP1 in dermal fibroblasts [190].

Elliot et al. showed that phosphorylation of S114 of the regulatory subunit of c-AMP dependent protein kinase (PKAR2B) is needed for nuclear import, thereby inhibiting IL-2 mRNA and protein synthesis in T cells [191]. The Y-binding box protein regulates transcription and translation and can bind both DNA as well as RNA. Phosphorylation of serine 176 was shown to be critical for the activation of NF-κB by YBX1 and also for the nuclear translocation of the protein [192]. Another well-known transcription factor, NFATC4 is phosphorylated on serine 213 and 217 by JNK1/2 which leads to the transactivation of the protein and induction its transcriptional activity [193]. According the measured phosphosite intensities is this activation dependent on substrate stiffness. FAM195B, also known as MCRIP1 was identified as a target of ERK. ERK-dependent phosphorylation of the protein plays an important role in ERK-induced epigenetic gene silencing during epithelial-mesenchymal-transition [194]. Two sites of MAF1 are increasingly phosphorylated, the more stiff the substrate is, serine 60 and serine 75. The phosphorylation of S75 inhibits MAF1 ubiquitination and therefore its turnover [195], furthermore attenuates the phosphosite the Pol III-repressive function of MAF1, so does S60 [196, 197]. Human MAF1 is a mTORC1 target and both sites are mTORC1 phosphorylation sites [197]. Symplekin (SYMPK) is also phosphorylated by ERK. The protein is localized to tight junctions and the nucleus and is involved in transcription modulation and mRNA maturation as well as tight junction assembly. Phosphorylation of T1275 promotes nuclear localization of symplekin and interaction with YBX3, which enhances cell proliferation [198].

FOXO3a is known to be hyperphosphorylated in IPF fibroblasts [199]. However, at the phosphorylation sites T32 and S253, which were both not measured in the stiffness regulated phosphoproteomics data set of this study. Nevertheless, increasing phosphorylation of S7 and S12 with increasing stiffness was observed for FOXO3a (**Figure 22 and Figure 24**). Celestini et al. hypothesizes that phosphorylation of S12 is induced upon metabolic stress, which causes an import of the protein into the mitochondria to activate mitochondrial gene expression. This supports mitochondrial metabolism and cell survival [200]. The transcriptional regulator SSB (Lupus La protein) shows decreasing phosphorylation of S366 the stiff the substrate is. The phosphorylation site is known to control tRNA maturation [201].

The phosphorylation sites HDAC4 S467, HSF1 S303/307/314, NELFE S115, GTF2F1 S385/389 and CBX3 S93 are assigned to cluster 5 and increase in phosphorylation with rising stiffness but were also measured on 0.5 kPa, however not peaking on soft conditions.

The heterochromatin protein CBX3 or HP1γ, binding to di- or trimethylated lysine 9 on histone H3 (H3K9), has an important role in chromatin packaging and the regulation of gene transcription. Recently, HP1γ has been involved in the development of cancer [202]. In this data set, S93 phosphorylation of CBX3 is elevated on stiff substrates, which directs the protein to sites of active transcription and upregulates proliferative genes [203]. Also HDAC4 plays an

important role in regulation of gene expression. Upon phosphorylation on S467 binding with 14-3-3 family proteins is facilitated leading to retention of the protein in the cytoplasm and thereby leading to enhanced transcriptional repression [204]. HSF1 is differentially phosphorylated on three residues within its regulatory domain upon mechanosensing of different substrate rigidities. However, a study by Budzynski et al. suggests that the phosphorylation signature alone is not an adequate marker for the activity of HSF1 [205]. Also phosphorylation of NELFE at residue 115 promotes binding of 14-3-3 family proteins which causes a rapid dissociation of the NELF complex from chromatin. This is followed by RNA polymerase II elongation [206]. GTF2F1 is the largest subunit of transcription factor TFIIFalpha with a serine/threonine kinase activity. The two residues serine 385 and 389 are autophosphorylated. Rossignol et al. showed that the deletion of the two phosphosites leads to an upregulation of transcription [207].

Taken together, these results indicate that several key regulators of cell shape and motility and also various transcriptional master regulators are differentially phosphorylated in dependence of substrate stiffness. This clearly reflects the great influence an underlying substrate has on a cells fate.

Profiling of kinase activities regulated by substrate stiffness

The casein kinase II (CK II α, CK2A1, CSNK2A1) was identified as top upstream regulator in the IPA analysis (**Figure 20 E**). This result is based on the phosphorylation status of known CK2A1 targets (**Figure 23 A**). The protein phosphorylation of almost all of those sites is increasing with increasing substrate stiffness. This suggests that the activity of the CK2A1 kinase is elevated on rigid substrates.
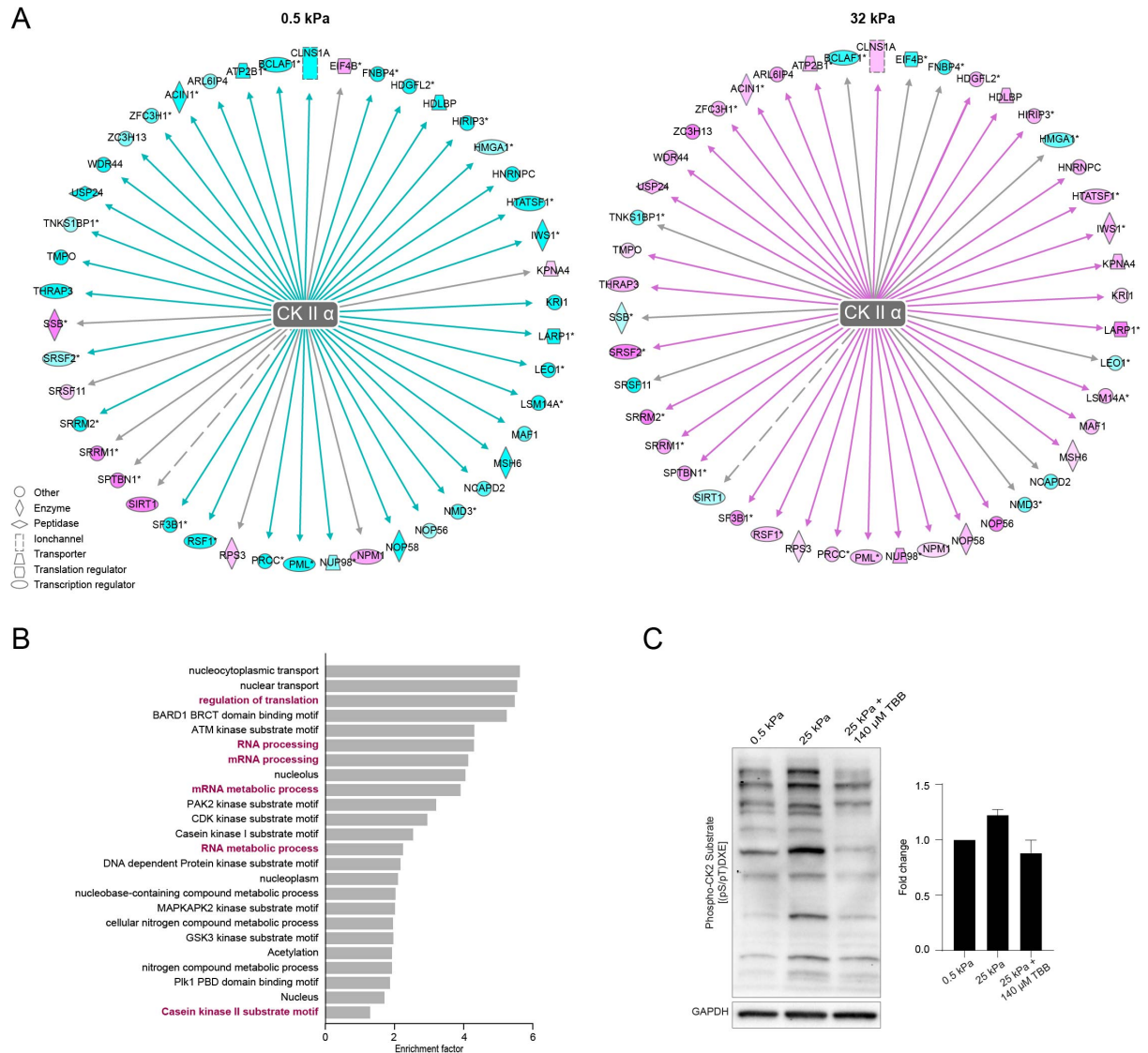

Figure 23 I Activation of kinase CK II alpha on stiff substrates. A The graphs show CK2A1 targets predicted by IPA and their phosphorylation status in the phosphoproteomic data set. Turquoise color shades indicate low phosphorylation and pink color shades indicate high phosphorylation. Doted lines indicate an indirect interaction and continuous lines specify a direct interaction. **B** Enrichment analysis of phosphoproteomic data for enhanced annotations using Fisher exact test (FDR 0.05 %) **C** Immunoblot analysis of equal amounts of proteins from total cell lysates seeded for 120 min on 0.5 and 25 kPa substrates or 25 kPa + CKII inhibitor, probed with an antibody specific for proteins containing a pS/pTDXE motif, which represents a CK2 phosphorylation consensus sequence. GAPDH served as a loading control. Increasing phosphorylation of CK2 substrates is observed, if cells are seeded on 25 kPa substrates compared to 0.5 kPa substrates The increase is phosphorylation on stiff substrates could be blocked by treating the cells with 140 µM TBB, a CK II alpha inhibitor.

A Fischer's exact test was performed with the sites predicted by IPA to be CK2A1 targets to identify statistically enriched protein annotations. Terms as 'regulation of translation' and 'mRNA processing' and also the CK2A1 substrate motif were found to be overrepresented (**Figure 23 B**). To validate the *in silico* finding of enhanced CK II activity in vitro, cell lysates of cells seeded for 120 min on 0.5 kPa and 25 kPa and were probed with an antibody specific for phosphorylated pS/pTDXE motif. This motif is a CK2A1 consensus sequence [208]. More phosphorylation intensity was detected in cell lysates of cells cultured on stiff substrates compared to soft substrates. Furthermore, in cells treated with the CK2A1 specific kinase inhibitor TBB and cultured on stiff substrates the phosphorylation level was decreased. So the increase of phosphorylation on stiff substrates could be blocked by treating the cells with 140 µM TBB, a CK II alpha inhibitor. Hence, the activity of CK2A1 is enhanced in cells encountering a more stiff substrate. However, no statement is possible whether the activation is directly dependent on substrate stiffness or of indirect nature.

When comparing the CK2A1 substrates predicted by IPA with the phosphorylation sites phosphorylated *in vivo* by CK2A1 according to the PSP database, there is no consistency (**Figure 24 CK2A1**). Eleven phosphosites in the significantly regulated data have CK2A1 assigned as putative *in vivo* kinase. However, five of those sites are increasingly phosphorylated with elevated substrate stiffness.

Also other kinases were predicted as upstream regulator of the change in phosphorylation with stiffness, such as CDK1, CDK5, AKT1, MAPK1 and MAPKAP12 (**Figure 20 E**). Also those kinases seem to be more activated above a rigidity threshold of 8 kPa. Within the phosphorylation sites which are assigned to a putative *in vivo* kinase, the most of those sites are also increased with increasing substrate stiffness (**Figure 24**). For the kinases CK2A1, CDK2, CDK1, mTOR, PKACA, ERK1/2 and GSK3B at least six or more phosphosites known to be assigned to those kinases were found to be regulated in a stiffness dependent manner. For all the other kinases only one to three target sites were differentially phosphorylated with substrate stiffness. No clear activation of certain kinases can be deduced from the different phosphorylation states of the known targets. However, most of the kinases seem to be more active with increasing substrate stiffness. Especially mTOR targets are increasingly phosphorylated with rising substrate stiffness. Also the autophosphorylation site of mTOR S2481 gets more phosphorylated on the stiffer the substrates. This site regulates among other processes, the enzymatic activity of the protein [209]. GRK5 activity is regulated by autophosphorylation as well. The sites S484 and T485 are increasingly phosphorylated with rising substrate stiffness, hence the enzymatic activity of GRK5 is enhanced [210]. It is noticeable that kinases which phosphorylate sites that increase with substrate stiffness does

not overlap with kinases that phosphorylate sites that are only strongly phosphorylated to 0.5 kPa in this dataset. Solely, CK2A1, CDK1/2 and PKACA phosphorylate targets of various clusters including increasing and decreasing phosphorylation with increasing substrate rigidity. PDK1, Pim2, PRKD1, SMG1, TTK, UL97, WNK1/2 and MEK1 have a tendency to be more active on soft substrates according to the phosphorylation status of their targets. On the contrary, ROCK, AKT1, AMPKA1, GRK5, CAMK1A, HER2, JNK2, Myt1, p90RSK, PLK1, PKCD, CK1A, CDK3, Chk1, DYRK2 and PAK1 appear to operate more actively when cells encounter stiffer substrates. For most of the rigidity-regulated phosphorylation sites no kinase-substrate relationship is known so far. Altogether, these results demonstrate the involvement of various kinases in mechanical signaling, suggesting that mechanical signaling is integrating many pathways to build a signaling network with various self-regulations and feedback connections.
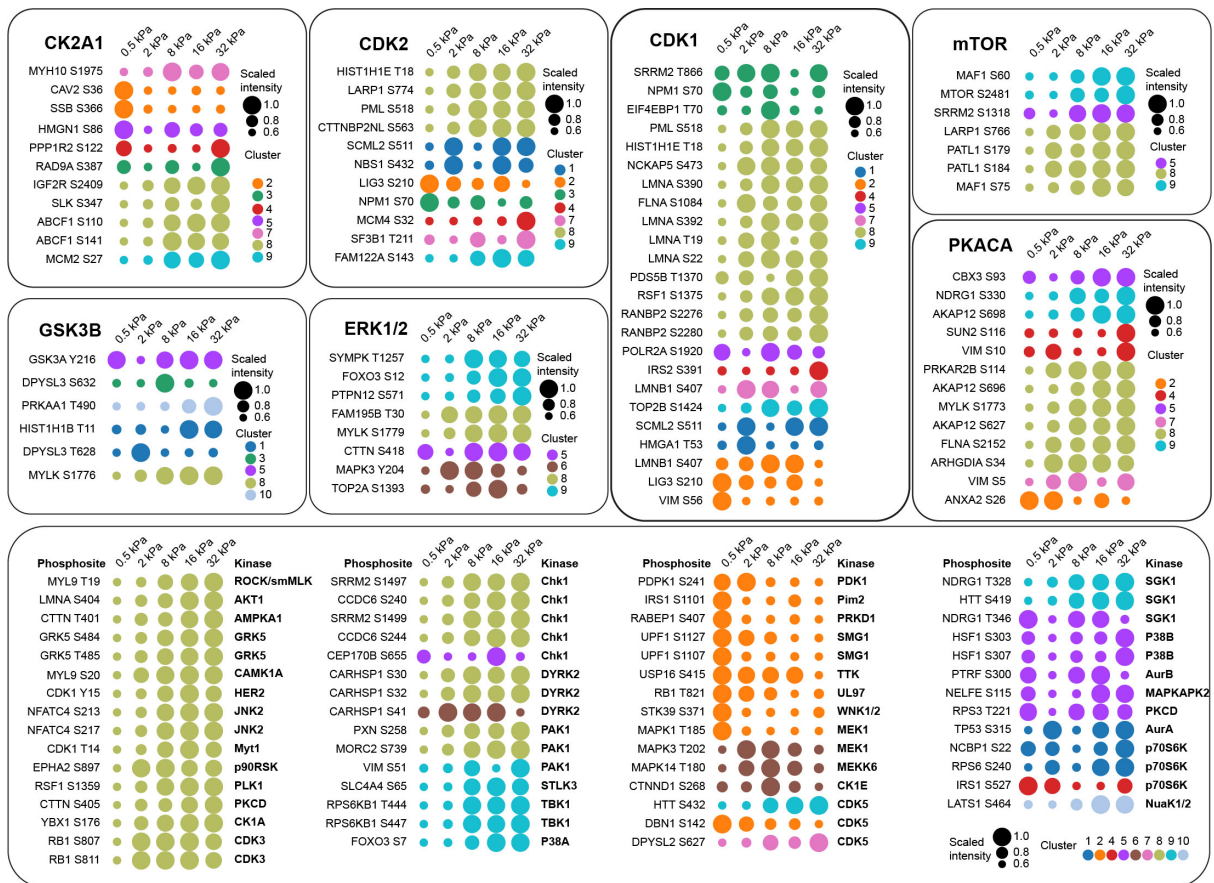

Figure 24 I Regulated phosphorylation sites known to be putative substrates of distinct kinases in vivo. Dot plots showing the dynamics of scaled phosphorylation intensities on soft to stiff substrate of selected phosphosites with known upstream kinases (dots are color-codes per cluster as presented in **Figure** 20 **B**).

Validation of phosphorylation sites in human lung fibrosis

To further validate stiffness regulated phosphorylation of distinct sites in human lung fibrosis, I stained human tissue sections for phosphorylated PXN at residue 126 and for phosphorylated CBX3 at serine 93. Indeed, less phosphorylation of PXN at serine 126 was detected in the alveolar space of healthy control lungs compared to tissue section of IPF lungs (**Figure 25 upper panel**). However, the phosphorylation of PXN was primarily seen in hyperplastic epithelial cells and not so much in interstitial cells where one would expect the fibroblasts. I expected to see the increase in phosphorylation rather in fibroblasts in fibrotic areas with high ACTA2 expression. PXN phosphorylation was also detected in those areas, but not as prominent as in the hyperplastic cells.
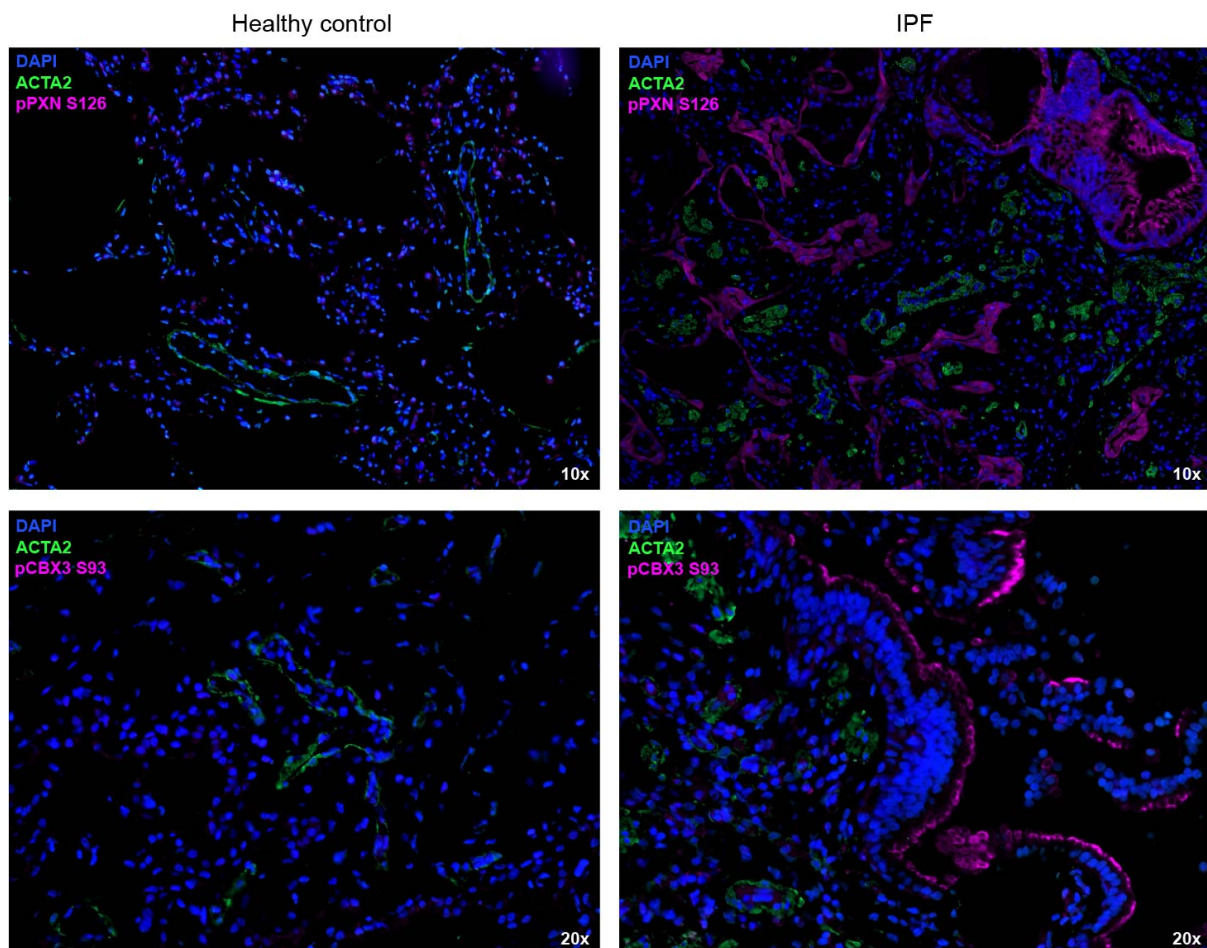

Figure 25 I Phosphorylated PXN and CBX3 in human lung fibrosis. Upper panel: FFPE sections from non-fibrotic controls and fibrotic regions of IPF patient lungs were stained against ACTA2 (green), pPXN S126 (magenta), and DAPI (blue) revealing pronounced phosphorylation of PXN at S126 in fibrotic tissue. **Lower panel:** FFPE sections from non-fibrotic controls and fibrotic regions of IPF patient lungs were stained against ACTA2 (green), pCBX3 S93 (magenta), and DAPI (blue) revealing pronounced phosphorylation of CBX at S93 in fibrotic tissue.

An increase in phosphorylated CBX3 at serine 93 in IPF lung tissue was also seen (**Figure 25 lower panel**) compared to healthy lung tissue with almost no phosphorylation of CBX3. CBX3 phosphorylation was visible in close proximity to ACTA2 expression, but also very strong in epithelial cells in areas of hyperplasia and airway remodeling.

Taken together, both PXN phosphorylation at S126 as well as CBX3 phosphorylation at S93 are elevated in IPF lung tissue section even if the increase in phosphorylation is not primarily seen in fibroblasts.

Mapping phosphorylation sites in human lung fibroblasts during a time course of cell spreading on stiff substrate

Cell spreading is usually isotropic in the first 30-60 min during the area-increase phase (**Figure 26 A**). This means that the cell spreading is identical in all directions. In the second phase stress fibers are formed and focal adhesions are reorganized while the cells gradually elongate with only minor changes in cell area [44]. Immunofluorescence staining of PXN, phospho T18/S19 MYL9 and the actin cytoskeleton depicts the cytoskeletal rearrangement process, which the CCL151 human lung fibroblasts are undergoing during spreading. Here, cells were fixed after 20 and 240 min of seeding time. After 240 min of spreading are a lot stress fibers (seen in the phalloidin staining) are being formed and many focal adhesions can be seen (spots with high intensity of PXN staining).
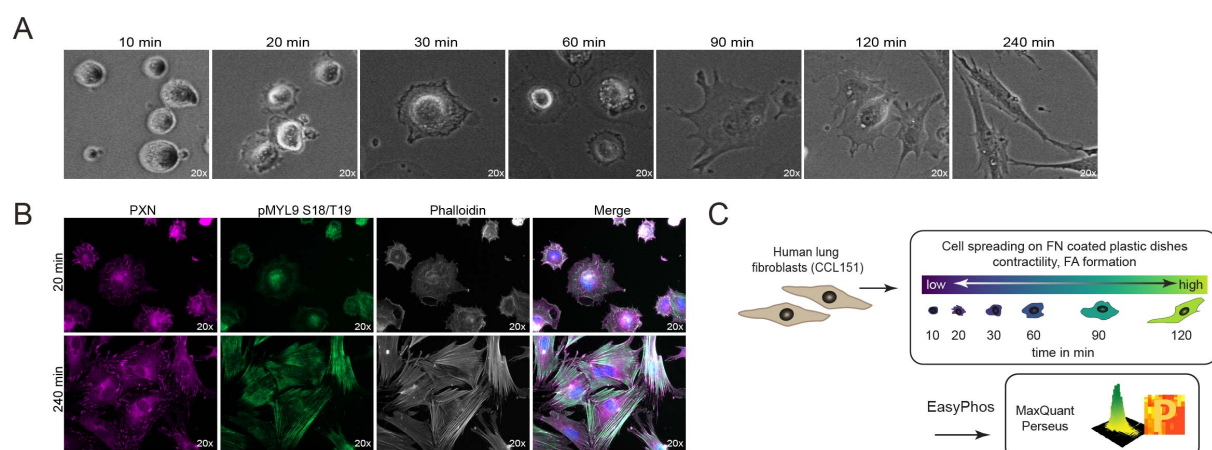

Figure 26 I Cell spreading and phosphoproteomic workflow. A Shows a series of cell images on fibronectin-coated solid glass after 10 to 240 min of spreading time. **B** Fluorescent immunostainings of CCL151 cells spreading from 20 and 240 min after cell seeding show PXN in magenta, phosphorylated MYL9 (Thr18/Ser19) in green and actin (Phalloidin) in white. **C** Experimental workflow to analyze the phosphoproteome of human lung fibroblasts during cell spreading.

Also the diphosphorylation of MYL9 on T18 and S19 is increased in contrast to only 20 min of spreading time. The dephosphorylation of MYL9 results in an continued increase of the actin-activated Mg^{2+}-ATPase activity and myosin IIA is very much activated and is responsible for

the proper spread of the cell [211]. In order to identify phosphorylation sites which are temporally regulated upon cell attachment and during the process of cell spreading, phosphoproteomes were measured after 10, 20, 30, 60, 90, and 120 min after seeding. Therefore, CCL151 cells were expanded, released from their culture dishes, kept in suspension for 30 min and afterwards reseeded on fibronectin coated culture dishes. Cell lysis, phosphopeptide enrichment and sample preparation for MS was performed in the same way as for the phosphoproteomes on various substrate rigidities (**Figure 26 C**).

In the cell spreading phosphorylation data, even more phosphosites could be identified than in the substrate stiffness phosphoproteomic data set. A total of 12364 class I phosphosites were detected. The single replicates of each time point cluster relatively close together in a PCA analysis. The location of the time points in the PCA analysis follows the time line except for time point of 90 minutes of cell spreading, but shows a good agreement of the biological samples (**Figure 27 A**).
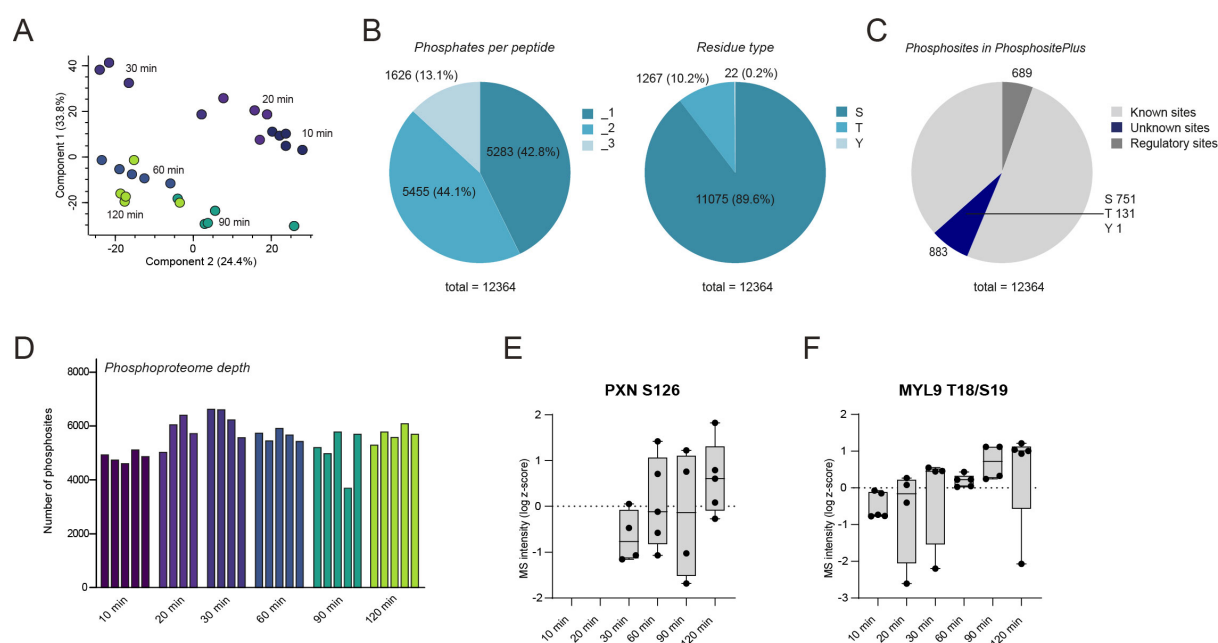

Figure 27 I Description of the phosphoproteomic data set during the process of cell spreading. A PCA of the regulated phosphoproteome during cell spreading. Two major components separate the data according to spreading time. **B** Right panel: pie chart presenting the percentage of identified phosphorylated serines (S), threonines (T) and tyrosines (Y) residues in the cell spreading data set. Left panel: pie chart presenting the percentage of identified singly, doubly and triply (or more) phosphorylated peptides in the spreading data set. **C** Pie chart showing the number of already known sites, previously unreported sites and known sites with an assigned regulatory function in the PhosphoSitePlus database of the spreading data set. **D** Phosphoproteome depth of the phosphoproteomic data set during cell spreading. **E** Phosphorylation of PXN on serine residue 126 is increasing during cell spreading**.** MS intensity values are log z-scored and shown without imputation. **F** Phosphorylation of MYL9 on threonine residue 18 and serine residue 19 is increasing with spreading time. MS intensity values are log z-scored and shown without imputation.

The distribution of the singly, doubly and triply phosphorylated peptides is almost the same as in the other data set, 42.8 % are singly, 44.1 % are doubly and 13.1 % are triply phosphorylated

(**Figure 27 B**). In case of the three different residue types the percental distribution is very similar to the rigidity data set, with serine being the most phosphorylated residue, followed by threonine and only very little tryrosine phosphorylations were captured (**Figure 27 B**). According to PhosphoSitePlus the data set contains 689 regulatory phosphosite with a known function. Nevertheless, 883 sites are unknown and were probably captured for the first time, consisting of only one new tyrosine phosphorylation site, but 131 threonine sites and 751 phosphorylated serines (**Figure 27 C**). The average phosphoproteome depth per replicate was 7224 (**Figure 27 D**). I searched the dataset for specific positive control phosphosites to validate the accuracy of the performed experiment. An increase in PXN phosphorylation can be seen over time, as expected. As shown in the immunostaining, the phosphorylation intensity of T18/S19 of MYL9 is also increasing over time during cell spreading, going along with increased contractility of the cell increases (**Figure 26 B**).

Identification of phosphorylation sites regulated during cell spreading

To explore the temporal regulation of phosphorylation upon cell attachment to fibronectin ANOVA analysis (1 % FDR) of various timepoints resulted in 1265 significantly regulated phosphosites (**Figure 28 A**). Also for this data set a combination of ANOVA testing with and without prior imputation was performed. These regulated sites account for around 12 % of the phosphorylation sites in the total data set and belong to 569 different proteins. Mainly phosphosites with phosphorylation on serine residues were regulated, namely 1174 sites, and only 87 threonines and four tyrosines were found to be regulated in the process of cell spreading. A heatmap depicting the course of phosphorylation over time was generated by hierarchical clustering (Pearson correlation) of the z-scored MS intensities. If one would divide the data, roughly three groups are emerging. On the one hand phosphorylation events which come very early during cell attachment (10-30 min) and on the other hand phosphorylation which occurs rather late during the time course (60-120 min), as well as phosphorylation events peaking at 20-60 min (**Figure 28 A**). Nevertheless, this categorization is very broad and was more refined by hierarchical clustering of the sites which resulted in eleven different cluster trends. The courses of the clusters are depicted in **Figure 28 B**. The 24 phosphosites in cluster 1 are increased at the beginning of the cell spreading process (10-20 min) and decrease afterwards. Cluster 2 contains 41 phosphorylation sites. The intensity of those sites is rather stable over time but decreases from 10 to 20 min enormously. In cluster 3 by contrast, the phosphorylation intensity of the contained sites is increasing with time, peaking at 30 min and then declines strongly but increases again until 120 min. The cluster with the most members is represented by cluster 4 with 459 sites being regulated in a similar way. Phosphorylation over 10, 20 and 30 min is relatively high but then decreases steeply and stays on a low level. Cluster 5 has only around half the number of sites as cluster 4 has. The profile

of cluster 5 is increasing with time and peaking at 30 min, then decreases strongly and forms a plateau at 90-120 min after seeding. The 50 phosphorylation sites of cluster 6 are increasing in phosphorylation up to 60 min of cell spreading but then decrease again only to be followed by an increase, peaking at 120 min.
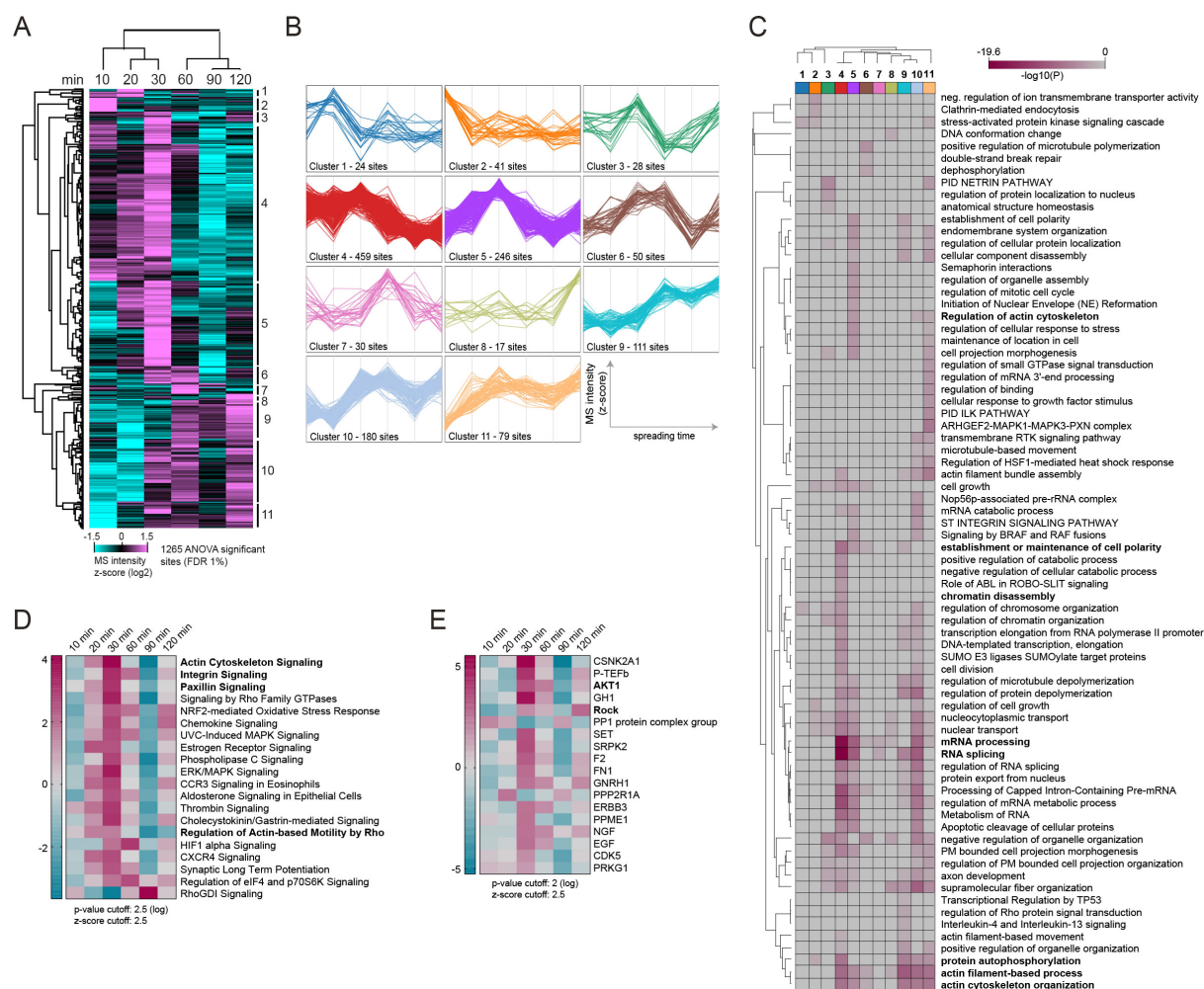

Figure 28 | Identification and dynamics of phosphorylation events in spreading cells.
A Hierarchical clustered heat map with the intensities (log2 z-scored normalized) of regulated phosphosites (1265 ANOVA significant phosphosites) during the process of cell spreading **B** Clustering analysis of phospho-regulated sites The 10 clusters were defined by hierarchical clustering (Pearson correlation). **C** Heat map showing enriched terms across gene lists of clusters 1 -10, colored by p-values. Enrichment analysis was performed with Metascape (www.metascape.org). **D, E** Phosphoproteomic data was analyzed in IPA. Regulated pathways belonging to "Canonical pathways" **(D)** and predicted "Upstream regulator" **(E)** with significant enrichment are shown and color-coded according to their activation z-score.

The cluster profile of cluster 7 behaves almost as cluster 6, being increasingly phosphorylated up to 60 mins but then the intensity is decreasing and stays rather on the same level. Cluster 8 contains only 17 phosphorylation sites. The intensity of those sites is rather stable over time but increases from 90 to 120 min enormously. Low phosphorylation status after 10, 20 and 30 min with steep in rise in phosphorylation intensity to 60 min and continued high phosphorylation on 90 and 120 min characterizes the 111 sites contained in cluster 9. Cluster

10 shows an increase in phosphorylation after 20 min and stays on the a high level over time. The phosphorylation intensity of the 79 sites contained in cluster 11 is nearly identical to cluster 10 but the initial increase is more prominent and the slight drop of phosphorylation intensity at 90 min is not so prominent.

Analysis of annotations enriched within the set of phosphorylation sites in a given cluster was performed with Metascape [172]. An overview of the different terms enriched across the eleven clusters is shown in **Figure 28 C**. The analysis demonstrated, that especially the clusters 4, 5, 9, 10 and 11 are enriched with sites corresponding to 'protein autophosphorylation', 'supramolecular fiber organization', 'actin filament based process' and 'actin cytoskeleton organization'. Particularly, cluster 4 showed a strong enrichment of terms belonging to RNA processing and splicing, which were however also found in cluster 5 and 10. Processes such as the 'establishment or maintenance of cell polarity' were found to be enriched in cluster 4, 5 and 10 as well. Many proteins belonging to the ARHGEF2-MAPK1-MAPK3-PXN complex were increasingly phosphorylated and statistically enriched in cluster 11.

For the prediction of pathway activities and potential upstream regulators, each time point was analyzed separately using IPA. The separate analyses revealed a similar list of pathways and upstream regulators which were compiled onto an integrated view (**Figure 28 D** and **E).** All enriched signaling pathways have the highest activation z-score at the 30 min time point, except for RhoGDI Signaling which is activated the most at 90 min after cell seeding and HIF1alpha signaling and Regulation of eiF4 and p70S6K Signaling being highest activated at the 60 min timepoint. Furthermore, the data shows a decline in activation of almost all signaling pathways at 90 min. Many pathways related to cell spreading are predicted to be regulated, such as Actin Cytoskeleton Signaling, Paxillin Signaling, Integrin Signaling and Regulation of actin based motility by Rho. The highest activation of most upstream regulators is corresponding to the activation pattern of the signaling pathways, peaking at 30 min after initial cell seeding. CK2A1 is as well found as one of the top upstream regulators in the spreading data set. In addition also other kinases such as AKT, ROCK, CDK5, SRPK2, ERBB3, PRKG1 were regulated in activity. Since signaling is not only regulated though addition of phosphates but also by dephosphorylation it is not surprising that phosphatases are differently activated in the time course, too. PP1 and PPP2R1A have unlike the other upstream regulators their peak in activity at 10-20 min. However, upstream regulators are not restricted to phosphatases and kinases, proteins as FN1, hormones (GH1 and GNRH1) and transcription factors such as P-TEFb seem to be regulated in activity during cell spreading.

Additionally, a schematic representation of phosphorylation sites found to be significantly regulated during cell spreading in this study has been drawn, and were mapped on proteins known from the literature to be functionally relevant in distinct signaling pathways (**Figure 29**).

Sections of the pathways ERK/MAPK signaling, actin cytoskeleton signaling, integrin signaling, phospholipase C signaling, Paxillin signaling, signaling by Rho GTPases signaling, HIF1a signaling, Regulation of eiF4 and p70S6K signaling are illustrated. A lot of those, pathway annotated, phosphosites do not have a known function yet, but seem to be regulated in the process of cell spreading. Further investigations will be needed to assign functional relevance to them.
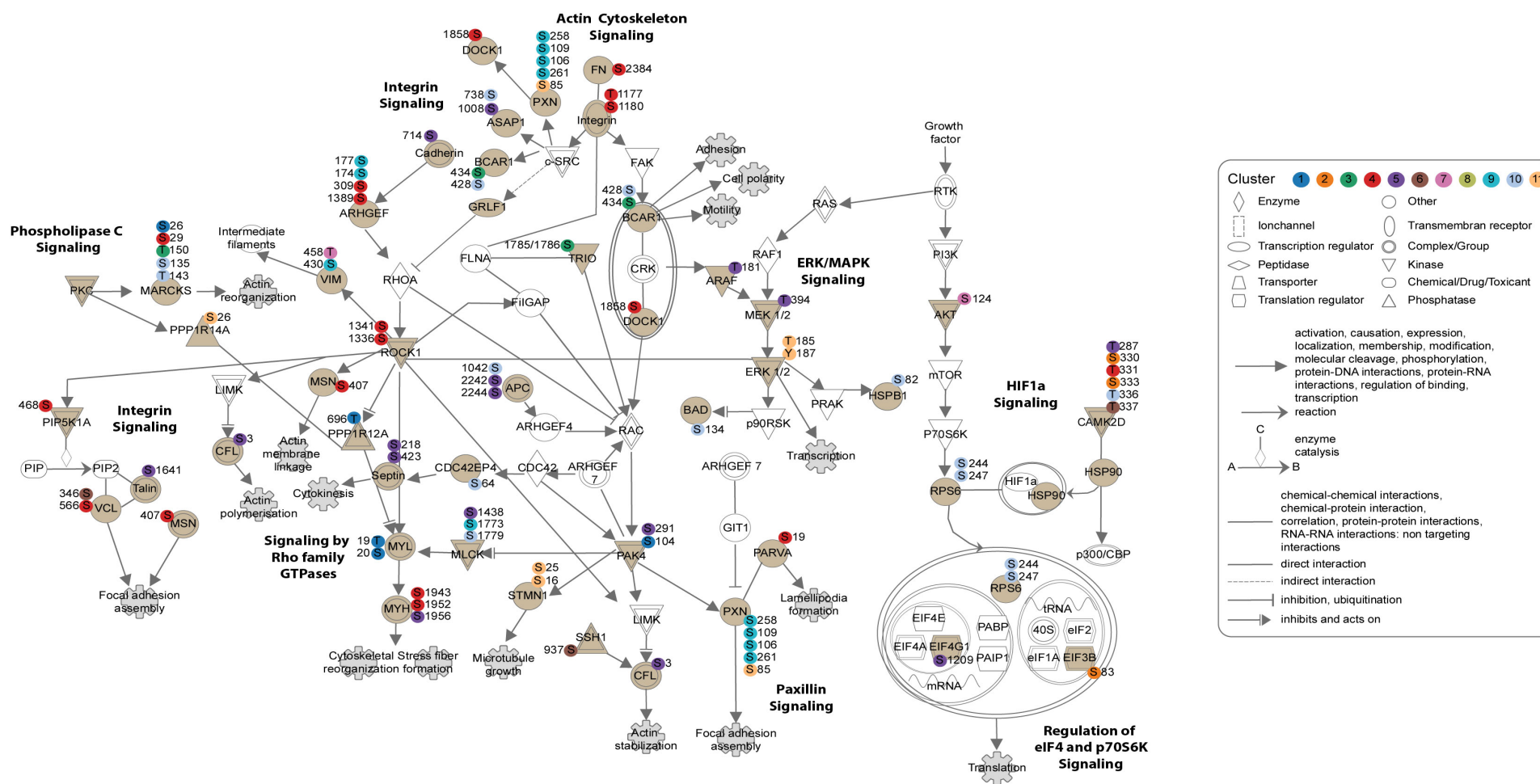
Figure 29 I Mapping of a subset of regulated phosphosites during cell spreading on canonical signaling pathways/networks. Phosphosites are color-coded according to their dynamic in the spreading time course as presented in **Figure** 20 **B**. Proteins color coded in light brown are contained in the regulated data. The white colored proteins where either not found to be phosphorylated in the data set or measured but were exclude by the settings of the performed ANOVA test.

Using the same approach as for the rigidity dependent phosphorylation events, 90 known regulatory phosphosites were identified among the ANOVA significantly regulated sites. I sorted the phosphorylation sites by their regulatory site process known from literature such as cell adhesion, cytoskeletal reorganization, cell motility, cell growth and transcription. The dynamics of those sites over spreading time were summarized according to their phosphorylation status and assigned cluster (**Figure 30**).
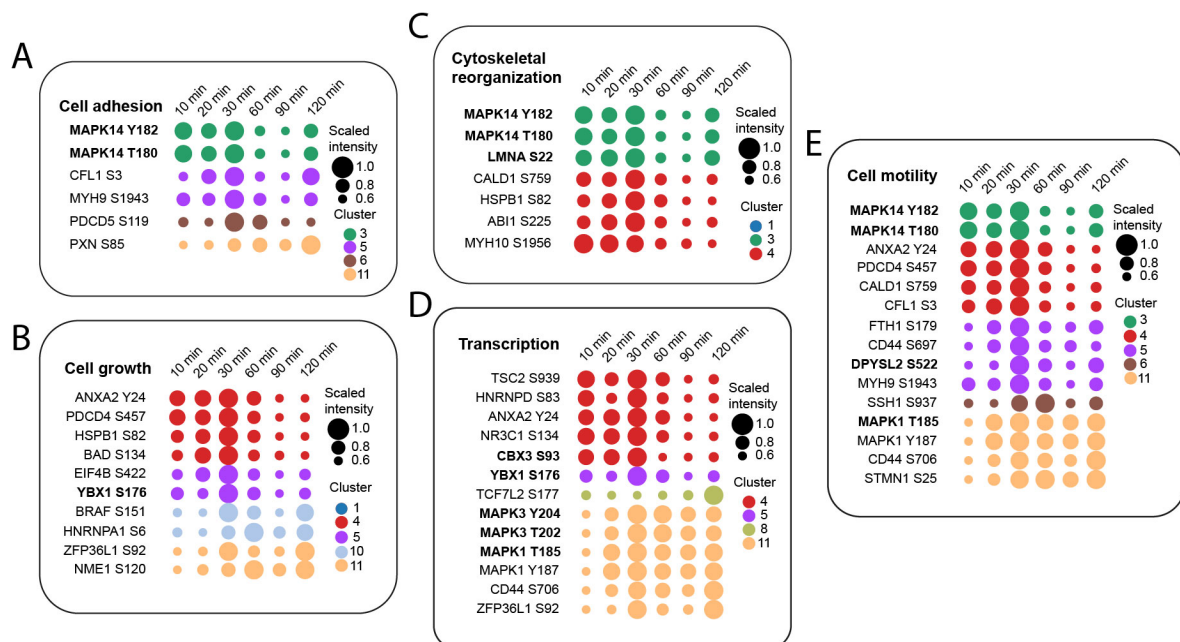

Figure 30 I Course of phosphorylation of known regulatory phosphosites during cell spreading. Dot plots showing the dynamics of scaled phosphorylation intensities over spreading time of selected phosphosites associated with the regulatory sites process **A** 'Cell adhesion', **B** 'Cell growth', **C** 'Cytoskeletal reorganization', **D** 'Transcription' and **E** 'Cell motility. Phosphosites written in bold were also identified in the phosphoproteomic data set regulated by substrate stiffness. (dots are color-codes per cluster as presented in **Figure 28 B**).

As an example for regulated focal adhesion proteins, the adaptor protein paxillin, is increasingly phosphorylated over spreading time at serine 85. This specific phosphosite is cell adhesion-dependent, which explains the low phosphorylation at early spreading time points. Phosphorylation at this site is important for regulation of focal adhesion dynamic and the interaction with talin and therefore needed for cell migration [212]. CFL, MYH9 and PDCD5 phosphorylation on serine 3, 1943 and 119 respectively, are also known to be relevant in cell adhesion. All three sites are peaking at 30 min of spreading time. The actin-binding protein cofilin is phosphorylated by ROCK2 on S3 thereby regulation actin polymerization. Upon phosphorylation the actin association of cofilin is disabled and thus prevents actin remodeling [213]. MYH9 phosphorylation at serine 1943 in the C-terminal part of the protein is known to be relevant for upstream focal adhesion signaling and focal adhesion stabilization. Furthermore, the phosphosite has been shown to be regulated during TGFß-induced

epithelial-mesenchymal transition and might be critical during invasion processes [214]. Phosphorylation sites known to be of relevance in cytoskeletal rearrangements like CALD1 S504, HSPB1 S82, ABI1 S225 and MYH10 S1956 are solely highly phosphorylated during the first 30 min of spreading. NMR spectroscopy showed that caldesmon phosphorylation at serine residue 759 alters the minimal inhibitory region of the protein (residue 750-779) leading to significantly reduced actin affinity thereby regulating actomyosin interactions [215]. Phosphorylation of the small heat shock protein HSPB1 in platelets leads to stimulating effect of actin polymerization and is also relevant for cell growth [216]. ABI1 is part of the WAVE2 regulatory complex, which is activated upon phosphorylation and in turn then activates actin assembly via Arp2/3. So phosphorylation on serine 225 is needed for functional interaction of the WAVE2 regulatory complex with Arp2/3 [217].

Interestingly, phosphorylation sites involved in cell growth are mainly phosphorylated at later time points. Yuan et al. reported that phosphorylation of ANXA2 on tyrosine 24 is required for breast cancer proliferation, invasion and metastasis by being able to bind and activate STAT3 [218]. Phosphorylation of BAD on serine 134 acts in an antiapoptotic manner and seems to be critical in survival signaling of tumor cells [219]. The translational inhibitor PDCD4 gets degraded upon phosphorylation on S457. This downregulation of the protein in turn promotes proliferation, survival and cell migration in breast cancer cells [220]. BRAF phosphorylation on serine 151 is caused by activated ERK. This hinders binding of BRAF to activated Ras and also contributes to the interruption of BRAF/C-RAF heterodimers, thereby altering the signaling via feedback phosphorylation [221]. In colorectal cancer, the phosphorylation of HNRNPA1 at S6 leads to reprogramming of the glucose metabolism and cell growth, associated with reduced survival rates in patients with high S6 phosphorylation [222]. The phosphorylation on serine 92 stabilizes the ZFP36L1 protein and inhibits its binding to RNA. Phosphorylation on this site may also inhibit cell growth [223].

Phosphorylation sites are often implicated in more than one cellular process, such as phosphorylation of MAPK14 which is relevant in cell adhesion, cytoskeletal rearrangement and cell motility. The same phosphorylation site can affect different protein complexes that are important in different cellular functions. Phosphorylation of CD44, STMN1, SSH1, FTH1 and MYH9 play also a role in cell movement. For maintenance of cell migration properties the phosphorylation of STMN1 at serine 25 is required. Furthermore, it was shown that this phosphosite is associated with shorter disease-free survival in breast cancer [224]. Phosphorylation of the phosphatase SSH1 on serine 937 leads to reduced binding capabilities with 14-3-3 proteins. Without being linked to 14-3-3, SSH1 can be activated by F actin which results in dephosphorylation of cofilin and thereby in local activation of cofilin in lamellipodia [225].

Cell spreading on a substrate induces tension-dependent changes in cell morphology, which are tightly related to gene expression, growth regulation as well as survival. The combination chemical and mechanical signals is believed to be essential for the control of these cellular functions [226]. For that reason it is not surprising that many proteins involved in transcriptional regulation are differential phosphorylated in the process of cell spreading. TSC2, HNRNPD, ANXA2, NR3C1, and CBX3 are highly phosphorylated in the early phase of spreading. TCF7L2 is only phosphorylated after 120 min of spreading time. And phosphorylation of MAPK3, MAPK1, CD44 and ZFP36L1 is increasing with time and persisting until 120 min. Tuberin phosphorylation at S939 limits its ability to inhibit p70S6K activity and also its ability to trigger apoptosis [227]. HNRNDP is involved in transcriptional regulation, phosphorylation of S83 suppresses the transactivator domain of the protein, thereby inhibiting transcription [228]. Phosphorylation of Ser134 on NR3C1 serves as a molecular sensor, controlling the cellular stress level to redirect the glucocorticoid-regulated pathway by changing the binding of the 14-3-3 zeta factor and recruiting promoters [229]. TCF7L2 is part of the Wnt signaling pathway. Mutation of the phosphorylation site abrogates the TNIK induced TCF/LEF transcriptional activity in colon cancer cells. This indicates that the phosphosites regulated transcriptional activity of TCF7L2 [230].

All phosphorylation sites marked in bold in **Figure 30** were also found to be differentially regulated by substrate stiffness. Their function was already explained in chapter: **Identification of stiffness-dependent regulated phosphorylation sites.** However, it seems that those sites are not only relevant in terms of mechanosensing and mechanotransduction but also of importance in the process of cell spreading.

Profiling of kinase activities in the course of cell spreading

The known kinase-substrate relationships of putative *in vivo* kinases of distinct phosphorylation sites were obtained from the database PhophoSitePlus. The course of phosphorylation for substrates and their responsible kinase were summarized (**Figure 31**). The kinases CDK1, AKT1, CK2A1, GSK3B, PKACA, Chk1 and ERK1/2 are assigned to most known target sites in this data regulated during cell spreading. The majority of the substrates of those kinases is found in cluster 4 and consequently strongly phosphorylated in the first 30 minutes after initial cell seeding. But also many sites following the course of phosphorylation of cluster 5 and 11 are seen. However, the kinases could not be assigned to be active in just one distinct cluster. Kinases assigned to only few substrates in the data set seem to be more specific for a distinct activity time window such as p70RS6K, CAMK2A, MEK1, GRK5, SRPK1, PLK1 and ROCK1. The kinases WNK1/2, PKCI and ATM seem to be activated in the very

early spreading process around 10 min, since the phosphorylation of their substrates is decreasing afterwards. But for most of the regulated phosphorylation sites in the spreading process no kinase-substrate relationship is known so far.
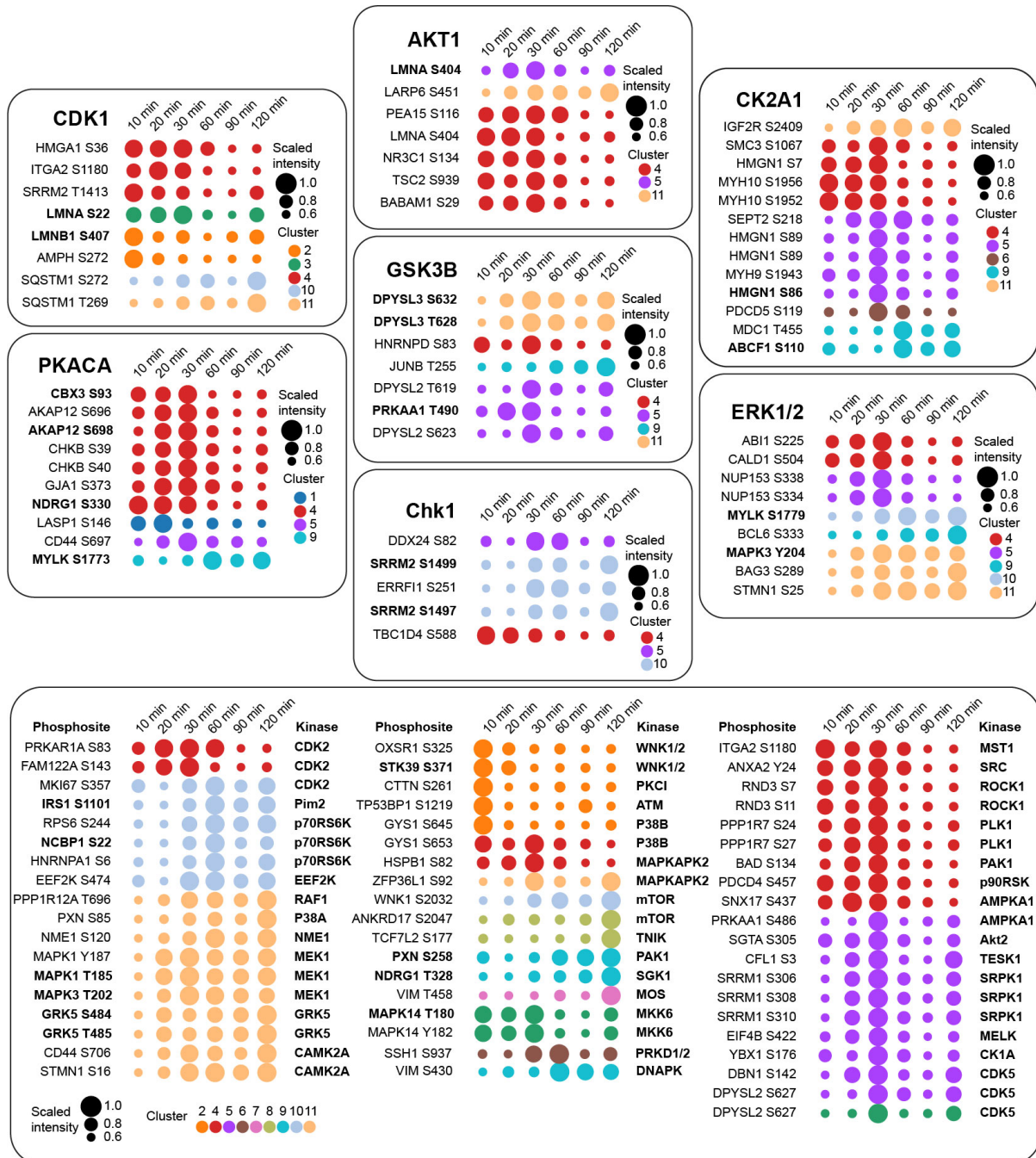

Figure 31 I Regulated phosphorylation sites during cell spreading known to be putative substrates of distinct kinases in vivo. Dot plots showing the dynamics of scaled phosphorylation intensities over time of selected phosphosites with known upstream kinases (dots are color-codes per cluster as presented in **Figure 28 B**).

Substrates marked in bold were also found in the phospho data regulated with substrate stiffness. For example, CBX3 is highly phosphorylated at S93 during early cell spreading and also found to be increasingly phosphorylated with enhanced substrate rigidity. The overlap of regulated phosphorylation sites between those two data sets will be discussed further in the following chapter.

Identification of phosphorylations sites which are regulated in terms of substrate stiffness and also during cell spreading

More rigid substrates result in highly spread (possibly polarized) cells with pronounced focal adhesions and stress fibers, but very soft substrates result in a less developed cytoskeleton and much less cell spreading [231]. Therefore, cell spreading is faster on stiff substrates than on soft substrates [232]. This means that mechanosensing and cell spreading are tightly connected. To identify phosphorylation sites, that are regulated both by substrate stiffness and in the process of cell spreading and to find common nodes in signaling but also to illustrate differences between the two processes, the two data sets were compared. Moreover, the phosphorylation data of the spreading time course can be used to identify when stiffness sensing occurs. If stiffness sensing takes place early (first 30 min), the underlying mechanism might be completely different that for later occurring phosphorylation. Therefore, I want to infer which stiffness sensitive phosphorylation sites are directly influenced by substrate stiffness and which phosphosites require the adaption of the cell to specific contractility and shape and are more directly influenced by substrate stiffness.
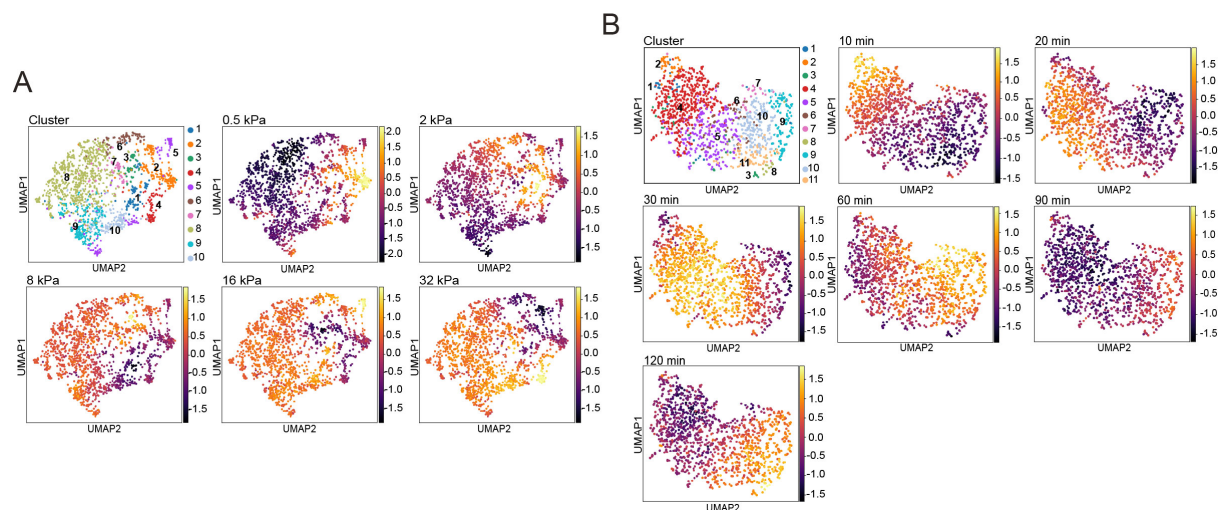

Figure 32 I A UMAP view of phosphosites regulated by substrate stiffness. The first UMAP depicts the distribution of the different clusters throughout the regulated sites. Every dot represents one phosphorylation site. The UMAPs for each substrate rigidity are color-coded according to the phosphorylation intensity of each site and visualize the course of phosphorylation across different substrate stiffnesses (Settings: n_pcs = 10, n_neighbours = 15, resolution = 0.5). **I B UMAP view of regulated phosphosites during the process of cell spreading.** The first UMAP depicts the distribution of the different clusters throughout the regulated sites. Every dot represents one phosphorylation site. The UMAPs for each substrate rigidity are color-coded according to the phosphorylation intensity of each site and visualize the changes in phosphorylation with spreading time. (Settings: n_pcs = 25, n_neighbours = 8, resolution = 1.2).

The phosphorylation profiles throughout the various substrate rigidities were visualized in two dimensions using the Uniform Manifold Approximation and Projection (UMAP) method [174], where every dot represents one single phosphorylation site (**Figure 32 A**). The first UMAP visualizes the different clusters in the map and the following UMAPs show the changes in intensity with increasing stiffness for each phosphorylation site. A similar approach was used for the regulated phosphosites during cell spreading (**Figure 32 B**). In order to able to better compare the two data sets, the phosphoproteomics data sets were combined (**Figure 33**).
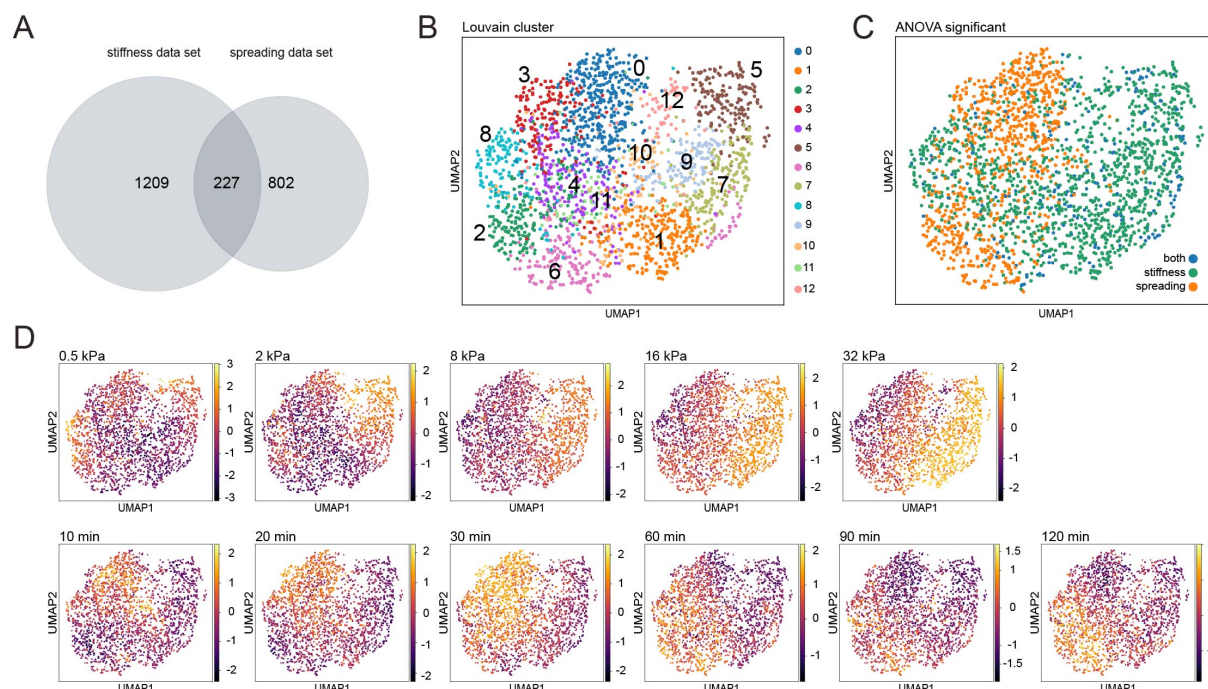

Figure 33 I Combined UMAP view of phosphosites regulated with changed substrate stiffness and during cell spreading. A The venn diagram depicts the overlap of significantly regulated phosphorylation sites in both datasets. **B** UMAP embedding colored by Louvain clusters demonstrates separation of phosphorylation sites according to their course of phosphorylation. Every dot represents one phosphorylation site (Settings: n_pcs = 30, n_neighbours = 8, resolution = 1). **C** UMAP color-coded according to ANAVA significance. **D** The UMAPs for each substrate rigidity and spreading timepoint are color-coded according to the phosphorylation intensity of each site and visualize the course of phosphorylation across both datasets.

Thus, only sites which were measured in both data sets were taken into account. About 74 % of the ANOVA significant, stiffness dependent phosphorylation sites were also measured in the spreading time course and about 63 % of ANOVA significant sites regulated during cell spreading were also measured in the rigidity data set. However, the overlap where phosphorylation sites are significantly regulated in both data sets amounts to 227 phosphosites (**Figure 33 A**). The data was visualized by generating a UMAP, divided in 13 Louvain clusters (**Figure 33 B**). The same UMAP was color coded according to the ANOVA significance of the phosphorylation sites (in both data sets, only in the one or the other) in order to spot the distribution of the 227 phosphorylation sites regulated in both experiments (**Figure 33 C**). This shows that those sites are not exclusively located in distinct clusters but are rather spread across the whole UMAP. Furthermore the z-scored

phosphorylation intensities for each stiffness condition and each spreading time point were overlaid on the UMAP (**Figure 33 D**). Although this reflects the different phosphorylation patterns well, it is difficult to identify the shared regulation of mechanosensing and cell spreading. For that reason, the 227 phosphorylation sites were clustered separately and the normalized intensities for each site for both datasets was combined in one heatmap (**Figure 34 A**).
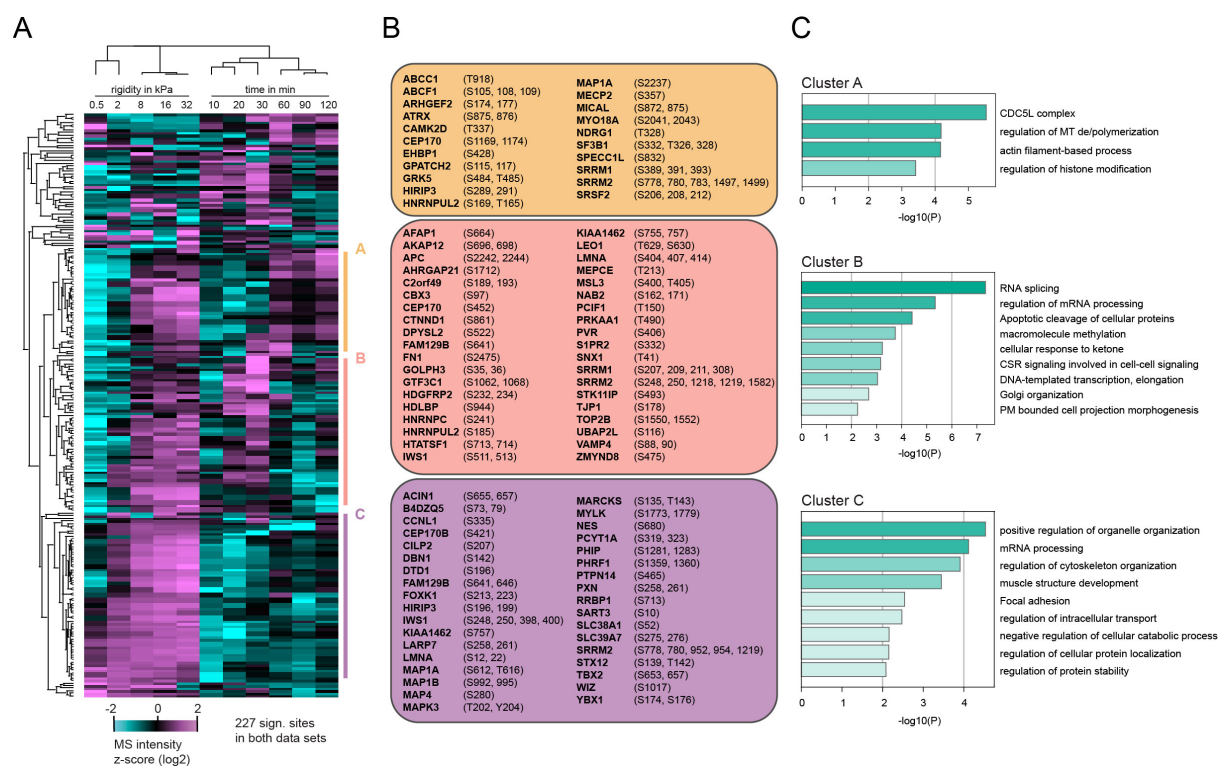

Figure 34 I Overlap of significantly regulated phosphorylation sites during cell spreading and mechanosensing. A Hierarchical clustered heat map with the intensities (log2 z-scored normalized) of stiffness sensitive phosphosites which are also regulated during cell spreading (227 phosphosites) **B** Corresponding proteins to the regulated phosphosites with their respective phosphorylated sites in the clusters A, B and C. **C** Bar graph showing enriched terms across gene lists of clusters A, B and C, colored by p-values. Enrichment analysis was performed with Metascape (www.metascape.org).

The sites were hierarchical clustered using the Pearson correlation. The clustering revealed three cluster A, B and C with an interesting progression. The phosphorylation intensity in cluster A is increasing from 8 to 32 kPa and in the spreading time course from 60 to 120 min. The 20 proteins with the corresponding 42 phosphosites are shown in in panel B of **Figure 34.** Furthermore, an enrichment analysis of biological processes and functions was performed with Metascape. Proteins associated with 'actin-filament based process', 'regulation of histone modification' and 'regulation of microtubule depolymerization' were overrepresented in cluster A. The cluster represents late stiffness sensitive sites which are more dependent on cytoskeletal rearrangement and formation of a more contractile cell shape. The proteins SF3B1, SRSF2, SRRM1 are members of the enriched term 'CDC5L protein complex'. This multiprotein complex is essential for the formation of pre-mRNA splicing [233], indicating that

mRNA splicing might be positively regulated by enhanced substrate rigidity but already early during cell spreading. The phosphorylation pattern in cluster B only differs from cluster A by different phosphorylation over time in the spreading process, because the phosphosites are also more strongly phosphorylated from a substrate stiffness of 8 kPa as seen in cluster A. Phosphorylation intensities in the spreading time course in cluster B is low at 10 min, peaks at 20 to 30 min and decreases afterwards, thereby representing phosphosites which are important in early cell spreading and are rather directly regulated by substrate stiffness. Cluster B contains 61 phosphorylation sites belonging to 38 proteins, which are enriched for GO terms such as 'RNA splicing' and 'regulation of mRNA processing' as top enriched annotations. Cluster C contains 63 phosphosites corresponding to 34 different proteins. Here the increase in phosphorylation is already observed form 2 kPa and also the phosphorylation status of the corresponding sites in the spreading time course are continually increasing over time, even though the rise is not so intense as for the stiffness dataset.

Only ten phosphorylation sites from those sites which were detected to be regulated during cell spreading and in dependence of substrate stiffness have a known functional role. Phosphorylation of ABCF1 at S109 (Cluster A) in the eIF2 binding domain of the protein is needed for association of eIF2 (translation initiation) with 80S ribosomal and polysomal fractions [234], indicating that increased stiffness promotes translation [235]. DPYSL2 phosphorylation at S522 (Cluster B) has been shown to be relevant in regulation of axon length [236] and thus might be important in fibroblasts for cell elongation. The phosphorylation of AKAP12 at S696 & S698 (Cluster B) in the binding domain of the protein for the receptor ß2AR is catalyzed by PKA and is functionally relevant for receptor resensitization [237]. LMNA, a component of the nuclear lamina is phosphorylated in both data sets on various sites: S12, 22, 404, 407 and 414. S22 (Cluster C) is required in the process of lamin A/C disassembly and is relevant during cytoskeletal rearrangement [185]. S404 (Cluster B) phosphorylation by marks prelamin A for degradation [238]. Phosphorylated YBX1 at S176 (Cluster C) is important for activation of NF-κB [192]. The actin cytoskeleton-organization protein DBN1 was shown to be phosphorylated in growth cone progress and thereby regulation neuronal migration [239]. Also the activity of MAPK3 (ERK1) is regulated via phosphorylation, here T202 and Y204 are the key phosphosites [181] and increased in phosphorylation on 2 and 8 kPa and also increasing with spreading time peaking at 30-60 min. Of note, seven phosphorylation sites APC S2242 & S2244, CEP170 S452, S1PR2 S332, B4DZQ5 S73 & S79 and MAP1A S2237 were previously unknown and were measured for the first time in this study.

The functions and roles of the differentially phosphorylated proteins contained in the clusters A, B and C were summarized in **Table 14.** As with the enrichment analysis in Metascape, a closer look at the individual protein information reveals that most proteins have a function in

the regulation of mRNA and the splicing machinery or are involved in the organization and rearrangements of the cytoskeleton.

Table 14 I Description of the function of proteins whose phosphorylation sites are regulated by substrate stiffness in the process of cell spreading. The provided protein information was taken from the UniProt database (**www.uniprot.org**) [240].

Protein	Phosphosite	Cluster	Description	Uniprot
ABCC1	T918	A	Mediator of export of drugs and organic anions from the cytoplasm	P33527
ABCF1	S105, 108, 109	A	Required for mRNA translation initiation	Q8NE71
ARHGEF2	S174, 177	A	Activator of Rho-GTPases involved in many cellular processes such as cell motility and polarization	Q92974
ATRX	S875, 876	A	Transcriptional regulator which is also involved in chromatin remodeling	P46100
CAMK2D	T337	A	Calcium/calmodulin dependent protein kinase implicated in the control of Ca2+ homeostasis and excitation-contraction coupling	Q13557
CEP170	S1169, 1174	A	Centrosomal protein involved in microtubule organization	Q5SW79
EHBP1	S428	A	Probably involved in actin reorganization and links clathrin-mediated endocytosis to the cytoskeleton	Q8NDI1
GPATCH2	S115, 117	A	G patch domain containing protein 2-like	Q9NWQ4
GRK5	S484, T485	A	Serine/threonine kinases which phosphorylates mainly activated GPCRs	P34947
HIRIP3	S289, 291	A	Interacts with HIRA and histones and thus might be important for chromatin function and histone metabolism	Q9BW71
HNRNPUL2	S169, T165	A	Protein involved in RNA binding	Q1KMD3
MAP1A	S2237	A	Structural protein participating in the filamentous bridging between microtubules and other cytoskeletal elements	P78559
MECP2	S357	A	Promotes transcriptional repression through interaction with histone deacetylase and the corepressor SIN3A	P51608
MICAL	S872, 875	A	Nuclear monooxygenase that enhances the depolymerization of F-actin by facilitating the oxidation of specific methionine residues on actin to generate methionine sulfoxide, which leads to the disintegration of actin filaments and prevents repolymerization	O94851
MYO18A	S2041, 2043	A	Might connect the Golgi membranes to the cytoskeleton and contribute in the tensile force required for the vesicles to sprout from the Golgi	Q92614
NDRG1	T328	A	Tumor suppressor in various cell types and regulator of microtubule dynamics	Q92597
SF3B1	S332, T326, 328	A	Component of the SF3B splicing factor complex and thus important in pre-mRNA splicing	O75533
SPECC1L	S832	A	Cytospin-A is essential in actin organization and microtubule stabilization and therefore involved in cell adhesion and migration	Q69YQ0
SRRM1	S389, 391, 393	A	Contributing to numerous processes in pre-mRNA processing also as part of multiprotein mRNP complexes	Q8IYB3
SRRM2	S778, 780, 783, 1497, 1499	A	Component of the spliceosome	Q9UQ35
SRSF2	S206, 208, 212	A	The factor is needed for formation of the ATP-dependent splicing complex and the pre-mRNA splicing	Q01130
AFAP1	S664	B	Actin filament-associated protein 1, crosslinker of actin filaments to bundles and networks, adapter molecule which links proteins to actin	Q8N556
AKAP12	S696, 698	B	Anchoring protein which regulates the compartmentation of PKA and PKC	Q02952
APC	S2242, 2244	B	Stabilizer of microtubules which regulates actin fiber dynamics	O95996
AHRGAP21	S1712	B	The depletion of ARHGAP21 initiates cell proliferation and accumulation of F-actin stress fibers	Q5T5U3
C2orf49	S189, 193	B	Protein of the ashwin family	Q9BVC5
CBX3	S97	B	Chromobox protein homolog which is probably part of heterochromatin-like complexes involved in transcriptional silencing	Q13185

CEP170	S452	B	Centrosomal protein involved in microtubule organization	Q5SW79
CTNND1	S861	B	Catenin delta-1 is a key regulator of cell-cell adhesion and is also involved in gene transcription.	O60716
DPYSL2	S522	B	Involved in neuronal developement, neuronal growth, cell migration and semaphorin class 3 signaling with subsequent cytoskeletal rearrangement	Q16555
FAM129B	S641	B	Protein Niban 2 might play a role in apoptosis suppression	Q96TA1
FN1	S2475	B	Fibronectin binds ECM proteins and cell surfaces and is involved cell adhesion and motility as well as cell shape maintenance	P02751
GOLPH3	S35, 36	B	Golgi phosphoprotein 3 links the cytokeleton with the Golgi membranes and is involved in vesicle budding from the Golgi	Q9H4A6
GTF3C1	S1062, 1068	B	General transcription factor 3C polypeptide 1 is needed for transcription mediated by RNA polymerase III	Q12789
HDGFRP2	S232, 234	B	Regulates expression of Cyclin D1 therby controlling cellular growth	Q7Z4V5
HDLBP	S944	B	Vigilin may play a role in protection from over-accumulation of cholesterol	Q00341
HNRNPC	S241	B	The protein may be involved in pre-mRNA splicing and the start of spliceosome assembly	P07910
HNRNPUL2	S185	B	Protein involved in RNA binding	Q1KMD3
HTATSF1	S713, 714	B	General transcription factor important for transcriptional elongation	O43719
IWS1	S511, 513	B	Transcription factor which defines the composition of RNA polymerase II elongation complex	Q96ST2
KIAA1462	S755, 757	B	Involved in cell adhesion	Q9P266
LEO1	T629, S630	B	Component of the PAF1 complex which is involved in transcription of Hox and Wnt target genes	Q8WVC0
LMNA	S404, 407, 414	B	Component of the framework for the nuclear envelope, the so called nuclear lamina. Important for chromatin organization and nuclear assembly	P02545
MEPCE	T213	B	Part of 7SK RNP complex and has an enzymatic methyltransferase activity	Q7L2J0
MSL3	S400, T405	B	Involved in transcriptional regulation and chromatin remodeling	Q8N5Y2
NAB2	S162, 171	B	Transcriptional repressor for the zinc finger transcription factor EGR1 and EGR2	Q15742
PCIF1	T150	B	Cap-specific adenosine methyltransferase	Q9H4Z3
PRKAA1	T490	B	Catalytic subunit of AMP-activated protein kinase (AMPK), an energy sensor protein kinase that plays a crucial role in controlling cellular energy metabolism	Q13131
PVR	S406	B	Promotes NK cell adhesion and enables NK cell effector functions	P15151
S1PR2	S332	B	Receptor for the lysosphingolipid sphingosine 1-phosphate	O95136
SNX1	T41	B	Engaged many stages of intracellular trafficking	Q13596
SRRM1	S207, 209, 211, 308	B	Contributing to numerous processes in pre-mRNA processing also as part of multiprotein mRNP complexes	Q8IYB3
SRRM2	S248, 250, 1218, 1219, 1582	B	Component of the spliceosome	Q9UQ35
STK11IP	S493	B	Controls function of kinase STK11/LKB1 via the subcellular localization	Q8N1F8
TJP1	S178	B	Scaffold protein which connect tight junction transmembrane proteins for example claudine, compound adhesion molecules and occludin to actin	Q07157
TOP2B	S1550, 1552	B	DNA topoisomerase inducing double-strand breaks	Q02880
UBAP2L	S116	B	Has an important role in the activation of the long-term repopulation of haematopoietic stem cells	Q14157
VAMP4	S88, 90	B	The vesicle-associated membrane protein 4 might be a marker for the sorting pathway which is important for the remodeling the secretory response of granule	O75379
ZMYND8	S475	B	Possible transcriptional corepressor for KDM5D and involved in down-regulation of many metastasis-associated genes	Q9ULU4
ACIN1	S655, 657	C	Part of the splicing-dependent multiprotein exon junction complex which is located at splice junctions on mRNAs	Q9UKV3
--	S73, 79	C		B4DZQ5
CCNL1	S335	C	Cyclin-L1 plays a role in pre-mRNA splicing	Q9UK58

CEP170B	S421	C	Involved in microtubule organization	Q9Y4F5
CILP2	S207	C	The protein might be involved in cartilage scaffolding	Q8IUL8
DBN1	S142	C	Drebrin is an actin-cytoskeleton-organizing protein and is important in cell projections	Q16643
DTD1	S196	C	ATPase probably important in DNA replication	Q8TEA8
FAM129B	S641, 646	C	Protein Niban 2 might play a role in apoptosis suppression	Q96TA1
FOXK1	S213, 223	C	Forkhead box protein K1 which can be a transcriptional activator or repressor depending on context playing a role in various processes for example glucose metabolism	P85037
HIRIP3	S196, 199	C	Interacts with HIRA and histones and thus might be important for chromatin function and histone metabolism	Q9BW71
IWS1	S248, 250, 398, 400	C	Transcription factor which defines the composition of RNA polymerase II elongation complex	Q96ST2
KIAA1462	S757	C	Involved in cell adhesion	Q9P266
LARP7	S258, 261	C	Binding protein of small nuclear RNA which regulates their function and processing	Q4G0J3
LMNA	S12, 22	C	Component of the framework for the nuclear envelope, the so called nuclear lamina. Important for chromatin organization and nuclear assembly	P02545
MAP1A	S612, T616	C	Structural protein participating in the filamentous bridging between microtubules and other cytoskeletal elements	P78559
MAP1B	S992, 995	C	Involved in microtubule polymerization and stabilization	P46821
MAP4	S280	C	A non-neuronal microtubule-associated protein which enhances microtubule assembly	P27816
MAPK3	T202, Y204	C	Serine/threonine kinase with an key role in MAP kinase signal transduction. Various cellular functions such as cell growth and survival, adhesion and differentiation are regulated by regulation of transcription and cytoskeletal rearrangements	P27361
MARCKS	S135, T143	C	MARCKS is a filamentous (F) actin cross-linking protein and the most prominent cellular substrate for protein kinase C and binds the proteins calmodulin, actin and synapsin	P29966
MYLK	S1773, 1779	C	Calcium/calmodulin-dependent myosin light-chain kinase involved in smooth muscle contraction through phosphorylation of myosin light chains (MLC). In addition, it controls the actin-myosin interaction through a non-kinase activity.	Q15746
NES	S680	C	Nestin enhances the degradation of phosphorylated vimentin intermediate filaments (IF) during mitosis and could be implicated in the trafficking of IF proteins	P48681
PCYT1A	S319, 323	C	The protein regulates phosphatidylcholine synthesis	P49585
PHIP	S1281, 1283	C	Involved in the control of cell morphology and cytoskeletal organization.	Q8WWQ0
PHRF1	S1359, 1360	C	Protein containing a PHD and RING finger domain	Q9P1Y6
PTPN14	S465	C	Protein tyrosine phosphatase, which is important in the regulation of lymphangiogenesis, cell-cell adhesion, cell-matrix adhesion, cell migration and growth and also regulates TGF-beta gene expression	Q15678
PXN	S258, 261	C	Cytoskeleton protein implicated in actin membrane fixation in focal adhesions	P49023
RRBP1	S713	C	The protein functions as a ribosome receptor and facilitates the interaction between the ribosome and the endoplasmic reticulum membrane	Q9P2E9
SART3	S10	C	U6 snRNP-binding protein that acts as a recycling factor of the splicing machine	Q15020
SLC38A1	S52	C	Acts as a sodium-dependent amino acid transporter	Q9H2H9
SLC39A7	S275, 276	C	Zinc transporter, which transports Zn2+ from the endoplasmic reticulum/Golgi apparatus to the cytosol	Q92504
SRRM2	S778, 780, 952, 954, 1219	C	Component of the spliceosome	Q9UQ35
STX12	S139, T142	C	SNARE protein which regulates protein transport between late endosomes and the trans-Golgi network	Q86Y82
TBX2	S653, 657	C	T-box transcription factor which regulates genes required for mesoderm differentiation	Q13207
WIZ	S1017	C	Might link the histone methyltransferases EHMT1 and EHMT2 in a heterodimer and stabilizes the complex	O95785
YBX1	S174, S176	C	DNA and RNA binding protein implicated in many processes like RNA stabilization, splicing and transcription regulation	P67809

The observed differential protein phosphorylation of PXN, MARCKS, FLNA and MAP1A are shown in more detail in **Figure 35**. Those sites were selected for a more detailed discussion since they might be promising targets for further functional studies. PXN is already a very well studied FA protein, nevertheless remains the functional role of the rather late phosphorylated serine 261 uncharacterized so far. The phosphorylation of FLNA and MARCKS are on the other hand, examples for early phosphorylation events in cell spreading and might be directly influenced by changes in the mechanical environment.
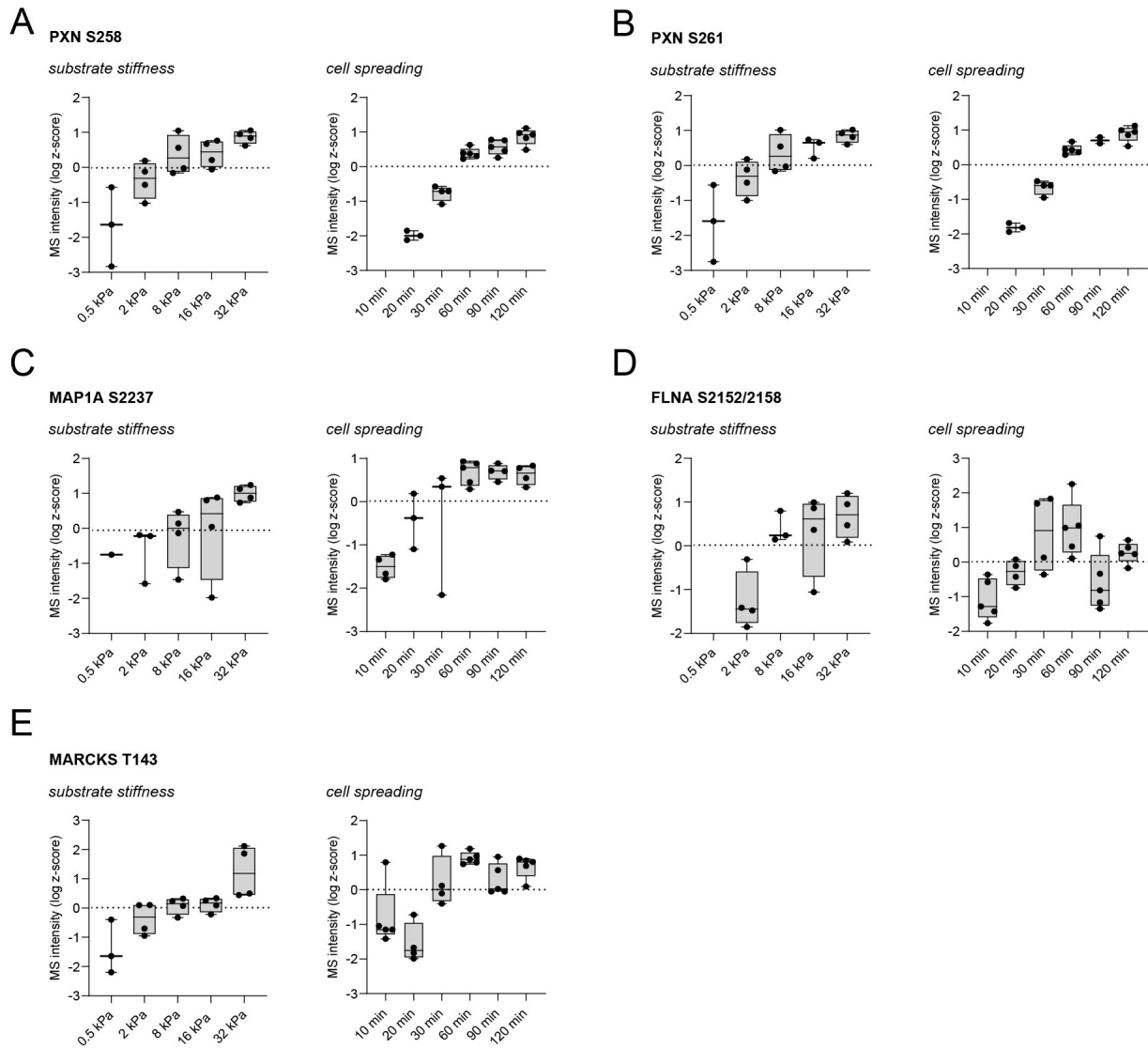

Figure 35 I A Phosphorylation status of A PXN S258, B PXN S261, C MAP1A S2237, D FLNA S2152/2158 and E MARCKS T143 on varying substrate stiffness and during cell spreading. MS intensity values are log z-scored and shown without imputation.

The phosphorylation of S258 of PXN by PAK1 negatively influences the association of TACE to paxillin thereby regulation lipid raft transfer [241]. However, no function is known for phosphorylation of serine 261. Both phosphorylation sites are highly upregulated in intensity

with increasing substrate stiffness and are also increasing in intensity over time with cell spreading (**Figure 35 A and B)**. Since paxillin is very important in cell spreading and focal adhesion regulation, phosphorylation of S261 has certainly also an important role in those processes. Filamin A phosphorylation of S2152/2158 is an early stiffness sensitive site, coming up already at 2 kPa and increases even more the stiffer substrate gets. On the other hand, the phosphorylation on those sites is also going up in cell spreading, peaking at 30 - 60 min but being still more phosphorylated at later time points than in early cell spreading (**Figure 35 D**). The phosphosite S2152 has been shown to be associated with several processes such as molecular association with transmembrane receptor protein complexes such as the glycoprotein Ib-IX complex [242], altered cell motility, cytoskeletal rearrangement and protein stabilization are linked. For instance, FLNA phosphorylated on Ser2152 is a target of caveloin-1 in IGF-I stimulated migration of MCF-7 breast cancer [243].

MAP1A is increasingly phosphorylated at S2237 both with enhanced substrate stiffness as well as with spreading time (**Figure 35 C**). The phosphosite has not been measured before and has therefore also no function assigned. However, the protein is well known for its role in stabilizing microtubules and also binds and interacts with signaling proteins and filamentous actin [244]. Also the function of T143 of MARCKS has no known function so far. The myristoylated alanine-rich C-kinase substrate (MARCKS) is one of the main substrates of PKC [245] and is part of the Phopholipase C Signaling pathway (**Figure 21**). Furthermore, a number of well-known functions of MARCKS comprise its association with and the control of cytoskeletal actin [245].

Integrated analysis of stiffness regulated phosphorylation in CCL151 cells and in primary human lung fibroblasts

To validate some of my observations I used primary human lung fibroblasts (phLF), which also behaved differently on varying substrate stiffnesses. After 180 min of seeding time the fibroblasts seeded on the soft substrates 0.5 and 2 kPa were rounded and spread less than the fibroblasts seeded on the rather stiff substrates. The spreading process was much more advanced on the stiff substrates. On 0.5 kPa the cells were still very round, compared to 2 kPa where the cell spreading was more advanced. Proper cell spreading was seen on 8-32 kPa. (**Figure 36 A**). The phosphoproteomic workflow was performed in the same way for those cells as for the CCL151 cells, however instead of four replicates per rigidity, five replicates were measured.
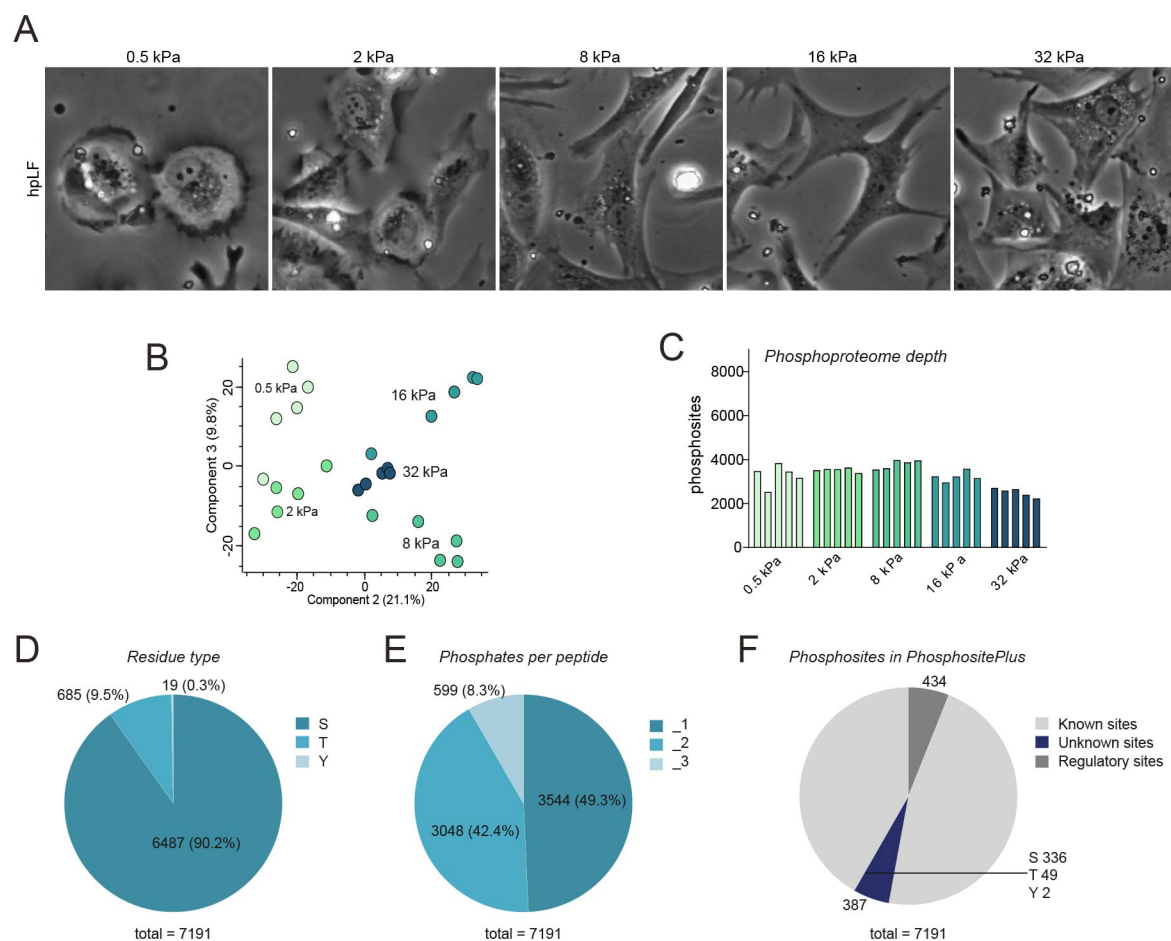

Figure 36 I Description of the phosphoproteomic dataset of primary human lung fibroblasts seeded on different substrate rigidities. A phLF cells seeded on FN-coated substrates with rigidities of 0.5 kPa, 2 kPa, 8 kPa, 16 kPa and 32 kPa after 180 min of spreading time. **B** Principal component analysis (PCA) of the stiffness regulated phosphoproteome. Two major components separate the data according to stiffness. **C** Phosphoproteome depth of the phosphoproteomic data set of varying substrate rigidities. **D** Pie chart presenting the percentage of identified phosphorylated serines (S), threonines (T) and tyrosines (Y) residues in the rigidity data set. **E** Pie chart presenting the percentage of identified singly, doubly and triply (or more) phosphorylated peptides in the rigidity data set. **F** Pie chart showing the number of already known sites, previously unreported sites and known sites with an assigned regulatory function in the PhosphoSitePlus database (www.phosphosite.org) of the rigidity data set.

The phosphorylation data set of phLF revealed 7191 class I phosphosites with a localization probability > 0.75. The performed principle component analysis shows a clear separation of the distinct substrate rigidities and a close clustering between the single replicates of each stiffness (**Figure 36 B**). The range of detected phosphorylation sites per replicate was roughly between 2000 and 4000 (**Figure 36 C**). The 7191 class I phosphosites correspond to mainly serine residues (S) with 6487 sites, followed by 685 phosphothreonines (T) and only 19 phosphorylated tyrosine residues (Y) (**Figure 36 D**). Almost half of all identified phosphosites (3544) are localized on phosphopeptides which have only one phosphate group as modification. But 3048 phosphosites are found on doubly phosphorylated peptides and 599 sites are located on phosphopeptides with at least three phosphorylations (**Figure 36 E**).

In this data set, 387 phosphosites were identified which were previously unknown without entry in the PhosphoSitePlus data base. Those sites split up in in phosphorylations on 336 serine, 49 threonines and two tyrosine residues. On the other hand, 434 phosphorylation sites identified are already better characterized and known to be functionally relevant (**Figure 36 F**). After filtering for sites at least measured four times in one of the stiffness conditions 4725 phosphorylation sites remained and were used for further analysis.

Also in this case the data was searched for already known phosphorylation sites in context of mechanosensing such as phosphorylation of threonine 18 and serine 19 of myosin light chain and various phosphorylation sites of the adaptor protein paxillin. Phosphorylation of T19 and S20 of myosin regulatory light chain (MYL9) showed the expected increase with increasing substrate stiffness (**Figure 37 A**). Phosphorylation of PXN on serine 126 was present with low intensity on 0.5 kPa and was not measured on 2 and 8 kPa, but increased on 16 and 32 kPa (**Figure 37 B**).
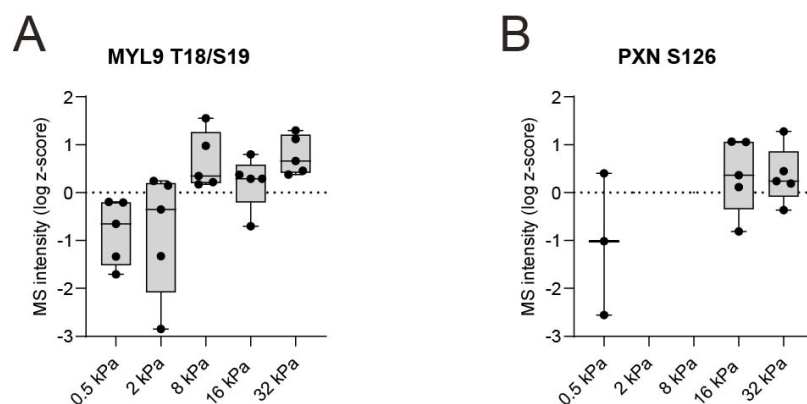

Figure 37 I Validation of the phosphoproteomic dataset of hpLF seeded on various substrate rigidities. A Phosphorylation of MYL9 on threonine residue 18 and serine residue 19 is increasing with spreading time. MS intensity is log z-scored and no imputed values are shown. **B** Phosphorylation of PXN on serine residue 126 is increasing during cell spreading. MS intensity values are log z-scored and shown without imputation.

After integration of both stiffness sensing data sets (CCL151 and phLF), 290 phosphorylation sites were found to be significantly regulated (ANOVA FDR 1 %) with different substrates rigidities. Those sites were imported into Scanpy and after calculation of the PCA, the phospho data was visualized in a UMAP, representing every phosphosite as single dot (**Figure 38 A**). Seven different Louvain clusters were defined according to the behavior of the single phosphorylation sites in both data sets. The z-scored phosphorylation intensities were overlaid over the UMAP.
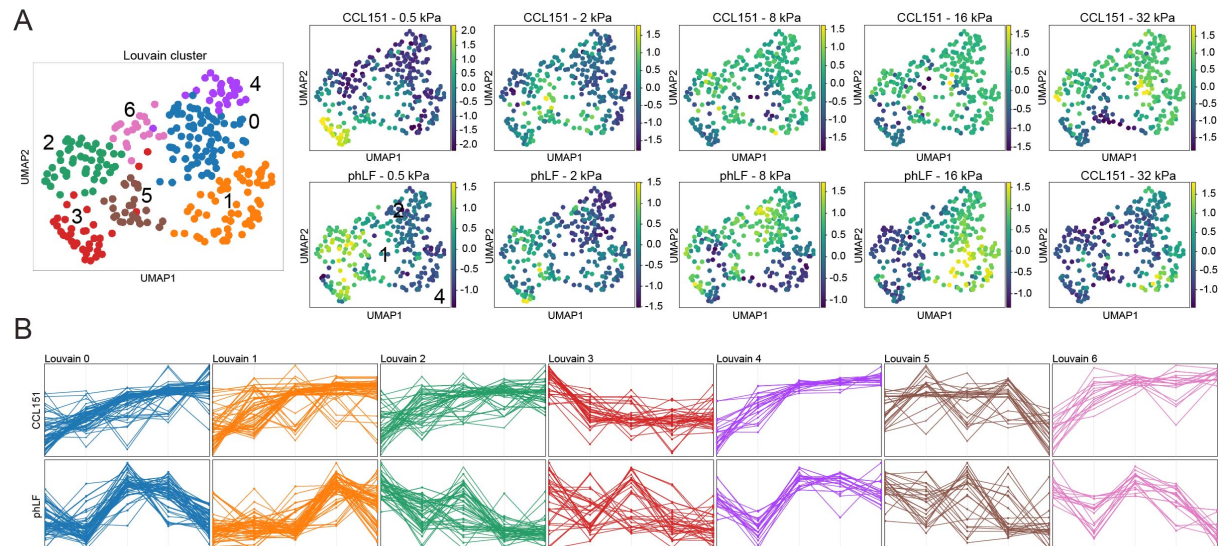

Figure 38 I Integration of stiffness dependent phosphorylation data from CCL151 cells and primary human lung fibroblasts. A UMAP embedding colored by Louvain clusters demonstrates separation of phosphorylation sites according to their course of phosphorylation (Settings: n_pcs = 30, n_neighbours = 10, resolution = 1.3). Every dot represents one phosphorylation site. The UMAPs for each substrate rigidity are color-coded according to the phosphorylation intensity of each site and visualize the course of phosphorylation across different substrate stiffnesses. **B** Illustration of the course of phosphorylation according to Louvain cluster for both datasets.

This shows the changes for both cell lines with varying substrates rigidities (**Figure 38 A**). The course of phosphorylation was visualized by importing the information on the assignment to the Louvain clusters and creating cluster profiles (**Figure 38 B).** This illustrates that, even though the phosphorylation sites are significantly regulated in both data sets with stiffness, they do not always exhibit the same behavior. Some clusters are even showing an opposite trend, such as Louvain cluster 2. Louvain cluster 1 and 4 were selected for further analysis, since the trend of change in phosphorylation is the same for both, CCL151 and phLF**.** Both cluster courses show increasing phosphorylation intensity with increasing substrates stiffness in both lung fibroblasts cell lines. If comparing the cluster profiles between the two data sets, I see that in Louvain cluster 1 and 4 the increase in phosphorylation is more gradually for the CCL151 cells. In the primary cells the increase is more volatile and is decreasing slightly at 32 kPa.The proteins of Louvain cluster 1 and 4 were submitted to Metascape enrichment analysis. The analysis revealed that Louvain cluster 1 is enriched for GO terms such as 'actin

cytoskeleton organization' and 'rRNA metabolic process' and also for reactome pathway RHO GTPases activate CIT. Citron kinase (CIT) apparently phosphorylates the myosin-regulating light chain at the same residues that are phosphorylated by ROCKs [246], indicating the involvement of the kinase in mechanical signaling. The GO term 'actin cytoskeleton organization' was enriched as well in Louvain cluster 4. Furthermore, the GO terms 'histone modification' and 'regulation of cell morphogenesis' as well as the reactome pathway RHO GTPases activate PAKs were statistically enriched. Interestingly, the increasingly phosphorylated proteins of Louvain cluster 4 were found to be relevant in 'fibromuscular dysplasia' and 'lung diseases' according to gene-disease associations database DisGenNET. The intensities of the phosphorylation sites of Louvain cluster 1 and 4 were hierarchically clustered in order to visualize the phosphorylation trends per individual site (**Figure 39 A**). The corresponding proteins with their phosphorylation sites are displayed in **Figure 39 B**.
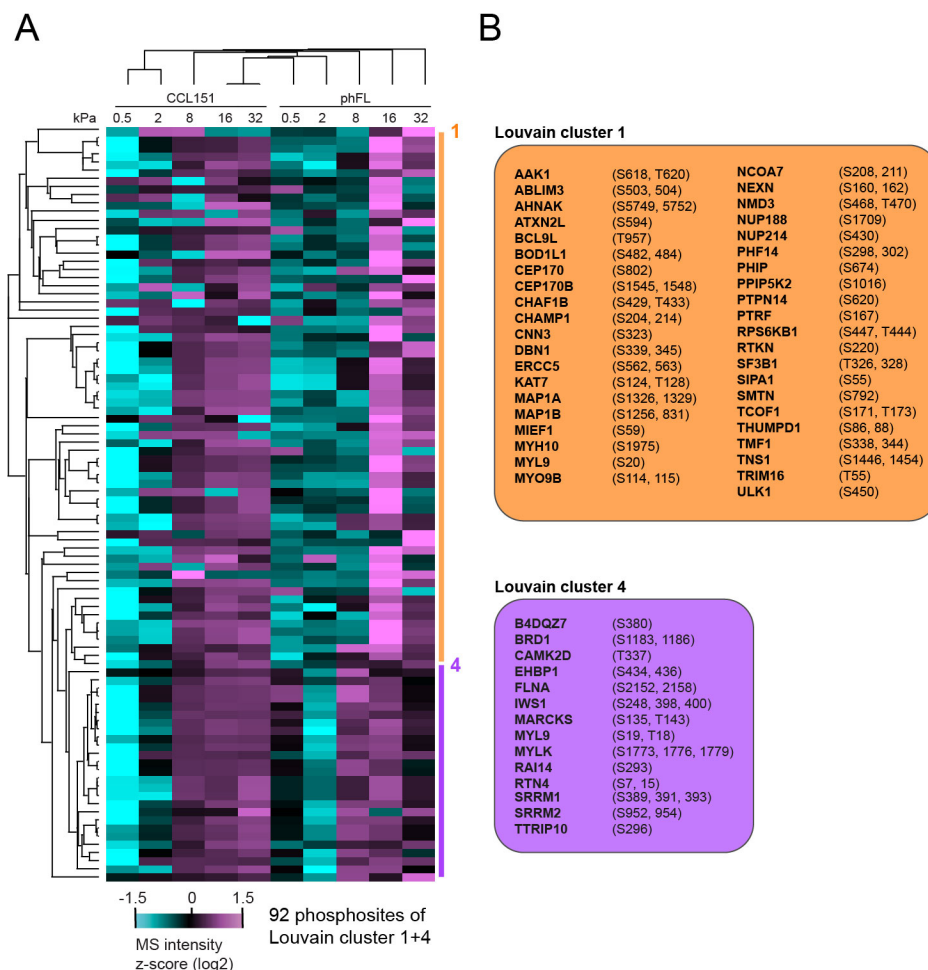

Figure 39 I Significantly increasing phosphorylation sites with increasing substrate stiffness in CCL151 cells and hpLF. A Hierarchical clustered heat map with the intensities (log2 z-scored normalized) of stiffness sensitive phosphosites which are regulated in both data sets of Louvain cluster 1 + 4 **B** Corresponding proteins to the regulated phosphosites with their respective phosphorylated sites in the Louvain clusters 1 + 4.

Only four phosphorylation sites from those sites which were detected to be regulated in dependence of substrate stiffness for both, CCL151 and hpLFs cells have a known functional role. In Louvain cluster 1 phosphorylation of S444/447 of RPS6KB1 is increased with enhanced activity, thereby regulating the enzymatic activity of the kinase [247]. The regulatory sites FLNA S2152 and MYL9 T18/S19 are contained in Louvain cluster 4. Of note, the phosphorylation site S380 on B4DQZ7 (undefined protein name) contained in Louvain Cluster 4 was previously unknown and was measured for the first time in this study.

Furthermore to better characterize in which cellular processes the differential phosphorylated proteins are involved, a short description of each protein is summarized in **Table 15.**

Table 15 I Description of the function of proteins whose phosphorylation sites are regulated by substrate stiffness in the cell line (CCL151) as well as in primary cells (phLF). The provided protein information was taken from the UniProt database (www.uniprot.org) [240].

Protein	Phosphosite	Louvain	Description	Uniprot
AAK1	S618, T620	1	AP2-asscoated protein kinase 1 involved in clathrin-mediated endocytosis and controls phosphorylation of other AP2 subunits and their cellular localization	Q2M2I8
ABLIM3	S503, 504	1	Actin-binding LIM protein 3 is probably a scaffold protein and regulates ABRA activity as well transcriptional activation of ABRA-dependent SRF	O94929
AHNAK	S5749, 5752	1	Might be needed for neuronal cell differentiation	Q09666
ATXN2L	S594	1	Contributes to the regulation of the development of stress grains and P-bodies	Q8WWM7
BCL9L	T957	1	Transcriptional activator which enhances ß-catenin transcription and is important in development of tumors	Q86UU0
BOD1L1	S484, 484	1	Part of the fork protection machine necessary to protect stalled/damaged replication forks from uncontrolled DNA2-dependent resection.	Q8NFC6
CEP170	S802	1	Centrosomal protein involved in microtubule organization	Q5SW79
CEP170B	S1545, 1548	1	Involved in microtubule organization	Q9Y4F5
CHAF1B	S429, T433	1	Chromatin assembly factor part of a complex which may control chromatin assembly in DNA repair and replication	Q13112
CHAMP1	S204, 214	1	Necessary for the correct alignment of chromosomes at the metaphase and their accurate separation during mitosis; Contributes to maintaining the binding of the spindle microtubules to the kinetochore during sister chromatid biorientation	Q96JM3
CNN3	S323	1	Thin filament-associated protein involved in the regulation and modulation of smooth muscle contraction. It is able to bind to actin, calmodulin, troponin C and tropomyosin.	Q15417
DBN1	S339, 345	1	Drebrin is an actin-cytoskeleton-organizing protein and is important in cell projections	Q16643
ERCC5	S562, 563	1	Single-stranded structure-specific DNA endonuclease important in DNA excision repair	P28715
KAT7	S124, T128	1	Histone acetyltransferase which is part of HBO1 complexes responsible for acetylation of histone H3 at Lys14 thereby mediating processes such as transcription, immune regulation and ubiquitination	O95251
MAP1A	S1326, 1329	1	Structural protein participating in the filamentous bridging between microtubules and other cytoskeletal elements	P78559
MAP1B	S831, 1256	1	Involved in microtubule polymerization and stabilization	P46821
MIEF1	S59	1	Protein of the mitochondrial outer membrane responsible for regulation of mitochondrial fission	Q9NQG6
MYH10	S1975	1	Cellular myosin important in cytoskeleton reorganization, focal adhesion formation, and lamellipodial extension; The function is mechanically antagonized by MYH9	P35580
MYL9	S20	1	Regulatory subunit of myosin, which is involved in regulating the contractile activity of both smooth muscle and non-muscular cells via phosphorylation; Important in cytokinesis, receptor capping and cell movement	P24844
MYO9B	S114, 115	1	Unconventional myosins are needed for intracellular movements. Binding actin with high affinity in the absence and presence of ATP, its mechanochemical activity is blocked by calcium ions	Q13459
NCOA7	S208, 2011	1	Coactivator mediating the transcriptional activity of various nuclear receptors	Q8NI08
NEXN	S160, 162	1	Nexilin plays an important role in cell migration via association with actin	Q0ZGT2
NMD3	S468, T470	1	Ribosomal export protein which functions as an adaptor for export of the 60S ribosomal subunit	Q96D46
NUP188	S1709	1	Component of the nuclear core complex	Q5SRE5
NUP214	S430	1	Component of the nuclear core complex and involved in nucleocytoplasmic transport	P35658
PHF14	S298, 302	1	Protein with zinc finger binding motif	O94880
PHIP	S674	1	Involved in the control of cell morphology and cytoskeletal organization	Q8WWQ0
PPIP5K2	S1016	1	Bifunctional inositol kinase that functions together with the IP6K kinases IP6K1, IP6K2 and IP6K3	O43314

PTPN14	S620	1	Protein tyrosine phosphatase, which is important in the regulation of lymphangiogenesis, cell-cell adhesion, cell-matrix adhesion, cell migration and growth and also regulates TGF-beta gene expression	Q15678
PTRF	S167	1	Important for caveolae formation and organization in all tissues	Q6NZI2
RPS6KB1	T444, S447	1	Serine/threonine protein kinase that acts downstream of mTOR signalling in a reaction to growth factors and nutrients to stimulate cell proliferation, cell growth and cell cycle progression	P23443
RTKN	S220	1	Rhotekin promotes the Rho signal to enable NF-kappa-B activation and could lead to increased resistance to apoptosis	Q9BST9
SF3B1	T326, 328	1	Component of the SF3B splicing factor complex and thus important in pre-mRNA splicing	O75533
SIPA1	S55	1	Activator of the GTPase for nuclear Ras-related regulatory proteins Rap1 and Rap2	Q96FS4
SMTN	S792	1	Smoothelin is a cytoskeletal structure protein	P53814
TCOF1	S171, T173	1	Nucleolar protein which functions as a regulator of RNA polymerase I	Q13428
THUMPD1	S86, 88	1	Works as a tRNA binding adapter to facilitate NAT10 dependent tRNA acetylation	Q9NXG2
TMF1	S338, 344	1	TATA element modulatory factor is a potential coactivator of the androgen receptor and modulates STAT3 degradation.	P82094
TNS1	S1446, 1454	1	Tensin-1 is implicated in the formation of fibrillar adhesions and May be implicated in cell migration, cartilage development and in the interconnection of signal transduction pathways with the cytoskeleton	Q9HBL0
TRIM16	T55	1	E3 ubiquitin ligase, which has an essential role in the regulation of autophagic response and ubiquitination in lysosomal and phagosomal defects.	O95361
ULK1	S450	1	Serine/threonine protein kinase which is implicated in autophagy in reaction to starvation.	O75385
BRD1	S1183, 1186	4	Bromodomain-containing protein 1 is a scaffold subunit of many histone acetyltransferase complexes	O95696
CAMK2D	T337	4	Calcium/calmodulin dependent protein kinase implicated in the control of Ca2+ homeostasis and excitation-contraction coupling	Q13557
EHBP1	S434, 436	4	Might contribute to actin reorganization and links clathrin-mediated endocytosis to the actin cytoskeleton.	Q8NDI1
FLNA	S2152, 2158	4	Filamin-A stimulates orthogonal branching of actin filaments and connects actin filaments with membrane glycoproteins. In addition, the protein anchors a variety of transmembrane proteins to the actin cytoskeleton and provides a scaffold for a vast range of cytoplasmic signalling proteins.	P21333
IWS1	S248, 398, 400	4	Transcription factor which defines the composition of RNA polymerase II elongation complex	Q96ST2
MARCKS	S135, T143	4	MARCKS is a filamentous (F) actin cross-linking protein and the most prominent cellular substrate for protein kinase C and binds the proteins calmodulin, actin and synapsin	P29966
MYL9	T18, S19	4	Regulatory subunit of myosin, which is involved in regulating the contractile activity of both smooth muscle and non-muscular cells via phosphorylation. Important in cytokinesis, receptor capping and cell movement	P24844
MYLK	S1773, 1776, 1779	4	Calcium/calmodulin-dependent myosin light-chain kinase involved in smooth muscle contraction through phosphorylation of myosin light chains (MLC). In addition, it controls the actin-myosin interaction through a non-kinase activity.	Q15746
RAI14	S293	4	Ankycorbin controls actin regulation in ectoplasmic specialization, a type of testicular cell junction.	Q9P0K7
RTN4	S15	4	Reticulon-4 is involved in induction of and stabilization of endoplasmic reticulum tubules	Q9NQC3
SRRM1	S289, 391, 393	4	Contributing to numerous processes in pre-mRNA processing also as part of multiprotein mRNP complexes	Q8IYB3
SRRM2	S952, 954	4	Component of the spliceosome	Q9UQ35
TRIP10	S296	4	Facilitates CDC42-induced actin polymerization by recruitment of WASL/N-WASP, which then activates the Arp2/3 complex	Q15642

The observed differential protein phosphorylation of MARCKS, CAMKD2, DBN1 and ABLIM3 are shown in more detail in **Figure 40**.

Interestingly, is increased phosphorylation of MARCKS also observed in primary human lung fibroblasts encountering different substrate rigidities (**Figure 40 A and B**). This might be a hint that those phosphorylation sites might be highly relevant in sensing the mechanical properties of the substrate.
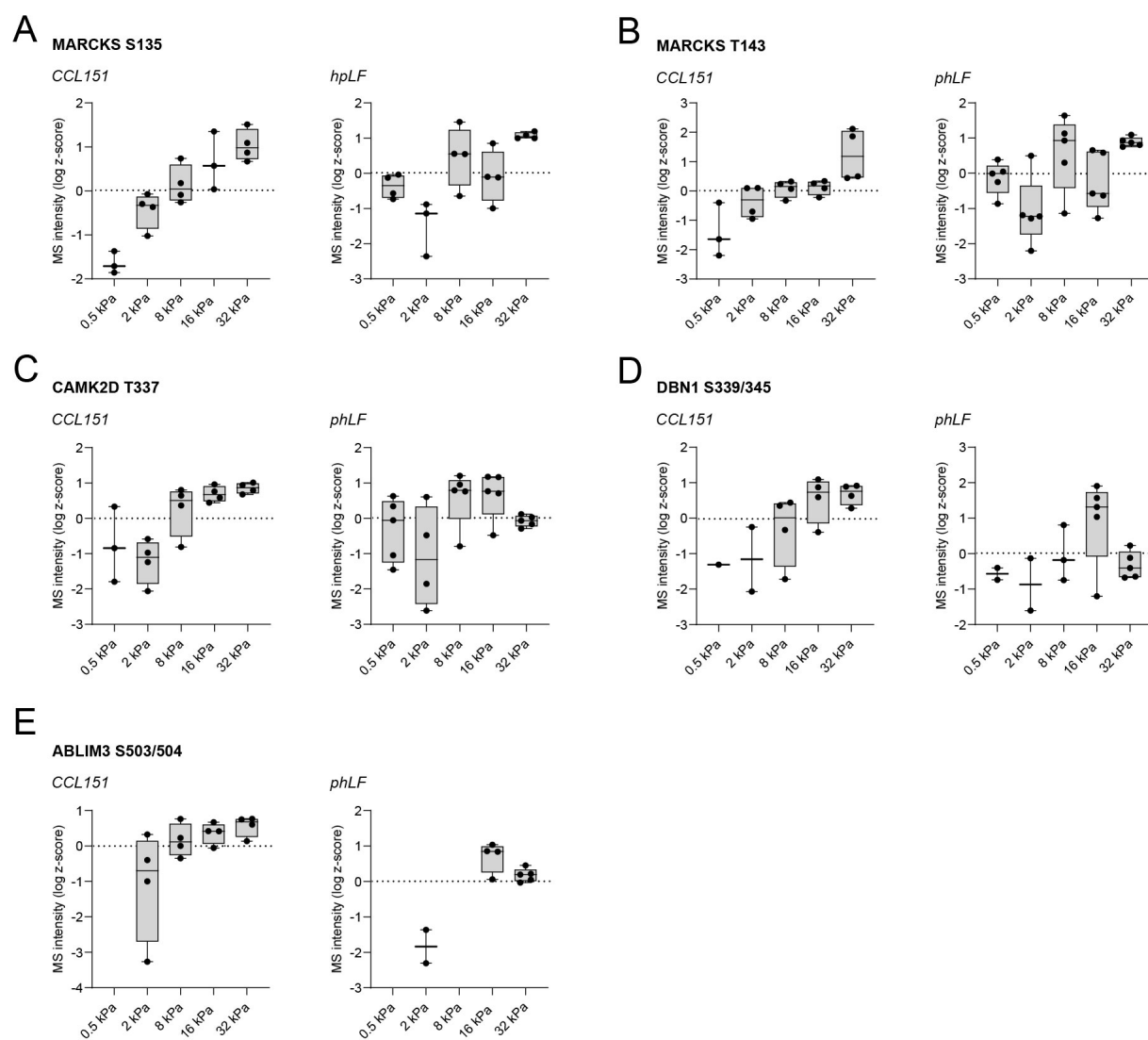

Figure 40 l A Phosphorylation status of A MARCKS S135, B MARCKS T143, C CAMK2D T337, D DBN1 S339/345 and E ABLIM3 S503/504 on varying substrate stiffness and during cell spreading. MS intensity values are log z-scored and shown without imputation.

The calmodulin and calcium dependent protein kinase CAMK2D is involved in HIF1a Signaling (**Figure 29**). Phosphorylation of threonine was observed to be increasing with substrate stiffness in both the CCL151 cell line and in primary human lung fibroblasts (**Figure 40 C**). No downstream effect of any of the various phosphorylation sites of this kinase is known so far. However, T337 phosphorylation was measured in a study where cell signaling was induced

by lysophosphatidic acid [248]. Nevertheless, the function of this phosphorylation site in cell spreading and during mechanosensing remains elusive.

Other interesting proteins linked to the cytoskeleton, whose phosphorylation has increased both in the cell line and in the primary cells are Drebrin 1 and ABLIM3 (**Figure 40 D and E**). Drebrin1 is an actin-filament binding protein and contains a cryptic F-actin-bundling activity which is regulated by phosphorylation of threonine 142 [187]. This site is increasingly phosphorylated with enhanced substrate stiffness in CCL151 cells but not observed in hpLFs. The phosphosites S339 and S345 however have no known function but could be relevant in cell adhesion and mechanosensing.

ABLIM3 has a so called LIM domain [249]. Proteins containing such domains might be potential tension sensors [18]. The increased phosphorylation of S503/504 on stiff substrates (**Figure 40 E**) might be of relevance for cytoskeletal signaling during mechanosensing.

Discussion

In the course of this study, I have determined the global changes in phosphorylation in two different experimental settings by mass spectrometry-based phosphoproteomics. The dynamic changes of phosphoproteomes of human lung fibroblasts were measured in reaction to substrate stiffness and during multiple timepoints of cell spreading on stiff substrates. As the main focus was to analyze large-scale phosphoproteomic data, the challenges and implications of large-scale PTM studies will be discussed in the first part. In the second part, the biological impact of this work for the field will be considered. Additionally, the phosphoproteins that appeared to be interesting candidates for further investigations will be highlighted and set into context of mechanosignaling, cell spreading and lung fibrosis.

Insights, implications and challenges of phosphoproteomics

The main goal of phosphoproteomics is the large-scale identification and quantification of phosphorylation sites [250]. Until now more than 100,000 unique phosphorylation events are detected in human cells enabled by the fast growing field of phosphoproteomics [94]. Considering the huge number of kinases, phosphatases, phosphorylatable amino acid residues and the ubiquitous biological role of phosphorylation, it can thus be expected that an individual protein occurs with multiple phospho-isoforms at a certain time. Not only are these isoforms different in the permutation of their phosphorylation sites but as well as in the occupancy for each site [98].

The bottleneck of low abundance and sub stoichiometric levels of phosphorylation in OMIC scale investigation of phosphorylation was overcome by development of several different enrichment strategies for phosphorylated peptides. This advancement increased site specific phosphorylation data enormously. Nevertheless, it has to be stated that, those enrichment techniques may introduce quantitative bias. This is caused by preferences of different techniques for certain phosphorylation populations due to sequence context and physicochemical characteristics [98]. Also due to certain levels of random phosphorylation, all phosphosites should undergo a prioritization process, where functional relevance is interfered [98]. The interrogation of the function of the modified site and protein is a huge challenge for phosphoproteomics but also for all other PTMs [94]. Very often it takes a lot of time and experiments to find out about the phenotypic effect of phosphosites. This explains why at present only 3 % of identified human phosphorylation sites have a known function assigned. Nevertheless, phosphorylation often represents essential key switches for cellular decision making. For example, the phosphorylation of pseudokinase MLKL by RIPK3 is enough to

trigger cell death via the necroptotic pathway [251]. To gain insights in potential functional relevance of phosphosites, it is useful to look at their topological localization e.g. within or between protein domains. Interestingly, the largest fraction of known phosphorylation sites is found in protein kinase domains, mainly in the conserved catalytic domain [252]. But also other protein domains are found to be often phosphorylated such as C2H2 zinc finger domain, RNA recognition motif domain and other repetitive domains. Transcription regulation by phosphorylation is the most common reported biological process [94]. The huge disparity between the reported functions, kinases and the documented phosphosites has led to the assumption that a substantial proportion of the phosphoproteome comprise "silent" phosphorylation sites, e.g. without functional consequence [253, 254]. Usually kinases are highly specific *in vivo* and in circumstances where kinases have insufficient specificity, obscure phosphorylations may be removed by phopsphatases via hydrolysis [255]. However, considering the size of the phosphoproteome, the extent of its functionality is difficult to assess [94].

Determination of the occupancy/stoichiometry of phosphorylation sites is a possibility to differentiate silent from functional phosphosites [98], which show that a substantial fraction of the sites are phosphorylated in high stoichiometry [94], for example during mitosis [256]. Global phosphorylation represents a rapid approach for cells and tissues to respond quickly to environmental changes and fine-tune reactions compared to transcriptional and translational control of protein abundance [94].

The transition of phosphoproteome analysis from discovery mode towards a more complete understanding of functional implications is already under way. Although this will require a thoughtful design of experiments under various cellular contexts and stimuli. The rebuilding of signaling networks from phosphoproteomics data requires large sample sizes, therefore efforts for cost reduction and invention of higher throughput methods are key. This makes it possible to include various conditions, time series and negative and positive controls in the experimental setup [94]. Also in the field of clinical proteomics, phosphoproteomics may become a key tool in diagnostics by analysis of large-scale datasets from patient-derived samples, which may enable to infer causal insights or find predictive markers in disease [257]. Needham et al. believe that in the years to come, the phosphorylation network status of patients could be a meaningful predictor of treatment responsiveness, as it accurately reflects the cell activity in the measured tissue. The continuous improvements in enrichment, labeling, and MS-methods will ease the generation of deep and high quality phosphoproteomics data and thereby increase the need for better data analysis and visualization strategies. But also

development in molecular biology tools, such as the CRISPR-Cas revolution, will help to shed more light on the "dark phosphoproteome" [94].

Complexity of analysis and reconstruction of signaling events

The identification of reaction networks that control the propagation of cellular signals through the cell to downstream transcriptional regulators is an important aspect of the holistic approach of systems biology [258]. Typically, phosphoproteomic experiments identify sites within a protein that are differently phosphorylated between two or more cell states. Nevertheless, the interpretation of these data is difficult due to the lack of methods that can translate site-specific information into global maps of active proteins and signaling networks [259]. Various databases have been established to record the interactions present in the signaling pathways and thus facilitate their access for computer-aided analysis. Despite the fact that these databases have been iteratively improved over the years, they remain largely built through extensive and tedious manual curation. Moreover, the proteins and interactions within the same pathway can differ significantly from one database to another [258]. Phosphoproteomics based on mass spectrometry is a very effective approach to investigate signal changes in cells under the influence of various stimuli or conditions. Phosphorylated peptides are identified by downstream computer-aided analysis and the modification site is localized. The depth of phosphoproteomic measurements in single experiments is already very good even though most phosphoproteomic studies suffer from under sampling (1), which is one of three major limitations. A phosphorylation change itself does not automatically mirror a difference in the signaling functionality of the phosphorylated protein (2), since the majority of known phosphosites has no functionality assigned. Furthermore, the identification of phosphosites alone does not lead to a holistic view of a larger signaling network (3). Most of the time, a list of regulated phosphosites that have been shown to differ across two or more cell states, is the final outcome of phosphoproteomic studies. There are only a couple of studies that continue with a functional investigation of only a very limited number of phosphosites [259].

MS-based phosphoproteomics provides not only insights into signaling networks but also the possibility to unravel new phosphorylation sites and discover new modes of protein regulation. The most serine and threonine phosphorylation sites are found in non-organized regions, those regions are often areas where protein association is mediated [131]. But also protein half-life and stability as well as the intracellular localization and the protein conformation can be influenced by phosphorylation [260] [28]. Even though, site information has been implemented in several databases like PhosphoSitePlus, PHOSIDA and Phospho.ELM, functional data is only obtainable for a minority of well investigated sites. The experimental

validation of the function of a site is difficult and often complicated, even if only a few sites are involved, so computational function prediction and modeling are urgently needed [254, 259].

Mechanosensing and signaling

Substrate stiffness has been shown to have a major impact on the behavior, adaptation and fate of a cell [261]. How much of this effect is a consequence of differential phosphorylation? In this thesis I documented the changes that occur in the phosphoproteome when cells are exposed to substrates of different stiffnesses and during the encounter and spreading process on a stiff substrate. I aligned the data with already known functional relevant phosphorylation sites, in order to draw conclusions about activated signaling pathways or changes in protein conformation and protein-protein interactions. In the field of mechanobiology, research is mostly conducted on the function of individual proteins in mechanosignaling rather than on a global scale. In order to gain a better understanding of how different molecular structures recognize and transduce physical forces, specific proteins are manipulated and cells are exposed to a physical force similar to that acting in the human body. Of primary interest are contractile cytoskeletal units, cytoskeleton-binding proteins, and integrin- and cadherin-based adhesion complexes, as they connect the cells with each other, and allow cellular interaction with the extracellular matrix. Several proteins found to be relevant in mechanosensing can be stretched, exposing domains that can bind other proteins or enable enzymatic reactions such as the transfer of a phosphate group. Those mechanisms are studied at the level of single proteins. However, a holistic view on signaling events which are caused by physical forces is lacking.

To my knowledge this work is the first unbiased quantitative phosphoproteomic study of mechanosensing and cell spreading to detect and characterize underlying phosphorylation events. In particular, 1631 phosphorylation sites have been identified that are regulated by changes in substrate stiffness and 1265 phosphorylation sites that significantly varied during cell spreading. Several functionally important phosphorylation sites were found that are obviously directly or indirectly regulated by substrate stiffness. Also during cell spreading, some previously well characterized phosphorylation sites were found to be dynamically altered. Many proteins important for the splicing and transcription machinery as well as a lot of cytoskeletal binding proteins were differentially phosphorylated under changing substrate rigidity conditions. Comparison to primary human lung fibroblasts enabled me to identify robust dynamic signals that were reproduced in independent experiments. In addition, the two data sets were analyzed together to identify phosphorylation sites that depend on substrate stiffness and are regulated differently during cell attachment. The integration of those data sets is especially important to be able to distinguish indirectly induced phosphorylation from

directly by substrate stiffness induced phosphorylation events from each other. Early events in stiffness sensing are rather directly influenced whereas phosphosites coming up late are probably more indirect affected. Those regulated phosphoproteins were summarized to obtain an overview of potential targets for further functional validation. Some of the very interesting single phosphorylation events are discussed in more detail in the following.

There is evidence that cells perceive mechanical stimuli via feedbacks of the acto-myosin cytoskeleton at focal adhesions with substrate stiffness, however, this process is incompletely understood [262]. Here, I can show that many well-known signaling pathways are involved in the process of mechanosensing in addition to Integrin, Actin Cytoskeleton and Paxillin Signaling. Proteins being part of signal transduction in the PI3K/AKT axis, mTOR Signaling, Phospholipase C Signaling, p38 MAPK Signaling and ERK5 Signaling are found to be differentially phosphorylated in dependence on substrate stiffness. This emphasizes that mechanical stimuli have global impacts on cells rather than only locally affecting the site of adhesion. It is reasonable that many proteins with binding functions for the cytoskeleton are affected by changes in matrix rigidity, since phosphorylation can change binding properties and open or close cryptic binding regions, and therefore influencing cytoskeletal remodeling. Strikingly, I also found many proteins with annotations such as mRNA regulation, splicing, RNA transport, mRNA processing to be differentially phosphorylated with changing substrate rigidity. This leads me to the assumption that the local sensing properties at the cell membrane are meaningful for cell fate decisions even after only two hours on a soft/stiff matrix. Gene expression is influenced by matrix stiffness, which was already shown for the prominent fibrosis marker alpha-SMA [263]. The importance of phosphorylation events in human pulmonary fibrosis was demonstrated by a study of Al-Tamari, where they suggests that FOXO3 is a key modulator of pro-fibrotic signaling in pulmonary fibrosis and is hyperphosphorylated in IPF fibroblasts on T32 and S253 [199]. However, I did not find those phosphorylation sites of FOXO3 to be regulated in the stiffness dataset, while S7 and S12 were indeed increasingly phosphorylated with substrate stiffness. To further explore the impact of matrix stiffness on transcriptional regulation, the data could be matched with RNAseq data of cells seeded on various substrate stiffnesses. Advances in the study of fibrosis, tissue repair, and the underlying mechanosensory signaling mechanisms have shown how mechanical environments are established in normal, injured, and fibrotic tissue and how these environments are maintained. The translation of this knowledge into clinical and therapeutic innovations could provide new strategies for the treatment of fibrotic tissue remodeling [53]. The insights of this phosphoproteomic study might serve as a starting point to identify new phospho-switches in the regulation of fibrosis.

I was able to validate the increase in phosphorylation with enhanced substrate stiffness of phosphorylation of CBX3 at S93 and PXN S126 in human IPF lung sections compared to healthy control sections, even if the increase in phosphorylation was not primarily seen in fibroblasts. By the combination of the stiffness data with time resolved phosphorylation data of cell spreading, I was able to identify phosphorylation sites which respond early in the spreading process and were stiffness sensitive. Indicating that those phosphorylation sites, such as FLNA S2152 and MARCKS T143, are directly sensing substrate stiffness. Other phosphorylation sites require first the formation of a specific cell shape and activity, suggesting that these later phosphorylation sites are possibly more indirectly influenced by substrate stiffness. Phosphorylation sites which are directly regulated by substrate rigidity might be important switches *in vivo* for adaption of cell migration and invasion. Nevertheless, further cell biological investigation will be needed to assign a functional role to those sites. Some promising targets for future research are discussed here.

Phospho-Paxillin

Paxillin is a scaffolding protein which has a key role in transduction of extracellular signals to the inside of a cell. This is induced by the engagement of integrins with the ECM and by formation of focal adhesions. Paxillin is one of the main players in FAs and also promotes the recruitment of structural proteins, cofactors, kinases and phosphatases implicated in intracellular signaling networks. Activation of these signaling cascades leads to turnover of FAs and cytoskeletal rearrangements, processes which are required for cell attachment, spreading and migration. Paxillin has a dual role in focal adhesions, at the leading edge the protein is recruited to nascent FAs and at the back end it is relevant for disassembly of FAs during cell movement [264]. However, paxillin is also important outside from FAs in the cytoplasm and nucleus, where it constitutes a link between the cytoskeleton, the plasma membrane and the nucleus and might be involved in transcription regulation [264].
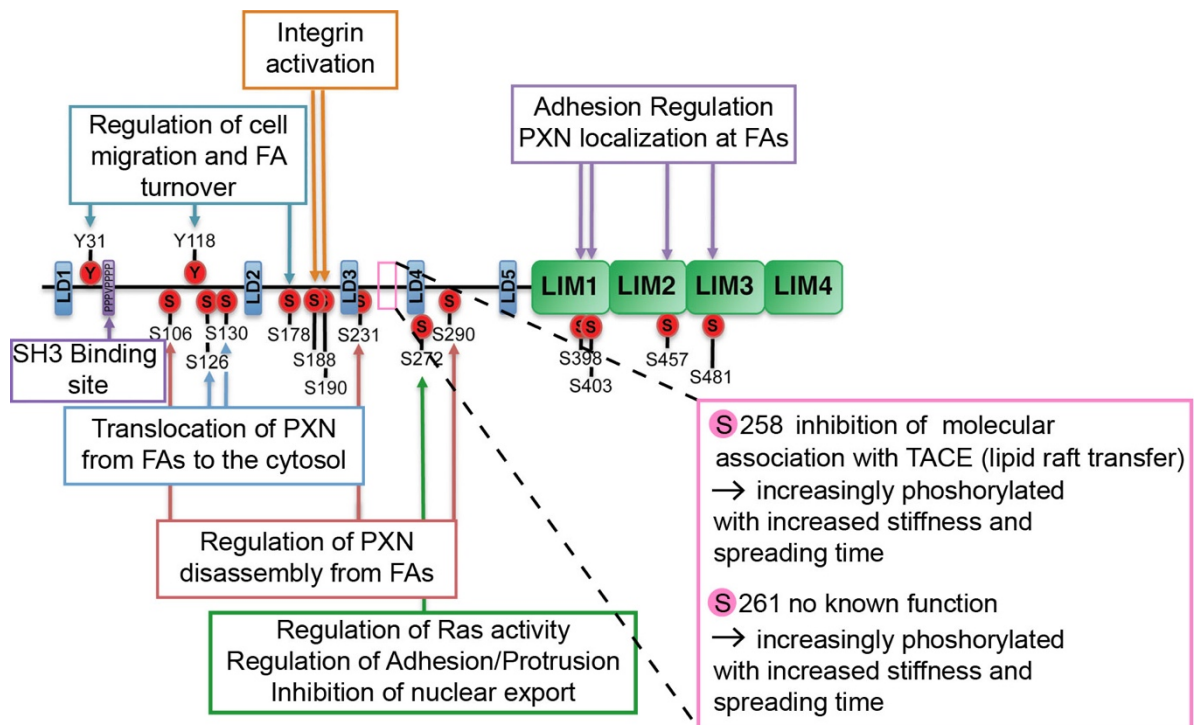
Figure 41 I Overview of structural and functional organization of Paxillin regarding its phosphorylation sites. Figure adapted from López-Colomé et al., 2017 [264] and extended.

Even though the protein has no intrinsic enzymatic activity it facilitates the formation of multiprotein complexes by functioning as a linker and docking protein. Many serine and also some tyrosine phosphorylations are regulating the respective binding and other functions of paxillin (**Figure 41**) [264].

In the present study I identified two phosphorylation sites of paxillin which are regulated with substrate stiffness and during cell spreading. Both phosphosites are increasingly phosphorylated the stiffer the FN-coated substrate is and also rise in phosphorylation over spreading time peaking at 120 min. Literature research revealed that the phosphorylation of serine 258 of paxillin is important for inhibition of molecular association with the protease TACE in lipid rafts [241]. However, no other functional role which could explain the increasing phosphorylation with increased substrate rigidity or the increasing phosphorylation during cell spreading was discovered so far. For the other regulated site on serine 261 no functional role is known at all. Nevertheless, the clear regulation of those sites with substrate stiffness and in the spreading process suggests a functional role of both phosphorylation sites. In order to explore the function of these phosphosites in mechanosensing and cell spreading CRISPR-Cas targeted mutation studies could be conducted. This approach may lead to identification of binding partners dependent on phosphorylation of S258 and S261. The serine residues are not located in one of the four LIM domains or in an LD motif but between LD3 and LD4 (**Figure 41**). In addition, the sites could control a change in conformation or the cellular localization of paxillin.

Phospho-Filamin A.

Cytoskeletal remodeling and rearrangement is controlled by a huge number of actin-binding proteins such as the filamins. Filamins are stabilizers for three-dimensional F-actin networks and connect those networks to the cell membrane by attaching to transmembrane receptors or ion channels. Filamins do not only bind F-actin but also to more than 70 different other proteins, including signaling molecules and transmembrane receptors, which are responsible for essential scaffolding functions and enable the integration of different cellular behaviors. Filamins affect mechanical properties of cells by generating dynamic orthogonal F-actin networks, thus ensuring membrane integrity and the resistance of cells against mechanical stress [265]. In the present study, increased phosphorylation with enhanced substrate stiffness of two residues (S2152 & S2158) was observed. The phosphorylation could not be measured on very soft conditions, such as a substrate stiffness of 0.5 kPa. In addition, phosphorylation of S2152/2158 was also regulated with spreading time, peaking at 60 min after cell seeding but retaining also high phosphorylation after 120 min. Filamin A consists of a N-terminal F actin binding domain and rod segment that is constructed of up to 24 repeats with approximately 96 amino acids each, two hinge regions and a C-terminal dimerization domain. The rod segment is split into two rod domains between the homologous repeats 15 and 16 [265]. The amino acid residues 2152 and 2158 are located in the repeat 20 of Filamin A, a region where many different proteins bind to filamin, including transcription factors, GTPase-related proteins and cell adhesion and migration proteins. Furthermore, Garcia et al. showed that phosphorylation of S2152 in FLNA stabilizes the protein, whereas dephosphorylation results in calpain mediated degradation. They propose that S2152 phosphorylation is present in the normal cell state with a highly organized cytoskeleton [266]. This theory reflects my observation of increasing phosphorylation of S2152 with rising substrate rigidity and spreading time. On 0.5 kPa where no phosphorylation was detected, actin crosslinking via filamin A is almost not present because the filamin is dephosphorylated and degraded. Phosphorylation of S2158 has no known function so far but may also be responsible for stabilization of the protein itself. Filamin A could be interesting to study in the context of lung fibrosis, since pathogenic mutation of the FLNA gene is associated with childhood interstitial lung disease [267]. Therefore, aberrant phosphorylation of FLNA might also be relevant in disease progression in adult-onset ILD.

Phospho-MAP1A.

As part of the cytoskeleton, microtubules are crucial cell structures that are required for numerous processes, such as determination of cell shape, mitosis, motility, polarity and intracellular transport [244]. MAP1A belongs to a heterogeneous group of microtubule binding proteins. These proteins have a microtubule binding domain and a projection domain, which

appears as a thread-like structure. By attaching along the side of microtubules, they stabilize the microtubules [268]. The newly identified phosphosite on serine residue 2237 is located in the projection domain of the protein and not in the N-terminal microtubule binding region [268]. MAP1A is increasingly phosphorylated at S2237, both with enhanced substrate stiffness as well as with spreading time. There are several known phosphorylation sites on MAP1A, however no downstream effect of phosphorylation of MAP1A is known so far. The phosphorylation may alter the binding affinity of MAP1A to microtubules or other binding partners. Given the phosphorylation increase upon the mechanical stimulus a function of the phosphorylation sites seems reasonable. Cell biological studies making use of p-site mutation could be the next steps to elaborate the functional relevance of this PTM in cell spreading and mechanosensing.

Phospho-MARCKS

Originally, the membrane-associated protein MARCKS was discovered as a major target of protein kinase C. The protein is involved in many cellular processes such as cytoskeletal control, motility, mediation of inflammatory responses and exocytosis. Furthermore, Yang et al. showed that MARCKS is highly phosphorylated on serine 152 and 158 in IPF lung tissues and fibroblasts as well as in a mouse pulmonary fibrosis model [245]. Even though I did not detect these sites in any of the phosphoproteomics data sets, I found the neighboring phosphorylation sites at S135 and T143 highly upregulated with increasing substrate stiffness in both CCL151 and primary human lung fibroblast cells. Accordingly, T143 phosphorylation is also induced early during cell spreading after 30 min and remain highly phosphorylated. Also in other studies of cell spreading an increase of phosphorylated MARCKS was detected in myoblast spreading on fibronectin coated surfaces after 30 min, however not at threonine 143 but on serine 152 and 156 [269]. MARCKS has three highly conserved domains, a myristoylated N-terminal domain, a MH2 domain and a phosphorylation site domain (PSD). The PSD ranges from amino acid residues 152-176 [245]. The phosphorylation sites S135 and T143 were measured and found to be significantly regulated in this study is not located in the PSD, but in an unstructured region before the PSD . The regulation of T143 phosphorylation in cell spreading and with changing substrate stiffness could be a potential mechanism for organizing cytoskeletal rearrangement. The sites could also be a priming site for other phosphorylation sites in the PSD domain. Interestingly, phosphosite S135 is not regulated with spreading time and seems only relevant in mechanosensing. Taken together, MARCKS may be an interesting target for further research in context of pulmonary lung fibrosis.

Phospho-Drebrin1

Drebrin (DBN1) has been identified to be involved in brain development in chicken [270]. Drebrin is an actin-binding protein and has two actin-binding regions AB1 and AB2 [271]. Via these domains it binds to actin filaments and increases their stability by inhibiting the depolymerization of the actin filaments. Indeed, cells that overexpress Drebrin tend to have more cell-substrate adhesions than normal cells [272, 273]. Recently, it was shown that drebrin expression is elevated in lung myofibroblasts where it promotes the expression of fibrosis-related genes [274]. DBN1 function can be regulated by phosphorylation. CDK5 phosphorylation of serine 142 regulates a cryptic F-actin bundling activity [187]. In CCL151 cells I found the phosphorylation of S142 strongly decreased on stiff substrates, with a similar trend in hpLF. However, no functional role is known for the other regulated phosphorylation sites of DBN1 on S339 and S345 so far. Here the opposite effect is observed. The increasingly phosphorylated phosphosites with rising substrate stiffness are located in the potential helical domain of the protein ranging from residues 257-355 [187]. The helical domain of drebrin alone is sufficient to induce filopodia [187], suggesting that phosphorylation sites in the domain could be responsible of controlling filopodia formation. Overall, drebrin1 phosphorylation seems to be interesting to be studied in the context of lung fibrosis.

Phospho-CAMK2D

The Ca2+/calmodulin-dependent protein kinase regulates Ca2+-mediated changes in cellular function. The enzyme's multimeric structure and autoregulation allows the kinase to actively participate in the sensitivity, timing and location of its action, thereby processing information from extracellular stimuli and intracellular Ca2+ increase [275]. CAMK2D was increasingly phosphorylated on threonine 337 with rising substrate stiffness in both human lung fibroblast data sets. This amino acid residue is neither located in the autophosphorylation region nor in the catalytic domain of the kinase. T337 phosphorylation of CAMK2D has not yet been assigned a functional role. Chen et al. hypothesized that CAMK2D might be involved in activation of fibroblasts in cardiac fibrosis. However, a potential role of CAMK2D in lung fibrosis was not examined so far.

Phospho-ABLIM3

AbLIM family proteins are characterized by the LIM domain. It has been shown that proteins of the LIM domain play a crucial role in several biological processes including cell lineage determination, embryonic development and cancer differentiation. The LIM domain is a double-zinc finger structure that facilitates protein-protein interactions [249]. Furthermore, proteins containing such domains might be potential tension sensors [18]. ABLIM3 was found

to be a binding partner of striated muscle activator of Rho signaling and thus may serve as a scaffold for signaling modules of the actin cytoskeleton, consequently modulating transcription [276]. ABLIM3 may be involved in the pathophysiological response to biomechanical stress and may initiate upregulation of initial cellular adaptation mechanism. This mechanism could function via proteins of the LIM domain and boost transcriptional activation by mediating Rho signals from the cytoplasm into the nucleus. So far, no functional regulation of ABLIM3 by phosphorylation is reported. The increased phosphorylation of S503/504 on stiff substrates might be of relevance for cytoskeletal signaling during mechanosensing and could also be involved in cell fate decisions through modulation of transcription.

Conclusions and perspective

This thesis generated a first global map of cell adhesion mediated sensing of the mechanical properties of fibronectin based microenvironments. The produced data sets can be the basis for future functional studies of individual phosphoproteins or phosphorylation sites. The optimization of enrichment techniques and the performance of new mass spectrometers will in the future achieve even higher identification rates and consequently enable even more comprehensive maps of dynamic cellular signaling. Knowledgebases will also continue to grow, and increasingly elaborated modelling tools will be developed, leading to a more detailed and comprehensive picture of the cells interaction with its environment. However, the more saturated the phosphoproteome gets, the more important will be the identification of kinase and phosphatases upstream of phosphorylation sites and the assignment of functions to the substrates. Therefore, a thoughtful design of experiments to investigate the functional role of phosphorylation and the resulting phenotype in different cellular settings will be crucial. Especially, to decipher complex signaling networks a big sample size, manifold perturbations and time-series data are necessary [94]. This is facilitated not only by higher-sensitivity methods and better enrichment strategies but also by multiplexing (TMT labeling or EASI-tag) of samples which enables more precision and accuracy [277]. In addition, improved software for data visualization and analysis as well as advancements in cell biology will each have an impact to shed light on the so far underexplored phosphoproteome [94]. Overall, this work provides a unique resource and a valuable basis for further functional studies of mechano-sensitive protein targets by inhibition of kinases with small-molecules and p-site mutations

References

1.   Vogel, V. and M. Sheetz, *Local force and geometry sensing regulate cell functions.* Nat Rev Mol Cell Biol, 2006. **7**(4): p. 265-75.
2.   Jansen, K.A., et al., *A guide to mechanobiology: Where biology and physics meet.* Biochim Biophys Acta, 2015. **1853**(11 Pt B): p. 3043-52.
3.   Mohammed, D., et al., *Innovative Tools for Mechanobiology: Unraveling Outside-In and Inside-Out Mechanotransduction.* Front Bioeng Biotechnol, 2019. **7**: p. 162.
4.   Wasik, A.A. and H.B. Schiller, *Functional proteomics of cellular mechanosensing mechanisms.* Semin Cell Dev Biol, 2017. **71**: p. 118-128.
5.   Hoffman, B.D., C. Grashoff, and M.A. Schwartz, *Dynamic molecular processes mediate cellular mechanotransduction.* Nature, 2011. **475**(7356): p. 316-23.
6.   Hytonen, V.P. and B. Wehrle-Haller, *Mechanosensing in cell-matrix adhesions - Converting tension into chemical signals.* Exp Cell Res, 2016. **343**(1): p. 35-41.
7.   Choquet, D., D.P. Felsenfeld, and M.P. Sheetz, *Extracellular matrix rigidity causes strengthening of integrin-cytoskeleton linkages.* Cell, 1997. **88**(1): p. 39-48.
8.   Riveline, D., et al., *Focal contacts as mechanosensors: externally applied local mechanical force induces growth of focal contacts by an mDia1-dependent and ROCK-independent mechanism.* J Cell Biol, 2001. **153**(6): p. 1175-86.
9.   von Wichert, G., et al., *RPTP-alpha acts as a transducer of mechanical force on alphav/beta3-integrin-cytoskeleton linkages.* J Cell Biol, 2003. **161**(1): p. 143-53.
10.   Galbraith, C.G., K.M. Yamada, and M.P. Sheetz, *The relationship between force and focal complex development.* J Cell Biol, 2002. **159**(4): p. 695-705.
11.   Gillespie, P.G. and R.G. Walker, *Molecular basis of mechanosensory transduction.* Nature, 2001. **413**(6852): p. 194-202.
12.   Ingber, D.E., *Cellular mechanotransduction: putting all the pieces together again.* FASEB J, 2006. **20**(7): p. 811-27.
13.   Engler, A.J., et al., *Matrix elasticity directs stem cell lineage specification.* Cell, 2006. **126**(4): p. 677-89.
14.   Ingber, D.E., *Tensegrity-based mechanosensing from macro to micro.* Prog Biophys Mol Biol, 2008. **97**(2-3): p. 163-79.
15.   Polte, T.R., et al., *Extracellular matrix controls myosin light chain phosphorylation and cell contractility through modulation of cell shape and cytoskeletal prestress.* Am J Physiol Cell Physiol, 2004. **286**(3): p. C518-28.
16.   Chen, Y., et al., *Receptor-mediated cell mechanosensing.* Mol Biol Cell, 2017. **28**(23): p. 3134-3155.
17.   Schiller, H.B. and R. Fassler, *Mechanosensitivity and compositional dynamics of cell-matrix adhesions.* EMBO Rep, 2013. **14**(6): p. 509-19.
18.   Schiller, H.B., et al., *Quantitative proteomics of the integrin adhesome show a myosin II-dependent recruitment of LIM domain proteins.* EMBO Rep, 2011. **12**(3): p. 259-66.
19.   Holle, A.W. and A.J. Engler, *More than a feeling: discovering, understanding, and influencing mechanosensing pathways.* Curr Opin Biotechnol, 2011. **22**(5): p. 648-54.
20.   Tzima, E., et al., *A mechanosensory complex that mediates the endothelial cell response to fluid shear stress.* Nature, 2005. **437**(7057): p. 426-31.
21.   Lo, C.M., et al., *Cell movement is guided by the rigidity of the substrate.* Biophys J, 2000. **79**(1): p. 144-52.
22.   Martino, F., et al., *Cellular Mechanotransduction: From Tension to Function.* Front Physiol, 2018. **9**: p. 824.
23.   Abercrombie, M. and G.A. Dunn, *Adhesions of fibroblasts to substratum during contact inhibition observed by interference reflection microscopy.* Exp Cell Res, 1975. **92**(1): p. 57-62.
24.   Abercrombie, M., J.E. Heaysman, and S.M. Pegrum, *The locomotion of fibroblasts in culture. IV. Electron microscopy of the leading lamella.* Exp Cell Res, 1971. **67**(2): p. 359-67.
25.   Zamir, E. and B. Geiger, *Molecular complexity and dynamics of cell-matrix adhesions.* J Cell Sci, 2001. **114**(Pt 20): p. 3583-90.
26.   Case, L.B. and C.M. Waterman, *Integration of actin dynamics and cell adhesion by a three-dimensional, mechanosensitive molecular clutch.* Nat Cell Biol, 2015. **17**(8): p. 955-63.
27.   Dupont, S., *Role of YAP/TAZ in cell-matrix adhesion-mediated signalling and mechanotransduction.* Exp Cell Res, 2016. **343**(1): p. 42-53.
28.   Zaidel-Bar, R. and B. Geiger, *The switchable integrin adhesome.* J Cell Sci, 2010. **123**(Pt 9): p. 1385-8.
29.   Zaidel-Bar, R., et al., *Functional atlas of the integrin adhesome.* Nat Cell Biol, 2007. **9**(8): p. 858-67.
30.   Pasapera, A.M., et al., *Myosin II activity regulates vinculin recruitment to focal adhesions through FAK-mediated paxillin phosphorylation.* J Cell Biol, 2010. **188**(6): p. 877-90.
31.   Hynes, R.O., *Integrins: bidirectional, allosteric signaling machines.* Cell, 2002. **110**(6): p. 673-87.
32.   Wolfenson, H., B. Yang, and M.P. Sheetz, *Steps in Mechanotransduction Pathways that Control Cell Morphology.* Annu Rev Physiol, 2019. **81**: p. 585-605.
33.   Wasik, A. and H.B. Schiller, *Functional proteomics of cellular mechanosensing mechanisms.* Semin Cell Dev Biol, 2017.

34. McKee, C.T., et al., *Indentation versus tensile measurements of Young's modulus for soft biological tissues.* Tissue Eng Part B Rev, 2011. **17**(3): p. 155-64.

35. Smith, L.R., S. Cho, and D.E. Discher, *Stem Cell Differentiation is Regulated by Extracellular Matrix Mechanics.* Physiology (Bethesda), 2018. **33**(1): p. 16-25.

36. Park, J.S., et al., *The effect of matrix stiffness on the differentiation of mesenchymal stem cells in response to TGF-beta.* Biomaterials, 2011. **32**(16): p. 3921-30.

37. Pelham, R.J., Jr. and Y. Wang, *Cell locomotion and focal adhesions are regulated by substrate flexibility.* Proc Natl Acad Sci U S A, 1997. **94**(25): p. 13661-5.

38. Dupont, S., et al., *Role of YAP/TAZ in mechanotransduction.* Nature, 2011. **474**(7350): p. 179-83.

39. Gupta, M., et al., *Adaptive rheology and ordering of cell cytoskeleton govern matrix rigidity sensing.* Nat Commun, 2015. **6**: p. 7525.

40. Zhou, Y., et al., *Inhibition of mechanosensitive signaling in myofibroblasts ameliorates experimental pulmonary fibrosis.* J Clin Invest, 2013. **123**(3): p. 1096-108.

41. Liu, F., et al., *Feedback amplification of fibrosis through matrix stiffening and COX-2 suppression.* J Cell Biol, 2010. **190**(4): p. 693-706.

42. Discher, D.E., P. Janmey, and Y.L. Wang, *Tissue cells feel and respond to the stiffness of their substrate.* Science, 2005. **310**(5751): p. 1139-1143.

43. Yeung, T., et al., *Effects of substrate stiffness on cell morphology, cytoskeletal structure, and adhesion.* Cell Motility and the Cytoskeleton, 2005. **60**(1): p. 24-34.

44. Nisenholz, N., et al., *Active mechanics and dynamics of cell spreading on elastic substrates.* Soft Matter, 2014. **10**(37): p. 7234-46.

45. Fardin, M.A., et al., *Cell spreading as a hydrodynamic process.* Soft Matter, 2010. **6**(19): p. 4788-4799.

46. Aparna Nori, E.K.F.Y., Sulin Chen, Kam W. Leong, *Cell adhesion*, in *Principles of Regenerative Medicine*, R.L. Anthony Atala, James Thomson, Robert Nerem, Editor. 2008, Academic Press.

47. McGrath, J.L., *Cell spreading: The power to simplify.* Current Biology, 2007. **17**(10): p. R357-R358.

48. Sackmann, E. and R.F. Bruinsma, *Cell adhesion as wetting transition?* Chemphyschem, 2002. **3**(3): p. 262-269.

49. Cuvelier, D., et al., *The universal dynamics of cell spreading.* Current Biology, 2007. **17**(8): p. 694-699.

50. Chen, C.S., et al., *Geometric control of cell life and death.* Science, 1997. **276**(5317): p. 1425-1428.

51. Dulbecco, R. and M.G. Stoker, *Conditions determining initiation of DNA synthesis in 3T3 cells.* Proc. Natl. Acad. Sci. USA, 1970. **66**: p. 204-211.

52. Folkman, J. and A. Moscona, *Role of cell shape in growth control.* Nature, 1978(273): p. 345-349.

53. Tschumperlin, D.J., et al., *Mechanosensing and fibrosis.* J Clin Invest, 2018. **128**(1): p. 74-84.

54. Humphrey, J.D., E.R. Dufresne, and M.A. Schwartz, *Mechanotransduction and extracellular matrix homeostasis.* Nat Rev Mol Cell Biol, 2014. **15**(12): p. 802-12.

55. Wynn, T.A., *Cellular and molecular mechanisms of fibrosis.* J Pathol, 2008. **214**(2): p. 199-210.

56. Wells, R.G., *Tissue mechanics and fibrosis.* Biochim Biophys Acta, 2013. **1832**(7): p. 884-90.

57. Asano, S., et al., *Matrix stiffness regulates migration of human lung fibroblasts.* Physiol Rep, 2017. **5**(9).

58. Marinkovic, A., F. Liu, and D.J. Tschumperlin, *Matrices of physiologic stiffness potently inactivate idiopathic pulmonary fibrosis fibroblasts.* Am J Respir Cell Mol Biol, 2013. **48**(4): p. 422-30.

59. Southern, B.D., et al., *Matrix-driven Myosin II Mediates the Pro-fibrotic Fibroblast Phenotype.* J Biol Chem, 2016. **291**(12): p. 6083-95.

60. Parker, M.W., et al., *Fibrotic extracellular matrix activates a profibrotic positive feedback loop.* J Clin Invest, 2014. **124**(4): p. 1622-35.

61. Tschumperlin, D.J., *Matrix, mesenchyme, and mechanotransduction.* Ann Am Thorac Soc, 2015. **12 Suppl 1**: p. S24-9.

62. Thannickal, V.J., et al., *Matrix biology of idiopathic pulmonary fibrosis: a workshop report of the national heart, lung, and blood institute.* Am J Pathol, 2014. **184**(6): p. 1643-51.

63. Swartz, M.A., et al., *Mechanical stress is communicated between different cell types to elicit matrix remodeling.* Proc Natl Acad Sci U S A, 2001. **98**(11): p. 6180-5.

64. Xie, G., et al., *Role of differentiation of liver sinusoidal endothelial cells in progression and regression of hepatic fibrosis in rats.* Gastroenterology, 2012. **142**(4): p. 918-927 e6.

65. Martinez, F.J., et al., *Idiopathic pulmonary fibrosis.* Nat Rev Dis Primers, 2017. **3**: p. 17074.

66. Annesi-Maesano, I., et al., *Geriatric study in Europe on health effects of air quality in nursing homes (GERIE study) profile: objectives, study protocol and descriptive data.* Multidiscip Respir Med, 2013. **8**(1): p. 71.

67. Patterson, K.C., et al., *Interstitial Lung Disease in the Elderly.* Chest, 2017. **151**(4): p. 838-844.

68. Selman, M. and A. Pardo, *Idiopathic pulmonary fibrosis: an epithelial/fibroblastic cross-talk disorder.* Respir Res, 2002. **3**: p. 3.

69. Nathan, S.D., et al., *Effect of pirfenidone on mortality: pooled analyses and meta-analyses of clinical trials in idiopathic pulmonary fibrosis.* Lancet Respir Med, 2017. **5**(1): p. 33-41.

70. Noble, P.W., et al., *Pirfenidone for idiopathic pulmonary fibrosis: analysis of pooled data from three multinational phase 3 trials.* Eur Respir J, 2016. **47**(1): p. 243-53.

71. Noble, P.W., et al., *Pirfenidone in patients with idiopathic pulmonary fibrosis (CAPACITY): two randomised trials.* Lancet, 2011. **377**(9779): p. 1760-9.

72. King, T.E., Jr., et al., *A phase 3 trial of pirfenidone in patients with idiopathic pulmonary fibrosis.* N Engl J Med, 2014. **370**(22): p. 2083-92.

73.   Ley, B., et al., *Pirfenidone Reduces Respiratory-related Hospitalizations in Idiopathic Pulmonary Fibrosis.* Am J Respir Crit Care Med, 2017. **196**(6): p. 756-761.

74.   Richeldi, L., et al., *Efficacy of a tyrosine kinase inhibitor in idiopathic pulmonary fibrosis.* N Engl J Med, 2011. **365**(12): p. 1079-87.

75.   Richeldi, L., et al., *Efficacy and safety of nintedanib in idiopathic pulmonary fibrosis.* N Engl J Med, 2014. **370**(22): p. 2071-82.

76.   Somogyi, V., et al., *The therapy of idiopathic pulmonary fibrosis: what is next?* Eur Respir Rev, 2019. **28**(153).

77.   Wolters, P.J., H.R. Collard, and K.D. Jones, *Pathogenesis of idiopathic pulmonary fibrosis.* Annu Rev Pathol, 2014. **9**: p. 157-79.

78.   Thannickal, V.J., et al., *Idiopathic pulmonary fibrosis: emerging concepts on pharmacotherapy.* Expert Opin Pharmacother, 2004. **5**(8): p. 1671-86.

79.   Wynn, T.A., *Integrating mechanisms of pulmonary fibrosis.* J Exp Med, 2011. **208**(7): p. 1339-50.

80.   Rafii, R., et al., *A review of current and novel therapies for idiopathic pulmonary fibrosis.* J Thorac Dis, 2013. **5**(1): p. 48-73.

81.   Lehmann, M., et al., *Senolytic drugs target alveolar epithelial cell function and attenuate experimental lung fibrosis ex vivo.* Eur Respir J, 2017. **50**(2).

82.   Selman, M. and A. Pardo, *Revealing the pathogenic and aging-related mechanisms of the enigmatic idiopathic pulmonary fibrosis. an integral model.* Am J Respir Crit Care Med, 2014. **189**(10): p. 1161-72.

83.   Kendall, R.T. and C.A. Feghali-Bostwick, *Fibroblasts in fibrosis: novel roles and mediators.* Front Pharmacol, 2014. **5**: p. 123.

84.   Peter J. Barnes, J.M.D., Stephen I. Rennard, Neil C. Thomson, *Asthma and COPD: Basic Mechanisms and Clinical Management.* Elsevier Ltd., 2009. **2**.

85.   Jordana, M., et al., *Immune-inflammatory functions of fibroblasts.* Eur Respir J, 1994. **7**(12): p. 2212-22.

86.   Tomasek, J.J., et al., *Myofibroblasts and mechano-regulation of connective tissue remodelling.* Nat Rev Mol Cell Biol, 2002. **3**(5): p. 349-63.

87.   Hinz, B., *Mechanical aspects of lung fibrosis: a spotlight on the myofibroblast.* Proc Am Thorac Soc, 2012. **9**(3): p. 137-47.

88.   Wynn, T.A., *Common and unique mechanisms regulate fibrosis in various fibroproliferative diseases.* J Clin Invest, 2007. **117**(3): p. 524-9.

89.   Hoyles, R.K., et al., *An essential role for resident fibroblasts in experimental lung fibrosis is defined by lineage-specific deletion of high-affinity type II transforming growth factor beta receptor.* Am J Respir Crit Care Med, 2011. **183**(2): p. 249-61.

90.   Phillips, R.J., et al., *Circulating fibrocytes traffic to the lungs in response to CXCL12 and mediate fibrosis.* J Clin Invest, 2004. **114**(3): p. 438-46.

91.   Hung, C., et al., *Role of lung pericytes and resident fibroblasts in the pathogenesis of pulmonary fibrosis.* Am J Respir Crit Care Med, 2013. **188**(7): p. 820-30.

92.   Walsh, C.T., S. Garneau-Tsodikova, and G.J. Gatto, Jr., *Protein posttranslational modifications: the chemistry of proteome diversifications.* Angew Chem Int Ed Engl, 2005. **44**(45): p. 7342-72.

93.   Hunter, T., *Protein kinases and phosphatases: the yin and yang of protein phosphorylation and signaling.* Cell, 1995. **80**(2): p. 225-36.

94.   Needham, E.J., et al., *Illuminating the dark phosphoproteome.* Sci Signal, 2019. **12**(565).

95.   Cohen, P., *The origins of protein phosphorylation.* Nat Cell Biol, 2002. **4**(5): p. E127-30.

96.   Low, T.Y., et al., *Unraveling the ubiquitin-regulated signaling networks by mass spectrometry-based proteomics.* Proteomics, 2013. **13**(3-4): p. 526-37.

97.   Jin, J. and T. Pawson, *Modular evolution of phosphorylation-based signalling systems.* Philos Trans R Soc Lond B Biol Sci, 2012. **367**(1602): p. 2540-55.

98.   Low, T.Y., et al., *Widening the Bottleneck of Phosphoproteomics: Evolving Strategies for Phosphopeptide Enrichment.* Mass Spectrom Rev, 2020.

99.   Alberts B., J., A., Lewis J., *Molekular Biologie der Zelle*. Vol. 4. 2004, Weinheim: Wiley-Vch Verlag GmbH und Co. KGaA.

100.   Hunter, T., *Why nature chose phosphate to modify proteins.* Philos Trans R Soc Lond B Biol Sci, 2012. **367**(1602): p. 2513-6.

101.   Ciesla, J., T. Fraczyk, and W. Rode, *Phosphorylation of basic amino acid residues in proteins: important but easily missed.* Acta Biochim Pol, 2011. **58**(2): p. 137-48.

102.   Meins, M., et al., *Cysteine phosphorylation of the glucose transporter of Escherichia coli.* J Biol Chem, 1993. **268**(16): p. 11604-9.

103.   Bertran-Vicente, J., et al., *Site-specifically phosphorylated lysine peptides.* J Am Chem Soc, 2014. **136**(39): p. 13622-8.

104.   Elsholz, A.K., et al., *Global impact of protein arginine phosphorylation on the physiology of Bacillus subtilis.* Proc Natl Acad Sci U S A, 2012. **109**(19): p. 7451-6.

105.   Ardito, F., et al., *The crucial role of protein phosphorylation in cell signaling and its use as targeted therapy (Review).* Int J Mol Med, 2017. **40**(2): p. 271-280.

106.   Krebs, E.G., *An accidental biochemist.* Annu Rev Biochem, 1998. **67**: p. xii-xxxii.

107.   Manning, G., et al., *Evolution of protein kinase signaling from yeast to man.* Trends Biochem Sci, 2002. **27**(10): p. 514-20.

108. Manning, G., et al., *The protein kinase complement of the human genome.* Science, 2002. **298**(5600): p. 1912-34.

109. Caunt, C.J. and S.M. Keyse, *Dual-specificity MAP kinase phosphatases (MKPs): shaping the outcome of MAP kinase signalling.* FEBS J, 2013. **280**(2): p. 489-504.

110. Zhang, M., et al., *Viewing serine/threonine protein phosphatases through the eyes of drug designers.* FEBS J, 2013. **280**(19): p. 4739-60.

111. Chen, M.J., J.E. Dixon, and G. Manning, *Genomics and evolution of protein phosphatases.* Sci Signal, 2017. **10**(474).

112. Nair, A., et al., *Conceptual Evolution of Cell Signaling.* International Journal of Molecular Sciences, 2019. **20**(13).

113. Day, E.K., N.G. Sosale, and M.J. Lazzara, *Cell signaling regulation by protein phosphorylation: a multivariate, heterogeneous, and context-dependent process.* Current Opinion in Biotechnology, 2016. **40**: p. 185-192.

114. Marusyk, A., V. Almendro, and K. Polyak, *Intra-tumour heterogeneity: a looking glass for cancer?* Nature Reviews Cancer, 2012. **12**(5): p. 323-334.

115. Laklai, H., et al., *Genotype tunes pancreatic ductal adenocarcinoma tissue tension to induce matricellular fibrosis and tumor progression.* Nature Medicine, 2016. **22**(5): p. 497-505.

116. Dingal, P.C.D.P., Y.T. Xia, and D.E. Discher, *Fractal Heterogeneity in Minimal Matrix Models of Scars Modulates Stiff-Niche Stem-Cell Responses Via Nuclear Exit of a Mechanorepressor.* Biophysical Journal, 2016. **110**(3): p. 306a-306a.

117. Savage, S.R. and B. Zhang, *Using phosphoproteomics data to understand cellular signaling: a comprehensive guide to bioinformatics resources.* Clinical Proteomics, 2020. **17**(1).

118. Humphrey, S.J., S.B. Azimifar, and M. Mann, *High-throughput phosphoproteomics reveals in vivo insulin signaling dynamics.* Nat Biotechnol, 2015. **33**(9): p. 990-5.

119. Leutert, M., et al., *R2-P2 rapid-robotic phosphoproteomics enables multidimensional cell signaling studies.* Molecular Systems Biology, 2019. **15**(12).

120. White, F.M. and A. Wolf-Yadlin, *Methods for the Analysis of Protein Phosphorylation-Mediated Cellular Signaling Networks.* Annual Review of Analytical Chemistry, Vol 9, 2016. **9**: p. 295-315.

121. Clark, D.P. and N.J. Pazdernik, *Molekulare Biotechnologie - Grundlagen und Anwendungen*. 2009, Heidelberg: Spektrum Akademischer Verlag.

122. Mallick, P. and B. Kuster, *Proteomics: a pragmatic perspective.* Nat Biotechnol, 2010. **28**(7): p. 695-709.

123. Wilkins, M.R., et al., *From Proteins to Proteomes: Large Scale Protein Identification by Two-Dimensional Electrophoreses and Amino Acid Analysis.* Biotechnology, 1996. **14**.

124. Kenrick, K.G. and J. Margolis, *Isoelectric Focusing and Gradient Gel Electrophoresis: A two-dimensional technique.* Anal Biochem 1970. **33**: p. 204-207.

125. Henzel, W.J., et al., *Identifiying proteins from two-dimensional gels by electrophoresis by molecular mass searching of peptide fragments in protein sequence data bases.* Proc. Natl. Acad. Sci. USA, 1993. **90**: p. 5011 -5015.

126. Geiger, T., et al., *Comparative proteomic analysis of eleven common cell lines reveals ubiquitous but varying expression of most proteins.* Mol Cell Proteomics, 2012. **11**(3): p. M111 014050.

127. Clamp, M., et al., *Distinguishing protein-coding and noncoding genes in the human genome.* PNAS, 2007. **104**(49): p. 19428-19433.

128. Arabidopsis Genome, I., *Analysis of the genome sequence of the flowering plant Arabidopsis thaliana.* Nature, 2000. **408**(6814): p. 796-815.

129. Consortium, C.e.S., *Genome sequence of the nematode C. elegans: a platform for investigating biology.* Science, 1998. **282**(5396): p. 2012-8.

130. Bludau, I. and R. Aebersold, *Proteomic and interactomic insights into the molecular basis of cell functional diversity.* Nat Rev Mol Cell Biol, 2020.

131. Mayya, V. and D.K. Han, *Phosphoproteomics by mass spectrometry: insights, implications, applications and limitations.* Expert Rev Proteomics, 2009. **6**(6): p. 605-18.

132. Bodenmiller, B., et al., *Phosphoproteomic analysis reveals interconnected system-wide responses to perturbations of kinases and phosphatases in yeast.* Sci Signal, 2010. **3**(153): p. rs4.

133. Steen, H. and M. Mann, *The ABC's (and XYZ's) of peptide sequencing.* Nat Rev Mol Cell Biol, 2004. **5**(9): p. 699-711.

134. Aebersold, R. and M. Mann, *Mass-spectrometric exploration of proteome structure and function.* Nature, 2016. **537**(7620): p. 347-55.

135. Giansanti, P., et al., *Six alternative proteases for mass spectrometry-based proteomics beyond trypsin.* Nat Protoc, 2016. **11**(5): p. 993-1006.

136. Tsiatsiani, L. and A.J. Heck, *Proteomics beyond trypsin.* FEBS J, 2015. **282**(14): p. 2612-26.

137. Swaney, D.L., C.D. Wenger, and J.J. Coon, *Value of using multiple proteases for large-scale mass spectrometry-based proteomics.* J Proteome Res, 2010. **9**(3): p. 1323-9.

138. Zhou, F., et al., *Online nanoflow reversed phase-strong anion exchange-reversed phase liquid chromatography-tandem mass spectrometry platform for efficient and in-depth proteome sequence analysis of complex organisms.* Anal Chem, 2011. **83**(18): p. 6996-7005.

139. Manadas, B., et al., *Peptide fractionation in proteomics approaches.* Expert Rev Proteomics, 2010. **7**(5): p. 655-63.

140. Ruprecht, B., et al., *Comprehensive and reproducible phosphopeptide enrichment using iron immobilized metal ion affinity chromatography (Fe-IMAC) columns.* Mol Cell Proteomics, 2015. **14**(1): p. 205-15.

141. Ho, C.S., et al., *Electrospray Ionisation Mass Spectrometry- Principles and Clinical Applications.* Clin Biochem Rev, 2003. **24**.

142. Scheltema, R.A., et al., *The Q Exactive HF, a Benchtop mass spectrometer with a pre-filter, high-performance quadrupole and an ultra-high-field Orbitrap analyzer.* Mol Cell Proteomics, 2014. **13**(12): p. 3698-708.

143. Yoshida, T., et al., *Detection of High Mass Molecular Ions by Laser Desorption Time of Flight Mass Spectrometry.* 1987.

144. Konermann, L., et al., *Unraveling the mechanism of electrospray ionization.* Anal Chem, 2013. **85**(1): p. 2-9.

145. Chloupek, R.C., et al., *Study of the primary structure of recombinant tissue plasminogen activator by reversed-phase high-performance liquid chromatographic tryptic mapping.* J Chromatogr., 1989. **463**: p. 375-396.

146. Makarov, A. and M. Scigelova, *Coupling liquid chromatography to Orbitrap mass spectrometry.* J Chromatogr A, 2010. **1217**(25): p. 3938-45.

147. Eliuk, S. and A. Makarov, *Evolution of Orbitrap Mass Spectrometry Instrumentation.* Annu. Rev. Anal. Chem., 2015.

148. Scigelova, M. and A. Makarov, *Orbitrap mass analyzer--overview and applications in proteomics.* Proteomics, 2006. **6 Suppl 2**: p. 16-21.

149. Sleno, L. and D.A. Volmer, *Ion activation methods for tandem mass spectrometry.* J Mass Spectrom, 2004. **39**(10): p. 1091-112.

150. Michalski, A., et al., *A systematic investigation into the nature of tryptic HCD spectra.* J Proteome Res, 2012. **11**(11): p. 5479-91.

151. Yang, Y.H., et al., *Low mass cutoff evasion with q(z) value optimization in ion trap.* Anal Biochem, 2009. **387**(1): p. 133-5.

152. Roepstorff, P. and J. Fohlman, *Proposal for a common nomenclature for sequence ions in mass spectra of peptides.* Biomed Mass Spectrom, 1984. **11**(11): p. 601.

153. Nesvizhskii, A.I., O. Vitek, and R. Aebersold, *Analysis and validation of proteomic data generated by tandem mass spectrometry.* Nat Methods, 2007. **4**(10): p. 787-97.

154. Eng, J.K., A.L. McCormack, and J.R. Yates, *An approach to correlate tandem mass spectral data of peptides with amino acid sequences in a protein database.* J Am Soc Mass Spectrom, 1994. **5**(11): p. 976-89.

155. Cox, J., et al., *Andromeda: a peptide search engine integrated into the MaxQuant environment.* J Proteome Res, 2011. **10**(4): p. 1794-805.

156. Bantscheff, M., et al., *Quantitative mass spectrometry in proteomics: critical review update from 2007 to the present.* Anal Bioanal Chem, 2012. **404**(4): p. 939-65.

157. Bantscheff, M., et al., *Quantitative mass spectrometry in proteomics: a critical review.* Anal Bioanal Chem, 2007. **389**(4): p. 1017-31.

158. Grossmann, J., et al., *Implementation and evaluation of relative and absolute quantification in shotgun proteomics with label-free methods.* J Proteomics, 2010. **73**(9): p. 1740-6.

159. Chelius, D. and P.V. Bondarenko, *Quantitative profiling of proteins in complex mixtures using liquid chromatography and mass spectrometry.* J Proteome Res, 2002. **1**(4): p. 317-23.

160. Bondarenko, P.V., D. Chelius, and T.A. Shaler, *Identification and relative quantitation of protein mixtures by enzymatic digestion followed by capillary reversed-phase liquid chromatography-tandem mass spectrometry.* Anal Chem, 2002. **74**(18): p. 4741-9.

161. Cox, J. and M. Mann, *MaxQuant enables high peptide identification rates, individualized p.p.b.-range mass accuracies and proteome-wide protein quantification.* Nat Biotechnol, 2008. **26**(12): p. 1367-72.

162. Cox, J., et al., *Accurate proteome-wide label-free quantification by delayed normalization and maximal peptide ratio extraction, termed MaxLFQ.* Mol Cell Proteomics, 2014. **13**(9): p. 2513-26.

163. Tyanova, S., T. Temu, and J. Cox, *The MaxQuant computational platform for mass spectrometry-based shotgun proteomics.* Nat Protoc, 2016. **11**(12): p. 2301-2319.

164. Mertins, P., et al., *Reproducible workflow for multiplexed deep-scale proteome and phosphoproteome analysis of tumor tissues by liquid chromatography-mass spectrometry.* Nat Protoc, 2018. **13**(7): p. 1632-1661.

165. Humphrey, S.J., et al., *High-throughput and high-sensitivity phosphoproteomics with the EasyPhos platform.* Nat Protoc, 2018. **13**(9): p. 1897-1916.

166. Giorgianni, F. and S. Beranova-Giorgianni, *Phosphoproteome Discovery in Human Biological Fluids.* Proteomes, 2016. **4**(4).

167. Rappsilber, J., M. Mann, and Y. Ishihama, *Protocol for micro-purification, enrichment, pre-fractionation and storage of peptides for proteomics using StageTips.* Nat Protoc, 2007. **2**(8): p. 1896-906.

168. Kuo, J.C., et al., *Analysis of the myosin-II-responsive focal adhesion proteome reveals a role for beta-Pix in negative regulation of focal adhesion maturation.* Nat Cell Biol, 2011. **13**(4): p. 383-93.

169. Zemel, A., De R., and S.S. A., *Mechanical consequences of cellular force generation.* Current Opinion in Solid State and Material Science, 2011. **15**: p. 169-176.

170. Schwarz, U.S. and S.A. Safran, *Physics of adherent cells.* Reviews of Modern Physics, 2013. **85**: p. 1327-1381.

171. Tyanova, S., et al., *The Perseus computational platform for comprehensive analysis of (prote)omics data.* Nature Methods, 2016. **13**(9): p. 731-740.

172. Zhou, Y., et al., *Metascape provides a biologist-oriented resource for the analysis of systems-level datasets.* Nat Commun, 2019. **10**(1): p. 1523.

173. Wolf, F.A., P. Angerer, and F.J. Theis, *SCANPY: large-scale single-cell gene expression data analysis.* Genome Biology, 2018. **19**.

174. McInnes, L., J. Healy, and J. Melville, *Umap: Uniform manifold approximation and pro- jection for dimension reduction.* arXiv preprint 2018.

175. Vicente-Manzanares, M., et al., *Non-muscle myosin II takes centre stage in cell adhesion and migration.* Nat Rev Mol Cell Biol, 2009. **10**(11): p. 778-90.

176. Radtke, S., et al., *ERK2 but not ERK1 mediates HGF-induced motility in non-small cell lung carcinoma cell lines.* J Cell Sci, 2013. **126**(Pt 11): p. 2381-91.

177. Parrini, M.C., et al., *Dissecting activation of the PAK1 kinase at protrusions in living cells.* J Biol Chem, 2009. **284**(36): p. 24133-43.

178. Lekmine, F., et al., *Activation of the p70 S6 kinase and phosphorylation of the 4E-BP1 repressor of mRNA translation by type I interferons.* J Biol Chem, 2003. **278**(30): p. 27772-80.

179. Han, J.W., et al., *Rapamycin, wortmannin, and the methylxanthine SQ20006 inactivate p70s6k by inducing dephosphorylation of the same subset of sites.* J Biol Chem, 1995. **270**(36): p. 21396-403.

180. Lekmine, F., et al., *Interferon-gamma engages the p70 S6 kinase to regulate phosphorylation of the 40S S6 ribosomal protein.* Exp Cell Res, 2004. **295**(1): p. 173-82.

181. Singh, A.M., et al., *Signaling network crosstalk in human pluripotent cells: a Smad2/3-regulated switch that controls the balance between self-renewal and differentiation.* Cell Stem Cell, 2012. **10**(3): p. 312-26.

182. Raingeaud, J., et al., *MKK3- and MKK6-regulated gene expression is mediated by the p38 mitogen-activated protein kinase signal transduction pathway.* Mol Cell Biol, 1996. **16**(3): p. 1247-55.

183. Zheng, Y., et al., *Ras-induced and extracellular signal-regulated kinase 1 and 2 phosphorylation-dependent isomerization of protein tyrosine phosphatase (PTP)-PEST by PIN1 promotes FAK dephosphorylation by PTP-PEST.* Mol Cell Biol, 2011. **31**(21): p. 4258-69.

184. Kelley, L.C., et al., *Cortactin phosphorylated by ERK1/2 localizes to sites of dynamic actin regulation and is required for carcinoma lamellipodia persistence.* PLoS One, 2010. **5**(11): p. e13847.

185. Hamirally, S., et al., *Viral mimicry of Cdc2/cyclin-dependent kinase 1 mediates disruption of nuclear lamina during human cytomegalovirus nuclear egress.* PLoS Pathog, 2009. **5**(1): p. e1000275.

186. Goto, H., et al., *Phosphorylation and reorganization of vimentin by p21-activated kinase (PAK).* Genes Cells, 2002. **7**(2): p. 91-7.

187. Worth, D.C., et al., *Drebrin contains a cryptic F-actin-bundling activity regulated by Cdk5 phosphorylation.* J Cell Biol, 2013. **202**(5): p. 793-806.

188. Omarjee, S., et al., *The molecular mechanisms underlying the ERalpha-36-mediated signaling in breast cancer.* Oncogene, 2017. **36**(18): p. 2503-2514.

189. Brantley, M.A., Jr. and J.W. Harbour, *Inactivation of retinoblastoma protein in uveal melanoma by phosphorylation of sites in the COOH-terminal region.* Cancer Res, 2000. **60**(16): p. 4320-3.

190. Sen, S., et al., *Retinoblastoma Protein Modulates the Inverse Relationship between Cellular Proliferation and Elastogenesis.* Journal of Biological Chemistry, 2011. **286**(42): p. 36580-36591.

191. Elliott, M.R., et al., *Down-regulation of IL-2 production in T lymphocytes by phosphorylated protein kinase A-RIIbeta.* J Immunol, 2004. **172**(12): p. 7804-12.

192. Martin, M., et al., *Novel Serine 176 Phosphorylation of YBX1 Activates NF-kappaB in Colon Cancer.* J Biol Chem, 2017. **292**(8): p. 3433-3444.

193. Yao, K., et al., *Nuclear factor of activated T3 is a negative regulator of Ras-JNK1/2-AP-1 induced cell transformation.* Cancer Res, 2007. **67**(18): p. 8725-35.

194. Ichikawa, K., et al., *MCRIP1, an ERK substrate, mediates ERK-induced gene silencing during epithelial-mesenchymal transition by regulating the co-repressor CtBP.* Mol Cell, 2015. **58**(1): p. 35-46.

195. Wang, X.L., et al., *The RNA polymerase III repressor MAF1 is regulated by ubiquitin-dependent proteasome degradation and modulates cancer drug resistance and apoptosis.* Journal of Biological Chemistry, 2019. **294**(50): p. 19255-19268.

196. Shor, B., et al., *Requirement of the mTOR Kinase for the Regulation of Maf1 Phosphorylation and Control of RNA Polymerase III-dependent Transcription in Cancer Cells.* Journal of Biological Chemistry, 2010. **285**(20): p. 15380-15392.

197. Michels, A.A., et al., *mTORC1 Directly Phosphorylates and Regulates Human MAF1.* Molecular and Cellular Biology, 2010. **30**(15): p. 3749-3757.

198. Zhang, C., H.L. Mao, and Y. Cao, *Nuclear accumulation of symplekin promotes cellular proliferation and dedifferentiation in an ERK1/2-dependent manner.* Scientific Reports, 2017. **7**.

199. Al-Tamari, H.M., et al., *FoxO3 an important player in fibrogenesis and therapeutic target for idiopathic pulmonary fibrosis.* Embo Molecular Medicine, 2018. **10**(2): p. 276-293.

200. Celestini, V., et al., *Uncoupling FoxO3A mitochondrial and nuclear functions in cancer cells undergoing metabolic stress and chemotherapy.* Cell Death & Disease, 2018. **9**.

201. Intine, R.V.A., et al., *Control of transfer RNA maturation by phosphorylation of the human La antigen on Serine 366.* Molecular Cell, 2000. **6**(2): p. 339-348.
202. Zhou, J., et al., *Overexpression of HP1 gamma is associated with poor prognosis in non-small cell lung cancer cell through promoting cell survival.* Tumor Biology, 2014. **35**(10): p. 9777-9785.
203. Harouz, H., et al., *Shigella flexneri targets the HP1 gamma subcode through the phosphothreonine lyase OspF.* Embo Journal, 2014. **33**(22): p. 2606-2622.
204. Wang, A.H., et al., *Regulation of histone deacetylase 4 by binding of 14-3-3 proteins.* Molecular and Cellular Biology, 2000. **20**(18): p. 6904-6912.
205. Budzynski, M.A., et al., *Uncoupling Stress-Inducible Phosphorylation of Heat Shock Factor 1 from Its Activation.* Molecular and Cellular Biology, 2015. **35**(14): p. 2530-2540.
206. Borisova, M.E., et al., *p38-MK2 signaling axis regulates RNA metabolism after UV-light-induced DNA damage.* Nature Communications, 2018. **9**.
207. Rossignol, M., et al., *Kinase activity and phosphorylation of the largest subunit of TFIIF transcription factor.* Journal of Biological Chemistry, 1999. **274**(32): p. 22387-22392.
208. Meggio, F. and L.A. Pinna, *One-thousand-and-one substrates of protein kinase CK2?* Faseb Journal, 2003. **17**(3): p. 349-368.
209. Soliman, G.A., et al., *mTOR Ser-2481 autophosphorylation monitors mTORC-specific catalytic activity and clarifies rapamycin mechanism of action.* J Biol Chem, 2010. **285**(11): p. 7866-79.
210. Kunapuli, P., V.V. Gurevich, and J.L. Benovic, *Phospholipid-stimulated autophosphorylation activates the G protein-coupled receptor kinase GRK5.* J Biol Chem, 1994. **269**(14): p. 10209-12.
211. Hirata, N., M. Takahashi, and M. Yazawa, *Diphosphorylation of regulatory light chain of myosin IIA is responsible for proper cell spreading.* Biochem Biophys Res Commun, 2009. **381**(4): p. 682-7.
212. Kwak, T.K., et al., *Cell Adhesion-dependent Serine 85 Phosphorylation of Paxillin Modulates Focal Adhesion Formation and Haptotactic Migration via Association with the C-terminal Tail Domain of Talin.* Journal of Biological Chemistry, 2012. **287**(33): p. 27499-27509.
213. Newell-Litwa, K.A., et al., *ROCK1 and 2 differentially regulate actomyosin organization to drive cell and synaptic polarity.* Journal of Cell Biology, 2015. **210**(2): p. 225-242.
214. Rai, V., et al., *Myosin IIA Heavy Chain Phosphorylation Mediates Adhesion Maturation and Protrusion in Three Dimensions.* J Biol Chem, 2017. **292**(8): p. 3099-3111.
215. Patchell, V.B., et al., *Phosphorylation of the minimal inhibitory region at the C-terminus of caldesmon alters its structural and actin binding properties.* Biochim Biophys Acta, 2002. **1596**(1): p. 121-30.
216. Butt, E., et al., *Heat shock protein 27 is a substrate of cGMP-dependent protein kinase in intact human platelets - Phosphorylation-induced actin polymerization caused by Hsp27 mutants.* Journal of Biological Chemistry, 2001. **276**(10): p. 7108-7113.
217. Mendoza, M.C., et al., *ERK-MAPK Drives Lamellipodia Protrusion by Activating the WAVE2 Regulatory Complex.* Molecular Cell, 2011. **41**(6): p. 661-671.
218. Yuan, J., et al., *Tyr23 phosphorylation of Anxa2 enhances STAT3 activation and promotes proliferation and invasion of breast cancer cells.* Breast Cancer Research and Treatment, 2017. **164**(2): p. 327-340.
219. Polzien, L., et al., *BAD contributes to RAF-mediated proliferation and cooperates with B-RAF-V600E in cancer signaling.* J Biol Chem, 2011. **286**(20): p. 17934-44.
220. Cuesta, R. and M.K. Holz, *RSK-mediated down-regulation of PDCD4 is required for proliferation, survival, and migration in a model of triple-negative breast cancer.* Oncotarget, 2016. **7**(19): p. 27567-27583.
221. Ritt, D.A., et al., *Impact of feedback phosphorylation and Raf heterodimerization on normal and mutant B-Raf signaling.* Mol Cell Biol, 2010. **30**(3): p. 806-19.
222. Sun, Y., et al., *Phosphorylation of Ser6 in hnRNPA1 by S6K2 regulates glucose metabolism and cell growth in colorectal cancer.* Oncol Lett, 2017. **14**(6): p. 7323-7331.
223. Herranz, N., et al., *mTOR regulates MAPKAPK2 translation to control the senescence-associated secretory phenotype.* Nat Cell Biol, 2015. **17**(9): p. 1205-17.
224. Kuang, X., et al., *The phosphorylation-specific association of STMN1 with GRP78 promotes breast cancer metastasis.* Cancer Research, 2017. **77**.
225. Nagata-Ohashi, K., et al., *A pathway of neuregulin-induced activation of cofilin-phosphatase Slingshot and cofilin in lamellipodia.* J Cell Biol, 2004. **165**(4): p. 465-71.
226. Itano, N., et al., *Cell spreading controls endoplasmic and nuclear calcium: a physical gene regulation pathway from the cell surface to the nucleus.* Proc Natl Acad Sci U S A, 2003. **100**(9): p. 5181-6.
227. Freilinger, A., et al., *Tuberin activates the proapoptotic molecule BAD.* Oncogene, 2006. **25**(49): p. 6467-79.
228. Tolnay, M., Y.T. Juang, and G.C. Tsokos, *Protein kinase A enhances, whereas glycogen synthase kinase-3 beta inhibits, the activity of the exon 2-encoded transactivator domain of heterogeneous nuclear ribonucleoprotein D in a hierarchical fashion.* Biochemical Journal, 2002. **363**: p. 127-136.
229. Galliher-Beckley, A.J., J.G. Williams, and J.A. Cidlowski, *Ligand-independent phosphorylation of the glucocorticoid receptor integrates cellular stress pathways with nuclear receptor signaling.* Mol Cell Biol, 2011. **31**(23): p. 4663-75.
230. Shitashige, M., et al., *Traf2-and Nck-Interacting Kinase Is Essential for Wnt Signaling and Colorectal Cancer Growth.* Cancer Research, 2010. **70**(12): p. 5024-5033.
231. Bell, S., A.L. Redmann, and E.M. Terentjev, *Universal Kinetics of the Onset of Cell Spreading on Substrates of Different Stiffness.* Biophysical Journal, 2019. **116**(3): p. 551-559.

232. Li, J.J., D. Han, and Y.P. Zhao, *Kinetic behaviour of the cells touching substrate: the interfacial stiffness guides cell spreading (vol 4, 3910, 2014).* Scientific Reports, 2014. **4**.

233. Ajuh, P., et al., *Functional analysis of the human CDC5L complex and identification of its components by mass spectrometry.* EMBO J, 2000. **19**(23): p. 6569-81.

234. Paytubi, S., et al., *The N-terminal region of ABC50 interacts with eukaryotic initiation factor eIF2 and is a target for regulatory phosphorylation by CK2.* Biochemical Journal, 2008. **409**: p. 223-231.

235. Schlunck, G., et al., *Substrate rigidity modulates cell matrix interactions and protein expression in human trabecular meshwork cells.* Invest Ophthalmol Vis Sci, 2008. **49**(1): p. 262-9.

236. Cole, A.R., et al., *Distinct priming kinases contribute to differential regulation of collapsin response mediator proteins by glycogen synthase kinase-3 in vivo.* J Biol Chem, 2006. **281**(24): p. 16591-8.

237. Tao, J., H.Y. Wang, and C.C. Malbon, *Protein kinase A regulates AKAP250 (gravin) scaffold binding to the beta2-adrenergic receptor.* EMBO J, 2003. **22**(24): p. 6419-29.

238. Bertacchini, J., et al., *The protein kinase Akt/PKB regulates both prelamin A degradation and Lmna gene expression.* Faseb Journal, 2013. **27**(6): p. 2145-2155.

239. Uddin, B., et al., *The human phosphatase CDC14A modulates primary cilium length by regulating centrosomal actin nucleation.* Embo Reports, 2019. **20**(1).

240. UniProt, C., *UniProt: a worldwide hub of protein knowledge.* Nucleic Acids Res, 2019. **47**(D1): p. D506-D515.

241. Lee, J.H., et al., *HIV Nef, paxillin, and Pak1/2 regulate activation and secretion of TACE/ADAM10 proteases.* Mol Cell, 2013. **49**(4): p. 668-79.

242. Feng, Y. and C.A. Walsh, *The many faces of filamin: a versatile molecular scaffold for cell motility and signalling.* Nat Cell Biol, 2004. **6**(11): p. 1034-8.

243. Zhong, Z., et al., *Cyclin D1/cyclin-dependent kinase 4 interacts with filamin A and affects the migration and invasion potential of breast cancer cells.* Cancer Res, 2010. **70**(5): p. 2105-14.

244. Halpain, S. and L. Dehmelt, *The MAP1 family of microtubule-associated proteins.* Genome Biol, 2006. **7**(6): p. 224.

245. Fong, L.W.R., D.C. Yang, and C.H. Chen, *Myristoylated alanine-rich C kinase substrate (MARCKS): a multirole signaling protein in cancers.* Cancer Metastasis Rev, 2017. **36**(4): p. 737-747.

246. Yamashiro, S., et al., *Citron kinase, a Rho-dependent kinase, induces di-phosphorylation of regulatory light chain of myosin II.* Mol Biol Cell, 2003. **14**(5): p. 1745-56.

247. Gao, N., et al., *Role of PI3K/AKT/mTOR signaling in the cell cycle progression of human prostate cancer.* Biochem Biophys Res Commun, 2003. **310**(4): p. 1124-32.

248. Schreiber, T.B., et al., *An integrated phosphoproteomics work flow reveals extensive network regulation in early lysophosphatidic acid signaling.* Mol Cell Proteomics, 2010. **9**(6): p. 1047-62.

249. Krupp, M., et al., *Actin binding LIM protein 3 (abLIM3).* International Journal of Molecular Medicine, 2006. **17**(1): p. 129-133.

250. Machida, K., B.J. Mayer, and P. Nollau, *Profiling the global tyrosine phosphorylation state.* Mol Cell Proteomics, 2003. **2**(4): p. 215-33.

251. Murphy, J.M., et al., *The pseudokinase MLKL mediates necroptosis via a molecular switch mechanism.* Immunity, 2013. **39**(3): p. 443-53.

252. Finn, R.D., et al., *Pfam: the protein families database.* Nucleic Acids Res, 2014. **42**(Database issue): p. D222-30.

253. Landry, C.R., E.D. Levy, and S.W. Michnick, *Weak functional constraints on phosphoproteomes.* Trends Genet, 2009. **25**(5): p. 193-7.

254. Lienhard, G.E., *Non-functional phosphorylations?* Trends Biochem Sci, 2008. **33**(8): p. 351-2.

255. Sacco, F., et al., *The human phosphatase interactome: An intricate family portrait.* FEBS Lett, 2012. **586**(17): p. 2732-9.

256. Olsen, J.V., et al., *Quantitative phosphoproteomics reveals widespread full phosphorylation site occupancy during mitosis.* Sci Signal, 2010. **3**(104): p. ra3.

257. Mertins, P., et al., *Proteogenomics connects somatic mutations to signalling in breast cancer.* Nature, 2016. **534**(7605): p. 55-62.

258. Ritz, A., et al., *Pathways on demand: automated reconstruction of human signaling networks.* NPJ Syst Biol Appl, 2016. **2**: p. 16002.

259. Rudolph, J.D., et al., *Elucidation of Signaling Pathways from Large-Scale Phosphoproteomic Data Using Protein Interaction Networks.* Cell Syst, 2016. **3**(6): p. 585-593 e3.

260. Mayya, V. and K.H. D, *Proteomic applications of protein quantification by isotope-dilution mass spectrometry.* Expert Rev Proteomics, 2006. **3**(6): p. 597-610.

261. Yang, Y., et al., *Biophysical Regulation of Cell Behavior-Cross Talk between Substrate Stiffness and Nanotopography.* Engineering, 2017. **3**(1): p. 36-54.

262. Puleo, J.I., et al., *Mechanosensing during directed cell migration requires dynamic actin polymerization at focal adhesions.* Journal of Cell Biology, 2019. **218**(12): p. 4215-4235.

263. Angelini, A., et al., *Mechanosensing dysregulation in the fibroblast: A hallmark of the aging heart.* Ageing Res Rev, 2020. **63**: p. 101150.

264. Lopez-Colome, A.M., et al., *Paxillin: a crossroad in pathological cell migration.* J Hematol Oncol, 2017. **10**(1): p. 50.

265. Zhou, A.X., J.H. Hartwig, and L.M. Akyurek, *Filamins in cell signaling, transcription and organ development.* Trends Cell Biol, 2010. **20**(2): p. 113-23.

266.   Garcia, E., A. Stracher, and D. Jay, *Calcineurin dephosphorylates the C-terminal region of filamin in an important regulatory site: a possible mechanism for filamin mobilization and cell signaling.* Arch Biochem Biophys, 2006. **446**(2): p. 140-50.

267.   Sasaki, E., et al., *A review of filamin A mutations and associated interstitial lung disease.* Eur J Pediatr, 2019. **178**(2): p. 121-129.

268.   N. Hirokawa, R.T., *Microtubule-Associated Proteins*, in *Encyclopedia of Biological Chemistry.* 2013. p. 103-107.

269.   Disatnik, M.H., et al., *The bi-directional translocation of MARCKS between membrane and cytosol regulates integrin-mediated muscle cell spreading.* Journal of Cell Science, 2004. **117**(19): p. 4469-4479.

270.   Shirao, T. and K. Obata, *Two acidic proteins associated with brain development in chick embryo.* J Neurochem, 1985. **44**(4): p. 1210-6.

271.   Asada, H., K. Uyemura, and T. Shirao, *Actin-binding protein, drebrin, accumulates in submembranous regions in parallel with neuronal differentiation.* J Neurosci Res, 1994. **38**(2): p. 149-59.

272.   Mikati, M.A., E.E. Grintsevich, and E. Reisler, *Drebrin-induced stabilization of actin filaments.* J Biol Chem, 2013. **288**(27): p. 19926-38.

273.   Ikeda, K., et al., *Effect of a neuron-specific actin-binding protein, drebrin A, on cell-substratum adhesion.* Neurosci Lett, 1995. **194**(3): p. 197-200.

274.   Hironaka, T., et al., *Drebrin is induced during myofibroblast differentiation and enhances the production of fibrosis-related genes.* Biochemical and Biophysical Research Communications, 2020. **529**(2): p. 224-230.

275.   Hudmon, A. and H. Schulman, *Structure-function of the multifunctional Ca2+/calmodulin-dependent protein kinase II.* Biochemical Journal, 2002. **364**: p. 593-611.

276.   Barrientos, T., et al., *Two novel members of the ABLIM protein family, ABLIM-2 and -3, associate with STARS and directly bind F-actin.* J Biol Chem, 2007. **282**(11): p. 8393-403.

277.   Winter, S.V., et al., *EASI-tag enables accurate multiplexed and interference-free MS2-based proteome quantification.* Nature Methods, 2018. **15**(7): p. 527-+.

Abbreviations

2D	two-dimensional
3D	three-dimensional
ACN	actonitrile
ANOVA	analysis of variance
APS	Ammonium persulfate
ATP	adenosine triphophate
BCA	bicinchoninic acid assay
BSA	bovine serum albumin
CAA	2-chloracetamide
CCL151	normal human lung fiboblast cell line
CID	collision induced dissociation
CRM	charged residue model
DMEM	Dulbecco's modified Eagle's medium
DMSO	dimethyl sulfoxide
DTT	dithiortheitol
DWP	deep well plate
ECM	extra cellular matrix
EDTA	ethylendiamintetraacetic acid
ESI	electrospray ionization
ETD	electron transfer dissociation
FA	focal adhesion
FBS	fetal bovine serum
FDR	false discovery rate
FT	fourier transformation
FT-ICR	fourier transform ion cyclotron resonance
GdmCl	guanidinium chloride
HCD	high collision induced dissociation
HPLC	High performance liquid chromatography
hpLF	human primary lung fibroblast
IEM	ion evaporation model
IMAC	immobilized metal affinity chromatography
kPa	kilopascal
LC	liquid chromatography
LFQ	lable free quantification
MALDI	matrix-assisted laser desorption/ionization
MOPS	3-(N-morpholino)propanesulfonic acid
MRLC	myosin regulatory light chain
MS	mass spectrometry
MS/MS	tandem mass spectrometry
NCE	normalized collision energy

NP-40	nonyl phenoxypolythoxylethanol
o. n.	overnight
PBS	phosphate buffered saline
PCA	principle component analysis
PDMS	polydimethylsiloxane
PM	Plasma membrane
ppm	parts per million
PS	penicillin/streptomycine
PTM	post-translational modification
RIPA	Radioimmunoprecipitation assay buffer
RT	room temperature
SD	standard deviation
SDB-RPS	Styrene Divinylbenzene Reversed-Phase Sulfonate
SDS	sodium dodecyl sulfate
SDS-PAGE	sodium dodecyl sulfate polyacrylamide gel electrophoresis
SEM	standard error of the mean
TBS	tris-buffered saline
TBS-T	tris-buffered saline - tween
TEMED	Tetramethylethylendiamine
TOF	time of flight
Tris	Tris(hydroxymethyl)aminomethane
w/o	without

Proteins and gene names are based on UniProt.

Acknowledgements

First of all, I would like to thank my supervisor, Dr. Herbert Schiller, for giving me the opportunity to write my doctoral thesis in his lab. It was great to work in a laboratory with such advanced methods and techniques. I would also like to thank you for the fact that I was able to discuss things openly and that we were able to find solutions together. I think I have grown a lot both professionally and personally in these three years and have learned a lot about myself. I really appreciate the numerous opportunities you have given me to present my data at conferences and to learn new things, such as at the MaxQuant Summer School.

I am also very grateful to Prof. Dr. Bernhard Küster, my doctoral thesis supervisor at the Wissenschaftszentrum Weihenstephan of the Technical University Munich, for his valuable suggestions and support during the years. It was also his credit that I became so enthusiastic about proteomics. I wanted to work in this field since the basic proteomics lecture during my Bachelor's. My thanks also go to the other members of my thesis committee Prof. Dr. Silke Meiners and Prof. Dr. Maria Robles for productive discussions and very helpful advice.

I would also like to thank the CPC Research School for the successful learning sessions and for the support during the PhD. I would especially like to thank Claudia Staab-Weijnitz and Silke Meiners for their mental support during the ups and downs of doctoral life.

Above all, the strong team spirit in the Schiller laboratory was great. I really enjoyed working with all of you, Ilias, Christoph, Max, Gabi, Meshal, Paulina, Silvia, Baharak und Janine. You often put a smile on my face when I was dissatisfied with my progress and you always had an open ear for me! Thank you very much for the legendary "lab parties" with DJ Enrico Ostendorf and the Wiesenhits and for all the lunch and coffee breaks, the after work events and your friendship. Thank you so much for including me so well in your "boy group" and all the fun we had together, be it the Milky Way on the dance floor or the one or other after-work beer.

Caffeine has certainly been a very important part of the last three years, as well as the good company during the coffee breaks with Thomas Meul. Tom, you have rebuilt me so many times and have always motivated me to keep going and not give up. I had the luck to work with you, which was really a lot of fun, even though our CRIPSR Cas9 attempts failed miserably. But most of all you have changed from a good colleague to a good friend for me and I hope we will stay in touch even without seeing each other every day at CPC!

Laura Felicitas Mattner

*29.10.1991 in Munich, Germany

Education/Academic training

Since 10/2017:	Ph.D. candidate in the research group "Systems Medicine of Chronic Lung Disease" of Dr. Schiller at the Helmholtz Zentrum München, Institute of Lung Biology and Disease and the Comprehensive Pneumology Center (ILBD/CPC)
10/2014-07/2017:	M.Sc. in Molecular Biotechnology, Technische Universität München Master's thesis in the group of Dr. Schiller, CPC, Helmholtz-Zentrum München: "Functional proteomics of cellular rigidity sensing mechnisms"
10/2011- 07/2014:	B.Sc. in Molecular Biotechnology, Technische Universität München Bachelor's thesis in the group of Prof. Dr. Küster, TUM: „Proteomics with HDAC affinity matrices"
09/200 2 – 05/2011:	Abitur: Michaeli-Gymnasium München

Presentation at conferences

Talks:
Laura F. Mattner (Wanat), Anita A. Wasik, Matthias Mann, and Herbert B. Schiller (February 2018).Phosphoproteomics reveals the signaling landscape of lung fibroblast rigidity sensing. DZL Annual Meeting in Bad Nauheim, Germany.

Poster:
Laura F. Mattner (Wanat), Anita A. Wasik, Matthias Mann, and Herbert B. Schiller (February 2018).Phosphoproteomics reveals the signaling landscape of lung fibroblast rigidity sensing. DZL Annual Meeting in Bad Nauheim, Germany.

Laura F. Mattner (Wanat), Anita A. Wasik, Matthias Mann, and Herbert B. Schiller (March 2018).Phosphoproteomics reveals the signaling landscape of lung fibroblast rigidity sensing. European Respiratory Society (ERS) 16th Lung Science Conference in Estoril, Portugal.

Laura F. Mattner, Jan Daniel Rudolph, Jürgen Cox and Herbert B. Schiller (September 2019). Phosphoproteomics of cell adhesion and celluar mechanosensing.
ETRS Annual Meeting 2019: "From basic science to clinical translation", Munich, Germany

Scholarships and Awards

- Comprehensive Pneumology Center - Research Grant (amount: 2.000 EUR, 2019)

- Travel bursary for the European Respiratory Society (ERS) 16th Lung Science Conference in Estoril, Portugal (March 2018)

Publications

Strunz, M., Simon, L. M., Ansari, M., **Mattner, L. F**., Angelidis, I., Mayr, C. H., ... & Herbert B. Schiller. (2020). Longitudinal single cell transcriptomics of lung regeneration reveals a fibrogenesis specific epithelial cell state. Nat Commun. 2020 Jul 16;11(1):3559.
doi: 10.1038/s41467-020-17358-3. PMID: 32678092

Thomas Meul, Korbinian Berschneider, Sabine Schmitt, Christoph H. Mayr, **Laura F. Mattner**, Herbert B. Schiller, Ayse Yazgili, Xinyuan Wang, Bastian Popper, Christine von Toerne, Stefanie M. Hauck, ... , & Silke Meiners (2020). Adaptive mitochondrial regulation of the proteasome. Cell Rep. 2020 Aug 25;32(8):108059. doi:10.1016/j.celrep.2020.108059. PMID: 32846138

Mattner, L. F., , Mayr, C. H.,Ansari, M. ... & Herbert B. Schiller (2020).
in preparation

"In the end, you tried and you cared and sometimes that is enough."

Anonymous